İSTANBUL TECHNICAL UNIVERSITY ★ GRADUATE SCHOOL OF SCIENCE ENGINEERING AND TECHNOLOGY

FACTORS AFFECTING SOIL DAMPING

M.Sc. THESIS

Yeşim ÜNAL

Department of Civil Engineering

Soil Mechanics and Geotechnical Engineering

JUNE 2016

İSTANBUL TECHNICAL UNIVERSITY ★ GRADUATE SCHOOL OF SCIENCE ENGINEERING AND TECHNOLOGY

FACTORS AFFECTING SOIL DAMPING

M.Sc. THESIS

Yeşim ÜNAL
(501131313)

Department of Civil Engineering

Soil Mechanics and Geotechnical Engineering

Thesis Advisor: Prof. Dr. Ayfer ERKEN

JUNE 2016

İSTANBUL TEKNİK ÜNİVERSİTESİ ★ FEN BİLİMLERİ ENSTİTÜSÜ

ZEMİNLERİN SÖNÜMÜNÜ ETKİLEYEN FAKTÖRLER

YÜKSEK LİSANS TEZİ

Yeşim ÜNAL
(501131313)

İnşaat Mühendisliği Anabilim Dalı

Zemin Mekaniği ve Geoteknik Mühendisliği Programı

Tez Danışmanı: Prof. Dr. Ayfer ERKEN

HAZİRAN 2016

Yeşim ÜNAL, a **M.Sc.** student of ITU **Graduate School of Science Engineering and Technology**, student ID **501131313**, successfully defended the **thesis** entitled "**Factors Affecting Soil Damping**", which she prepared after fulfilling the requirements specified in the associated legislations, before the jury whose signatures are below.

Thesis Advisor:	**Prof. Dr. Ayfer ERKEN** Istanbul Technical University	.....
Jury Members:	**Yrd. Doç. Dr. Berrak TEYMÜR** Istanbul Technical University	.....
	Doç. Dr. Ayşe EDİNÇLİLER BAYKAL Boğaziçi University	.....

Date of Submission: 28 April 2016
Date of Defense: 09 June 2016

To my family,

FOREWORD

I would like to express my deepest gratitudes and thanks to my adviser Prof. Dr. Ayfer Erken for her kindness and understanding. Her knowledge and contribution made this thesis possible.

Also I would like to thank my family for their great love and support and for always believing in me.

May 2016

Yeşim Ünal
Civil Engineer

TABLE OF CONTENTS

Page

ABBREVIATIONS

AV sand	:Antelope valley sand
CL	: Lean clay
CTSS	: Cyclic torsional simple shear test
CTX	: Cyclic triaxial sand
EQ	: Earthquake Simulator
ESB	: Equivalent shear beam model container
DSDSS	: Double specimen direct simple shear device
GRM	: Gravel/sand mixture
HS	: Handspooning
KH	: Kobe strong event
KL	: Kobe weak event
KM	: Kobe moderate event
LVDT	: Linear variable differential transformers
ML	: Silt
RC	: Resonant column test
TOSS	: Torsional simple shear test
SRM	: Sand/rubber mixture
SM	: Silty sand
SM sand	: Santa Monica sand
UC	: Undercompaction
WCH	: West Canada strong event
WCL	: West Canada weak event
WCM	: West Canada moderate event

SYMBOL LIST

$\mathbf{A_{loop}}$	: Hysteresis loop area
B	: Skempton coefficient
$\mathbf{C_1}$	: Curve fitting constant
$\mathbf{C_1}$	: Stifness coefficient
$\mathbf{C_2}$	: Viscous damping coefficient
$\mathbf{C_c}$	: Compressibility of soil skeleton
$\mathbf{C_p}$	: Compressibility of pore water
$\mathbf{C_u}$	: Uniformity coefficient
d	: Dashpot
$\mathbf{d_{50}}$	: Mean grain size
D, $\mathbf{D_o}$, λ	: Damping ratio
DCF	: Calibration factor
$\mathbf{D_r}$	: Relative density
e	: Void ratio
F(e)	: Function of void ratio
G	: Shear modulus
$\mathbf{G_{max}}$	: Maximum shear modulus
$\mathbf{G/G_{max}}$	: Modulus reduction
$\mathbf{G_I}$	: Complex part
$\mathbf{G_{max}}$	: Maximum shear modulus
$\mathbf{G_R}$	: Real part
$\mathbf{I_p}$	: Plasticity index
k	: Spring constant
K(γ)	: Decreasing function of γ
LL	: Liquid limit
m(γ)	: Increasing function of γ
N	: Number of cycles
n($\mathbf{I_p}$)	: Function of I_p
OCR	: Overconsolidation ratio
PI	: Plasticity index
PL	: Plasticity limit
R	: Curve fitting constant
t	: Time
$\mathbf{t_d}$	: Arrival time
$\mathbf{T_r}$	: Relaxation time
$\mathbf{S_r}$	: Degree of saturation
u	: Particle displacement
v	: Particle velocity
$\mathbf{W_D}$	: Dissipated energy
$\mathbf{W_S}$	: Elastic strain energy
x	: Spatial coordinate

V_s : Shear wave velocity
α : Curve fitting constant
δ : Loss angle
Δ_1 : Logarithmic decreament
Δ_u : Change in pore water
$\Delta_{\sigma 1}$: Change in principal stress
Δ_x : Element spacing
η : Viscocity
γ : Cyclic shear strain
ω : Frequency
ϕ : Internal friction angle
ψ_1 : Incident angle
ψ_2 : Refraction angle
ψ_c : Critical angle
ρ : Mass density
σ'_3 : Confining pressure
σ' : Effective confining pressure
σ'_h : Horizontal effective stress
σ'_m : Mean effective confining pressure
σ_o : Mean principal stress
σ'_v : Vertical effective stress
σ'_{vc} : Effective consolidation stress
τ : Shear stress

LIST OF TABLES

Page

LIST OF FIGURES

Page

FACTORS AFFECTING SOIL DAMPING

SUMMARY

The behaviour of soil under cyclic loading like earthquake is very important and must be analyzed to solve problems. To comprehend the behaviour of soil, the dynamic soil parameters must be known. Two important dynamic soil parameters are damping and shear modulus which are related to shear strain. When the soil is subjected to cyclic loading, some of the energy is absorbed by soil which is called soil damping. So how bigger the energy absorbtion is, the soil damping is also big. In this thesis, especially damping had been examined.

Dynamic soil parameters can be evaluated from laboratory and field tests. Laboratory test results are more accurate because soil can be examined under different loadings and conditions. The key factor of choosing the test method is deformation levels. Laboratory tests are preferred for high deformation levels while the field tests are preferred for low deformation levels. Most performed laboratory tests are resonant column test, cyclic simple shear test and triaxial shear test. As a result of these tests, soil damping can be calculated from the stress-strain curves which are called hysteresis loops. Each loop is the amount of energy absorbtion by soil. Other than this, damping can be calculated by the developed formulas.

There are accepted curves for soil damping which are commonly used to compare the results of other investigations. Seed and Idriss (1970) curves are used for gravelly sands and sand, Vucetic and Dobry (1991) curves are used for plastic soils.

Soil damping is affected by the factors which are mentioned in this thesis; density, number of cycles, plasticity index, overconsolidation ratio, consolidation stress, compaction stress, saturation, mean grain size and uniformity coefficient. In chapter 3.3, these factors are examined comprehensively.

In recent years, the increment of traffic causes increment of waste tires. These waste tires are usually mixed with soil or asphalt to used in engineered fills, paving projects and other earthworks. Tire rubber has a high damping capacity thanks to its high elasticity and good fatique properties. Also it has a lightweight. On the other hand, fibers are used as a reinforcement in contruction materials for improvement of soil properties since prehistoric times.

Earthquake is an important fact for humanity. It is possible to decrease the affect of earthquake or other cyclic loadings with improving the dynamic soil properties. In this thesis, factors affecting soil damping are examined through literature. As a possible increasing factor on soil damping, soil mixed with granulated rubber and fiber are analyzed. For rubber effect Nakhaei et al. (2012) and Senetakis et al. (2012) curves were interpreted. Data from Torabi (2011) was used to determine damping values of fiber-sand mixtures and results were interpreted.

ZEMİNLERİN SÖNÜMÜNÜ ETKİLEYEN FAKTÖRLER

ÖZET

Deprem gibi tekrarlı yükler altında zeminin davranışı, problemlerin çözümlenebilmesi için çok önemlidir. Bu davranışı anlayabilmek için dinamik zemin özelliklerinin bilinmesi önem taşımaktadır. Dinamik zemin özelliklerinden en önemlileri sönüm ve kayma modulüdür. Bu iki özellik gerilme-şekil değiştirme karakteristiğine bağlı olarak incelenmektedir. Sönüm, malzemenin (zeminin) dinamik yükler altında enerji yutması demektir. Dolayısıyla sönümün büyük olması enerji yutumunun da fazla olduğunu göstermektedir. Bu özellik de deprem yüklerinin hasar etkisinin aza indirilmesinde büyük önem taşımaktadır. Bu tezde sönüm ve sönümü etkileyen faktörler ayrıntılı olarak incelenmiş ve sönümü arttırıcı malzeme olarak lastik ve fiber karıştırılmış zeminlerin davranışları incelenmiştir.

Dinamik zemin özellikleri laboratuar ve arazi deneyleri ile hesaplanabilmektedir. Labaratuar deneyleri zemin koşullarını gerçeğe daha yakın bir şekilde yansıtabilmektedir. Küçük deformasyon seviyeleri için arazi deneyleri tercih edilirken büyük deformasyon seviyeleri için laboratuar deneyleri tercih edilmektedir. En çok tercih edilen laboratuar deneyleri rezonant kolon testi, üç eksenli basınç deneyi ve basit kesme deneyidir. Laboratuar deneyleri sonucunda sönüm gerilme şekil değiştirme grafiği üzerinden hesaplanabilmektedir. Bu grafikte gerilme-şekil değiştirme davranışı histerez ilmekleri şeklinde olmaktadır. Her bir çevrimde sönümlenen enerji miktarı sönümleme oranı olarak tanımlanmaktadır. Ayrıca sönüm, yapılmış deneysel çalışmalar sonucunda geliştirilen formüller ile de hesaplanabilmektedir. Ray ve Woods (1988) Ramberg-Osgood modelini kullanırken, Zhang ve Aggour (1996) farklı yükleme çeşitleri için formüller geliştirmiştir. Bu tezde incelenmiş tüm geliştirilmiş formüller Çizelge 3.5'te özetlenmiştir.

Farklı zemin türleri için herkes tarafından kabul görmüş sönüm eğrileri bulunmaktadır. Bunlar özellikle çakıllı kum ve kumlar için Seed ve Idriss (1970), plastik zeminler için ise Vucetic ve Dobry (1991) tarafından çizilen eğrilerdir. Bu eğriler başka araştırmalarda ve yapılan deneylerde karşılaştırma eğrileri olarak sıkça karşımıza çıkmaktadır.

Sönüm bir çok faktörden etkilenmektedir. Bu tezde ele alınan başlıca faktörler; rölatif sıkılık, çevrim sayısı, plastisite, aşırı konsolidasyon oranı, konsolidasyon basıncı, yükleme tipi, test metodu, kompaksiyon basıncı, doygunluk ve ortalama tane çapıdır. Genel olarak sönüm rölatif sıkılık ve doygunluktan pozitif olarak etkilenirken diğer farktörlerden negatif etkilenmektedir. Kompaksiyon basıncı ve ortalama tane çapından ise etkilenmemektedir.

Son yıllarda trafikteki artış ile atık lastik sayısı da artmıştır. Geri dönüşüm olarak kullanılan bu lastikler dolgu malzemesi olarak, asfalt ile karıştırılıp yol kaplaması olarak ve diğer çeşitli mühendislik yapılarında kullanılmaktadır. Lastik elastisitesi yüksek ve dayanıklı bir malzeme olduğu için sönüm kapasitesi yüksektir. Ayrıca

hafif bir malzemedir. Zemine karıştırılarak sönüm arttırıcı özelliği ile ilgili araştırmalar yapılmıştır.

Zheng Yi ve Sutter (2000)'ın Ottowa kumu üzerinde yaptığı deneylere göre yüksek lastik içerikli numunelerde basınç arttıkça sönümde de artış görülmüştür. Bu davranış normal zemin davranışına terstir. Ayrıca lastik yüzdesi arttıkça sönümün de arttığı gözlemlenmiştir. Nakhaei ve diğerleri (2012)'nin daneli lastik ile karıştırılmış daneli zemin üzerinde yaptığı deneylere göre basınç 50 ve 100 kPa iken sönüm lastik yüzdesinin artışı ile düşmektedir. Bu davranış şu şekilde açıklanabilir: Düşük basınçlarda lastik yüzdesi arttıkça elastic deformasyonun artmasına sebep olmakta ve bunun sonucunda sönüm azalmaktadır. Basınç 200 ve 300 kPa olduğunda ise sönüm lastik yüzdesi arttıkça artmaktadır. Büyük basınçlar altında sıkışmış olan lastiğin esneksizliğinden dolayı rölatif deformasyon artmakta bu da plastik deformasyonu ve sönümü arttırmaktadır. Aynı zamanda lastiksiz zeminde sönüm basınç arrtıkça azalmaktadır ama normal davranışın aksine lastik karıştırılmış zeminlerde sönüm basınç arttıkça artmaktadır. Deviatör gerilme uygulandığında zemin danelerinin birbiri üzerinde kayışı arttığı için hem plastik deformasyonun hem de sönümün artışını sağlamaktadır.

Lastikli zeminin davranışını daha iyi anlayabilmek adına Nakhaei ve diğerleri(2012) tarafından çizilmiş olan eğrilerden belli bir deformasyon seviyesi seçilerek sönümün basınç ve lastik oranı ile değişimi incelenmiştir. Sadece lastiksiz zeminin sönümü basınç arttıkça azalmıştır. Basınç yaklaşık 150 kPa iken grafikteki eğriler için bir dönüm noktası oluşmuştur. Sönümün lastik ile değişimi incelendiğinde ise lastiksiz zeminde sönümün basınç arttıkça düştüğü gözlenlenmiş fakat bu davranış lastik oranı yaklaşık 3% oranına geldiğinde bir dönüm noktası oluşturarak tersine dönmüştür.

Artık lastiklerin yanısıra fiber de tarih öncesi dönemlerden beri güçlendirici yapı malzemesi olarak kullanılmaktadır. Fiber zeminin özelliklerini arttırıcı özellik taşımaktadır. Fiber ile ilgili çalışmalar sonucunda zeminin kayma direncini arttırdığı gözlemlenmiştir. Fiberin sönüm oranına etkisi ile ilgili çalışmalar ise çok kısıtlıdır.

Amir-Faryar ve Aggour (2016) iki farklı çeşit fiberi killi zemin ile karıştırarak deney yapmışlardır. Deneyler sonucunda maksimum kayma modülü fiber oranı ile artmıştır ancvak en yüksek değere 0.2% fiber ile ulaşmıştır. Ayrıca fibril yapılı olanın maksimum kayma modülü monofilament olan fibere göre daha yüksektir. Sönüm de fiber oranı arttıkça artmıştır. Fakat bu araştırma küçük deformasyon seviyelerinde yapılmıştır.

Mojtaba Torabi'nin 2011'de yazmış olduğu tezindeki deney verileri kullanılarak 100 kPa basınç uygulanan, rölatif sıkılığı 60% olan 0%, 0.1%, 0.5% ve 1% fiber karıştırılmış Akpınar kumunun sönümleri histerez ilmekleri yöntemi ile hesaplanmış ve sönümün deformasyon ile değişim eğrileri çizilmiştir. Sönüm temiz ve fiberli zeminler için önce artmış daha sonra azalmıştır. Gerilme şekil değiştirme grafiğinde histerez ilmekleri sönümün arttığı ve düştüğü çevrimler için incelendiğinde loop alanlarının büyüdüğü görülmüştür. Bu davranış boşluk suyu basıncının fazla artışı sonucunda numune etrafına sarılı membranın devreye girmesi sonucunda ortaya çıkması şeklinde açıklanabilir. Belli bir deformasyon seviyesi seçilerek fiberin sönüme olan etkisi incelenmiştir. Beklenenin aksine sönüm fiber oranı arttıkça azalmaktadır. Bu davranış da uygulanan basıncın yetersiz olması ile açıklanabilir.

Mojtaba Torabi'nin tezinden elde edilen sonuçlar Nakhaei ve diğerleri'nin (2012) lastik karıştırılmış zemin davranışı ile karşılaştırılmıştır. Farklı deformasyon seviyeleri olsa da 100 kPa için sönümün düştüğü iki araştırma için de geçerlidir. Ayrıca Senetakis ve diğerlerinin (2012) belli deformasyon seviyesi seçilerek çizilmiş sönümün lastikle değişimi eğrileri sonucunda da 100 kPa'da sönüm karıştırılmış malzeme lastik ya da fiber olsa da düşmektedir.

1.INTRODUCTION

The solution of the problems caused by cyclic loadings like earthquake, traffic vibrations etc., need the understanding of dynamic soil properties. Most important dynamic soil properties are soil damping and shear modulus. Evaluation of these parameters can be obtained by laboratory and field tests. Field tests are preferred mostly for low deformation levels while the laboratory tests are preferred for high deformation levels.

Soil damping can be calculated mostly with the general formula which is generated from the hysteretic stress-strain relationship loops. And also many researchers had developed different formulation for different conditions. For example, while Zang and Aggour (1996) developed equations for sinusoidal, random and impulse loading, Ray and Woods (1988) developed equation with using Ramberg-Osgood model. In chapter 3.1, these studied are comprehensively overviewed.

Seed and Idriss (1970) curves for gravelly soils and sands and Vucetic and Dobry (1991) curves for plastic soils are accepted as general curves for soil damping which are used mostly to compare of the results of studies.

Soil damping is affected by many factors which are examined in chapter 3.3: density, number of cycles, plasticity index, overconsolidation ratio, consolidation stress, compaction stress, saturation, mean grain size and uniformity coefficient.

In recent years, the number of waste tires increased due to the increment of traffic. These waste tires are usually mixed with soil or asphalt and used in geotechnical engineering such as lightweight fills, backfill materials, highway embankments, soil-retaining walls, paving projects etc.. Tire rubber is a light material, has high elasticity and good fatique properties so it has high damping capacity. On the other hand, fibers was using as a reinforcement in contruction materials for improvement of soil properties since prehistoric times.

In this thesis, factors affecting damping are examined through literature and As a possible increasing factor on soil damping, soil mixed with granulated rubber and fiber are analyzed. For rubber effect Nakhaei et al. (2012) and Senetakis et al. (2012) curves were interpreted. Data from Torabi (2011) was used to determine damping values of fiber-sand mixtures and results were interpreted.

2. DYNAMIC SOIL PROPERTIES

The response of soils to cyclic loading is very important to comprehend the nature of eartquake damage. Large part of this response is controlled by the mechanical properties of the soil. Important problems which are dominated by wave propagation effect induce low levels of strain in the soil and other important problems which involve the stability of masses induce large strains in the soil. The soil behaviour under cyclic loadings is governed by dynamic soil properties. (Kramer, 1996)

2.1 Soil Damping and Shear Modulus

Dynamic response analysis are very important to understand the soil behaviour under cyclic loadings such as earthquakes, machine foundations, waves, winds etc. Damping ratio (D) and the shear modulus (G) are the key parameters of dynamic response analysis because they are both dependent on the cyclic shear strain (γ). Cyclically loaded soil behaviour is related to soil stress-strain behaviour which is represented by Hysteresis loops. (Figure 2.1)

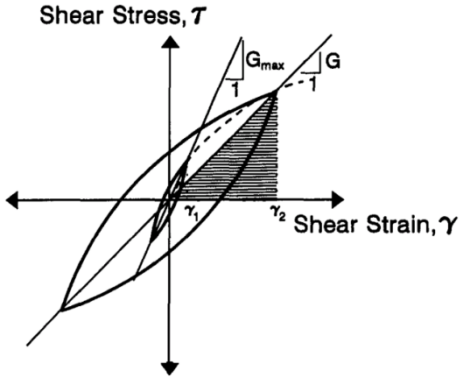

Figure 2.1: Hysteresis stress-strain relationships at different strain amplitudes (Rollins et al., 1998)

Damping is the energy dissipation or energy absorption of dynamically loaded material. For soils, it can be explained as a energy absorption in one loading cycle and this relation is defined as a damping ratio. Damping ratio (D) can be computed from the hysteresis loops as shown in Figure 2.1.

$$D = \frac{W_D}{4\pi W_S} = \frac{1}{2\pi} \times \frac{A_{loop}}{G\gamma^2} \quad (2.1)$$

where W_D is a measure of dissipated energy, W_S is the elastic strain energy or the area of the shaded triangle and A_{loop} is the area enclosed by the hysteresis loop.

The slope of the secant line connecting the higher tips on the hysteresis loop is defined as shear modulus.

$$G = \tau/\gamma \quad (2.2)$$

The shear modulus is at its maximum value (G_{max}) when the shear strain levels are very low (less than 10^{-4}%). G_{max} is the inclanation of the curve. (Fig 2.1) Best way to determining G_{max} is to measure shear wave velocity V_s with seismic geophysical in situ tests and then computing with the equation

$$G_{max} = \rho \times V_s^2 \quad (2.3)$$

where ρ is the mass density.(Rollins et al., 1998) On the other hand, Hardin and Richart (1963) defined G_{max} as a function of void ratio and confining pressure, which is also related to these properties and soil type.

$$G_{max} = A \times F(e) \times (\sigma'_m)^n \quad (2.4)$$

where A is an emperical coefficient which represents of the influence of soil type, F(e) is the void ratio function and σ'_m is the mean confining pressure with the power of n. Kokusho (1987) arranged the summary of these emperical equations. (Table 2.1)

Table 2.1: Constants in proposed emperical equations on small strain modulus (Kokusho, 1987) (Ishihara, 1996)

	References	A	$F(e)$	n	Soil material	Test method
Sand	Hardin–Richart (1963)	7000	$(2.17-e)^2/(1+e)$	0.5	Round grained Ottawa sand	Resonant column
		3300	$(2.97-e)^2/(1+e)$	0.5	Angular grained crushed quartz	Resonant column
	Shibata–Soelarno (1975)	42000	$0.67-e/(1+e)$	0.5	Three kinds of clean sand	Ultrasonic pulse
	Iwasaki *et al.* (1978)	9000	$(2.17-e)^2/(1+e)$	0.38	Eleven kinds of clean sand	Resonant column
	Kokusho (1980)	8400	$(2.17-e)^2/(1+e)$	0.5	Toyoura sand	Cyclic triaxial
	Yu–Richart (1984)	7000	$(2.17-e)^2/(1+e)$	0.5	Three kinds of clean sand	Resonant column
Clay	Hardin–Black (1968)	3300	$(2.97-e)^2/(1+e)$	0.5	Kaolinite, etc.	Resonant column
	Marcuson–Wahls (1972)	4500	$(2.97-e)^2/(1+e)$	0.5	Kaolinite, $I_p^{**}=35$	Resonant column
		450	$(4.4-e)^2/(1+e)$	0.5	Bentonite, $I_p=60$	Resonant column
	Zen–Umehara (1978)	2000 ~ 4000	$(2.97-e)^2/(1+e)$	0.5	Remolded clay, $I_p=0\sim50$	Resonant column
	Kokusho *et al.* (1982)	141	$(7.32-e)^2/(1+e)$	0.6	Undisturbed clays, $I_p=40\sim85$	Cyclic triaxial

*σ'_0 : kPa, G_0 : kPa, **I_p : Plasticity Index

The relation between the shear modulus G and the cyclic shear strain γ_c is typically expressed as a curve of G/G_{max} which is defined as modulus reduction. The basic relations of damping ratio and modulus reduction with cyclic shear strain is shown in Figure 2.2.

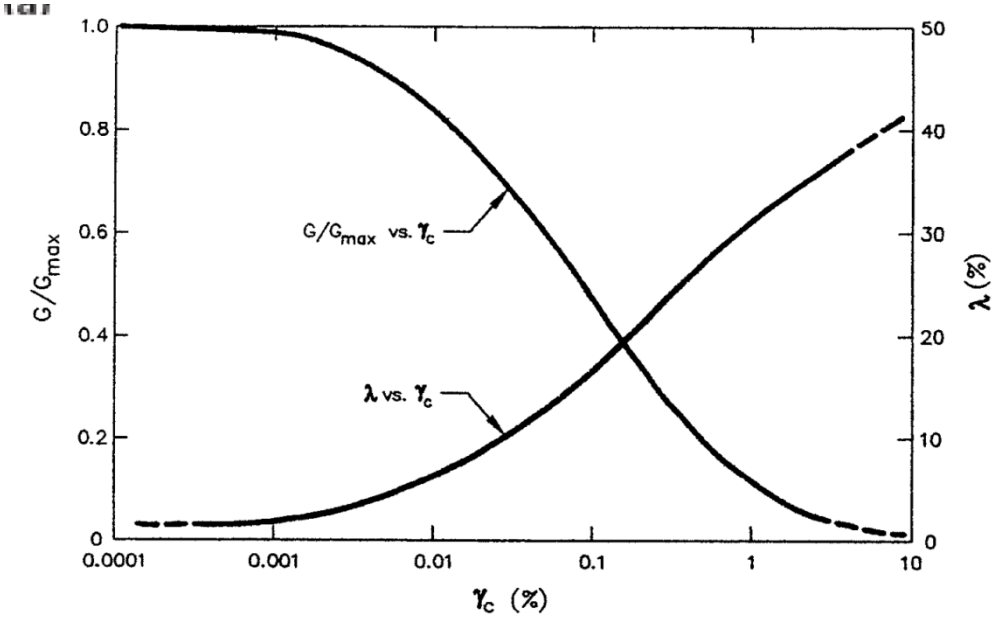

Figure 2.2: Variation of cyclic parameters with cyclic shear strain (Vucetic and Dobry, 1991)

As shown in Figure 2.2, as the shear strain increases, the damping ratio increases while the modulus reduction decreases.

2.2 Measurement of Dynamic Soil Properties

Laboratory tests and field tests are available for measurement of dynamic soil properties. Each test method has its own advantages and limitations depending on the problems. Some of the methods are oriented toward measurement of low strain properties and some of them toward of high strain properties. The selection of test method must be considered carefully for specific problems. (Kramer, 1996) The deformation and stress levels reached in soil are the most important differences between the different dynamic laboratory tests.

2.2.1 Field tests

Field tests are commonly used for estimation small strain dynamic soil properties. Field tests do not require sampling so soil can not be disturbed and can not change its

stress, chemical, thermal and structural conditions. But field tests do not allow to test the soil under different conditions also they do not allow for the controlled pore water drainage. On the other hand, the specific soil property of interest do not be measured directly but can be calculated with emperical relations or theoretical analysis related to shear wave velocity (V_s). Also soil profile type can be classified by determination of shear wave velocity.

2.2.1.1 Reflection method

A body wave is deflected when it comes across an interface of two media with different stiffness in according to Snell's law. If the incident angle (ψ_1) is smaller than the critical angle (ψ_c), the wave is refracted and propagates and if the refraction angle (ψ_2) is larger than angle of incidence, it have to be assumed that the wave travels faster in the second medium ($V_2>V_1$), as illustrated in Figure 2.3. But if the incident wave has larger angle than the critical angle, the wave is reflected into the first medium with same angle (ψ_R), as illustrated in Figure 2.4.

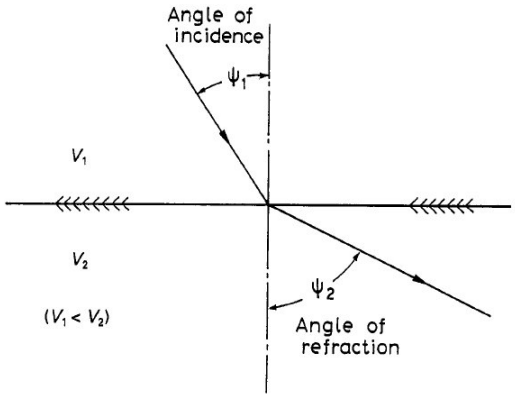

Figure 2.3: Refraction of a wave propagation across an interface (Ishihara, 1996)

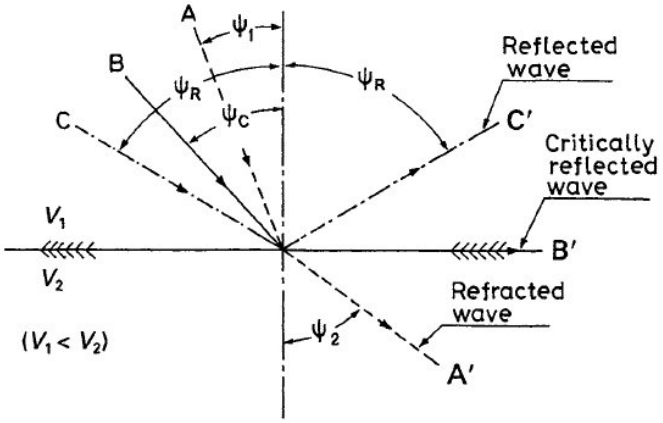

Figure 2.4: Critical angle of incidence ψ_c differentiating between reflection and refraction (Ishihara, 1996)

P-wave (longitudinal or compressional wave) is the fastest and it arrives first so it can be easily observed and identified at a point of monitoring on the ground surface. Figure 2.5 shows the illustration of the survey. (Ishihara, 1996)

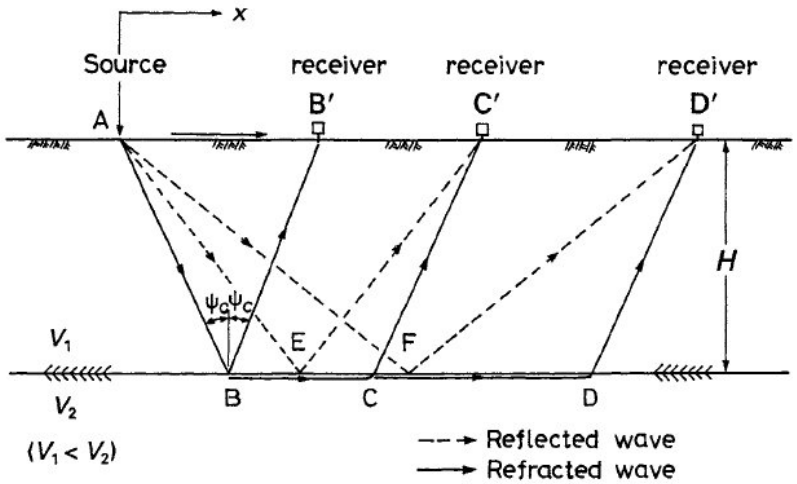

Figure 2.5: Propagation paths for reflected and refracted waves (Richart et al, 1970) (Ishihara, 1996)

If t_d is an arrival time of the P-wave through a direct path from the source A to a point such as B', C' or D', the velocity of propagation can be calculated by;

$$V_1 = \frac{x}{t_d} \tag{2.5}$$

2.2.1.2 Refraction method

To map out the soil profiles for wide areas, refraction method is the simpliest. In this method, there is a source such as impact or explosive energy and a receiver which capture the propagation at a distant point from the source. In Figure 2.6, the basic concept is illustrated.

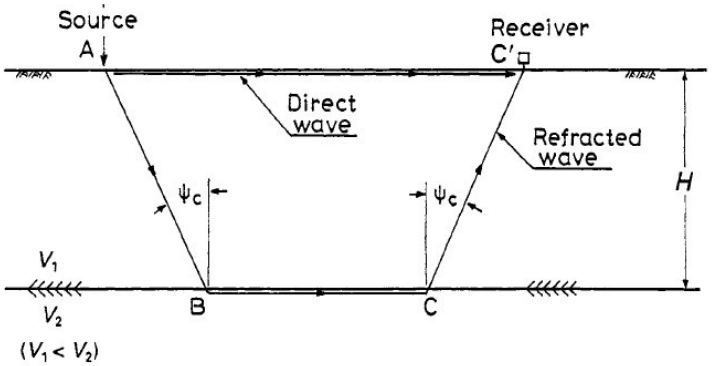

Figure 2.6: Travel path for a refracted wave (Ishihara, 1996)

The velocity of wave propagation through the surface layer is V_1 and through the underlaying layer is V_2. H is the thickness of surface layer. When an excitation is given at point A, most important waves are one travelling through surface (direct wave) and the other going down to point B, travelling along the interface and arriving at point C' (refracted wave). As illustrated in Figure 2.3, the angle of incident and refracted wave are denoted ψ_1 and ψ_2, respectively. According to Snell's law, the ratio between the wave propagation velocity which is related with the angles as;

$$\frac{\sin\psi_1}{\sin\psi_2} = \frac{V_1}{V_2} \tag{2.6}$$

For Figure 2.6, the refracted wave angle along the interface is given as ψ_2=90°. So the vertical angle of incidence is given by,

$$\sin\psi_c = \frac{V_1}{V_2} \tag{2.7}$$

since sin90°=1. (Ishihara, 1996)

2.2.1.3 Cross-hole method

Crosshole test configuration consists two or three boreholes. One of them is for source which generates shear wave or compressed wave and the other ones are for receivers which detect the waves propagation in the horizontal direction. Both source and receivers are placed at the same depth. (Figure 2.7)

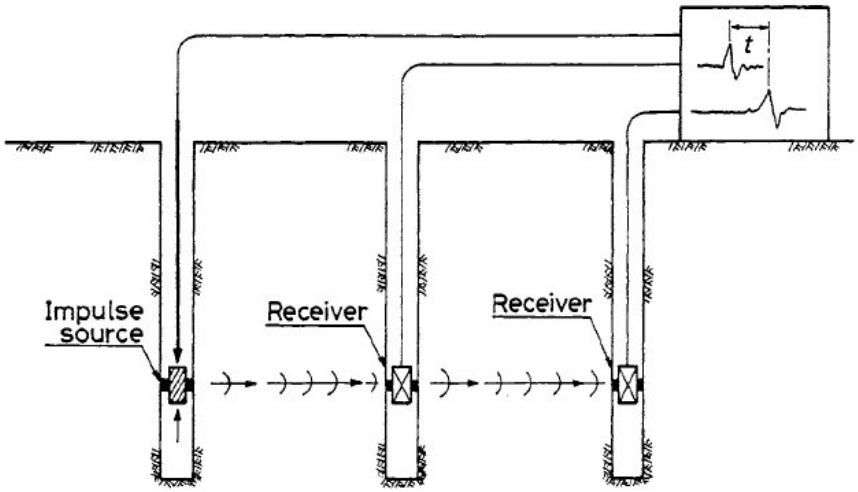

Figure 2.7: Velocity logging by crosshole method (Ishihara, 1996)

When the source is generated, geophones are sensing the vertical velocity and the signals from the geophones are monitored and stored in the oscilloscope. Shear wave velocity can be computed by the difference in travel time between two adjacent geophones. (Ishihara, 1996)

2.2.1.4 Up-hole and down-hole method

In the uphole method, source (generally explosives are fired) is generated in the borehole and its arrival is monitored on the surface by several receivers for both shear wave (S-wave) and longitudinal wave (P-wave). The propagation of P-wave is sufficiently faster than S-wave so in soil deposits with low to medium stiffness, P-wave can be distinguished from S-wave. But in the stiff soils or rocks, the difference can not be discerned.

In the downhole method, source is located on the ground surface and a receiver is fixed is against the walls of the borehole. On the surface, there is a clamped wooden plate which is hit manually by a hammer as a source. If the plate is hit horizontally, it generates a shear wave and if it is hit vertically, it generates longitudinal wave. This method is especially usefull for crowded city areas with limited space.

In Figure 2.8, downhole and uphole methods are illustrated and in Figure 2.9, an example of velocity logging by the downhole method is shown. The thickness of each layer and the velocity of propagation can be delineated by connecting the data points. (Ishihara, 1996)

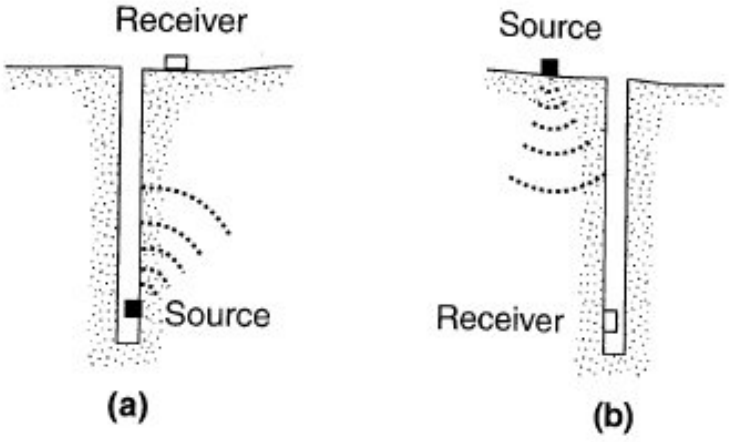

Figure 2.8: (a) Seismic up-hole test and (b) Seismic down-hole test (Kramer, 1996)

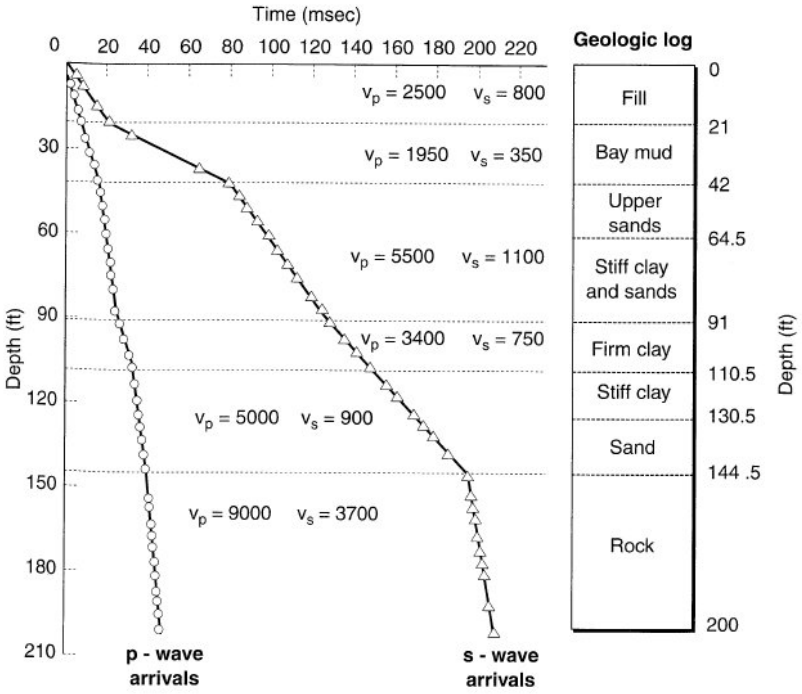

Figure 2.9: Travel-time curve from down-hole test in San Francisco Bay area. (After Schwarz and Musser, 1972) (Kramer, 1996)

2.2.1.5 Suspension sonde method

Shear waves are generated in all directions if an element of medium in a half space is displaced horizontally. In Figure 2.10, two typical shear waves (horizontal and vertical direction) and a compressional wave (in the horizontal direction) is shown.

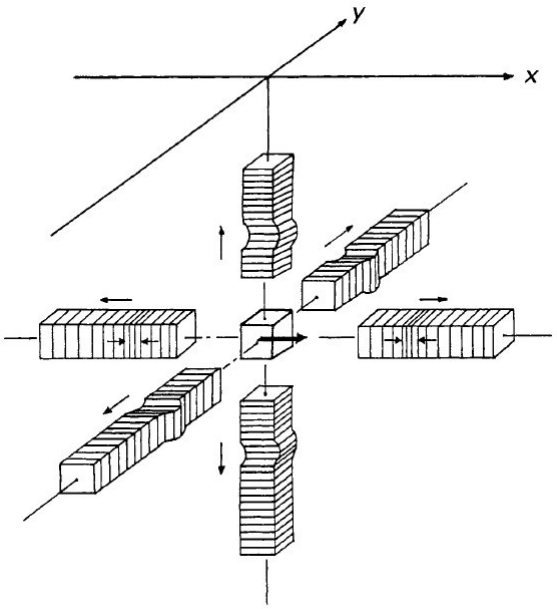

Figure 2.10: Mode of soil deformation within a half-space due to a horizontal impulse (Ishihara, 1996)

The sonde is suspended by a tension cable and lowered into a water filled hole. The sonde consists two geophones which are installed one meter apart, source driver and filter tube which is composed of a rubber tube contains compressed air and which provides a clear shear wave signals for geophones. (Figure 2.11) (Ishihara, 1996)

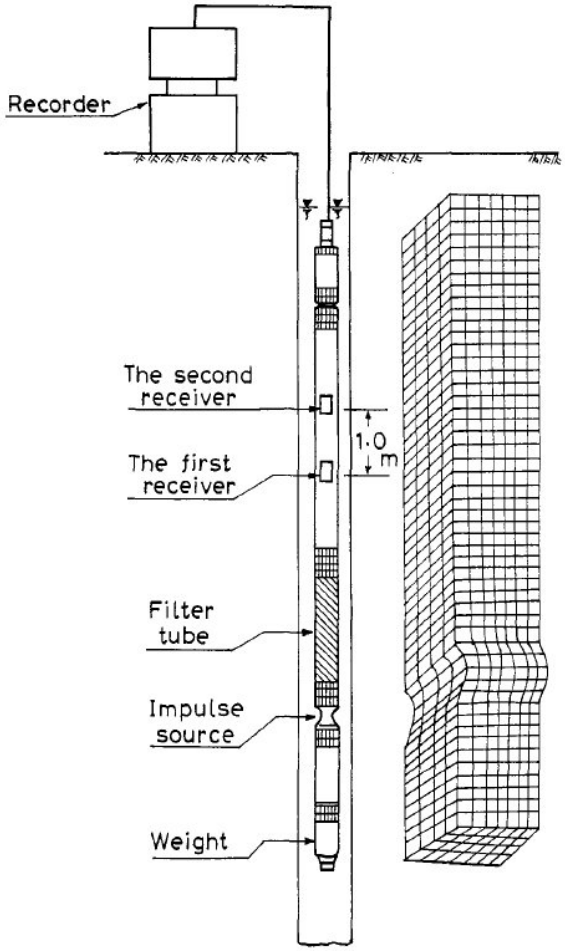

Figure 2.11: Velocity logging by suspension method (Nigbor and Imai, 1994) (Ishihara, 1996)

An electrical device generates an impulse. In Figure 2.12, the mode of deformation of the soil deposit cen be seen schematically. Also Figure 2.13 shows that the pair of records are helping to identify the travel time between the first and the second receiver. An example of velocity logging by suspension sonde can be seen in Figure 2.14.

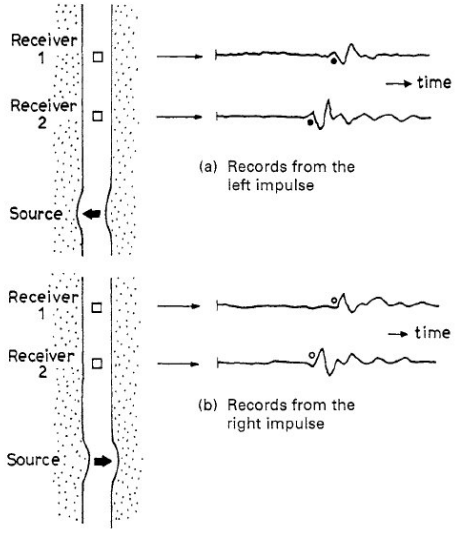

Figure 2.12: Monitoring of fronts of wave propagation by the suspension method (Kitsunezaki, 1982) (Ishihara, 1996)

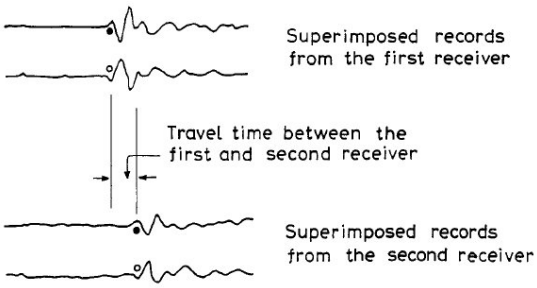

Figure 2.13: Reading of recorded motions in the suspension technique (Ishihara,1996)

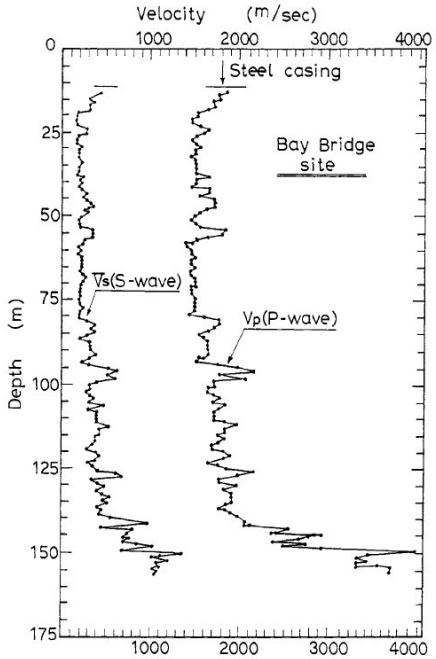

Figure 2.14: An example of at-depth velocity logging by the suspension method (Nigbor and Imai, 1994) (Ishihara, 1996)

2.2.2 Laboratory tests

Laboratory tests provide generally more accurate measurements for soil properties than in site tests. Pore water drainage can be controlled also soil properties can be measured at different confining stresses than those in situ. However, laboratory tests need soil sampling which cause disturbance of the soil. Also laboratory test results are representative for the entire test site because of the heterogeneous nature of the soil. Deformation levels are most important criterion for dynamic laboratory tests. (Figure 2.15)

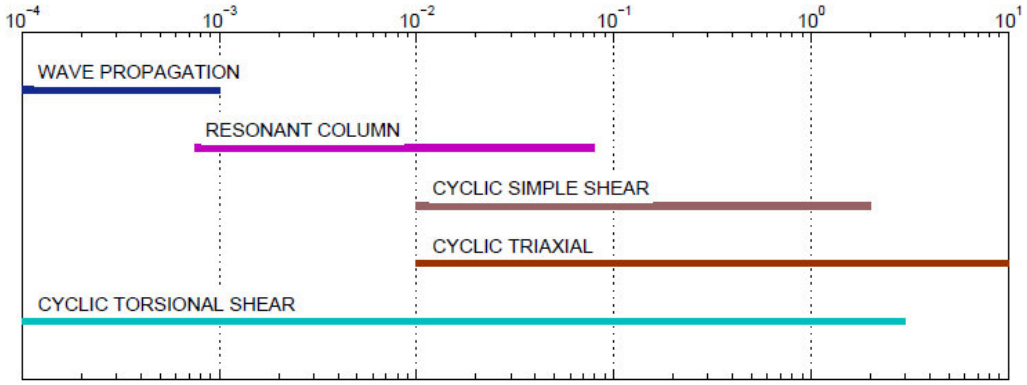

Figure 2.15: Deformation range in dynamic laboratory tests (Houbrechts et al., 2011)

2.2.2.1 Resonant column test

Resonant column test is used especially for measuring the low strain properties of soils. Cylindrical soil specimen is prepared and fixed in place in a triaxial cell. The pressure cell is closed, air pressure is applied to the soil specimen and the whole pressure cell. After that, dynamic excitation with a certain voltage and frequency is applied. Resonant frequency is the frequency of the maximum output amplitude. It is possible to back-calculate the velocity of wave propagation so the shear modulus with known value of the resonant frequency, sample geometry and conditions of end restraint. After the excitation is switched off, the specimen shows a free-decaying vibration which allows to determitaion of the damping property. The procedure is repeated for other excitation amplitudes and also for different cell pressures. (Ishihara, 1996)

There are most common two version of resonant column test apparatus which are shown in Figure 2.16. They are called free-free and fixed-free. The difference of these apparatus is the driving force is applied at the bottom for Figure 2.16(a) but it is

applied at the top for Figure 2.16(b). However, the response is picked up at the top for both of them.

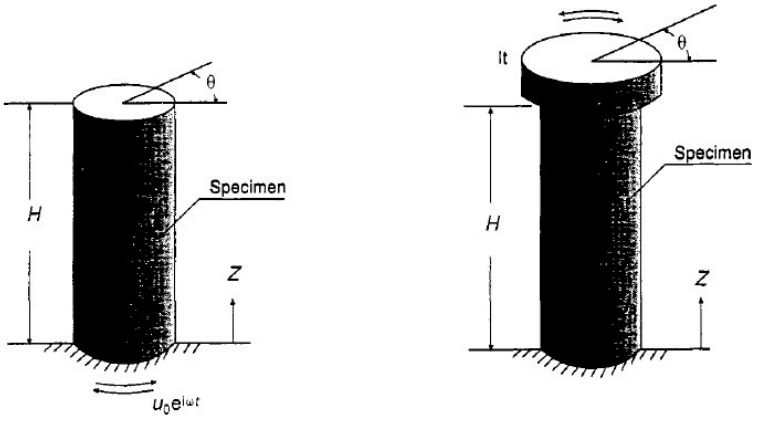

Figure 2.16: Two types of the resonant column test apparatus (Ishihara, 1996)

In Figure 2.17, resonant column apparatus designed by Drnevich (1972) can be seen.

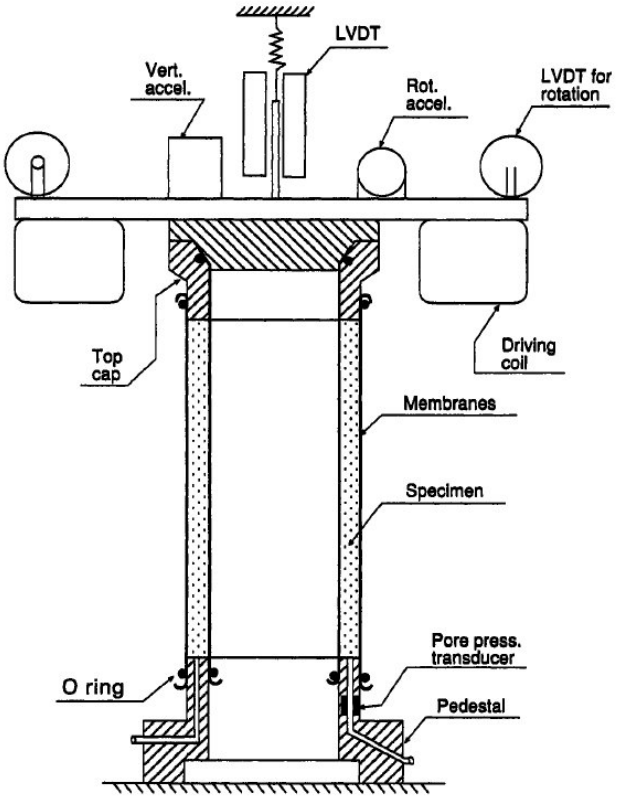

Figure 2.17: Resonant column test apparatus (Dmevich, 1972) (Ishihara, 1996)

As mentioned, the damping ratio is determined from the observation of an amplitude decay curve for free vibration. In Figure 2.18, decay of free vibration and logarithm of the amplitude versus cycles illustraions can be seen.

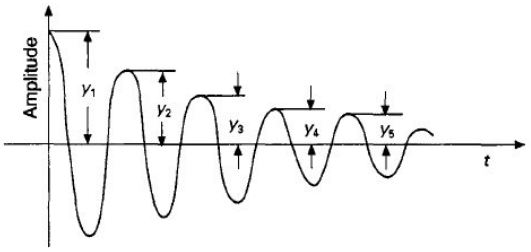

(a) Decay of free vibration

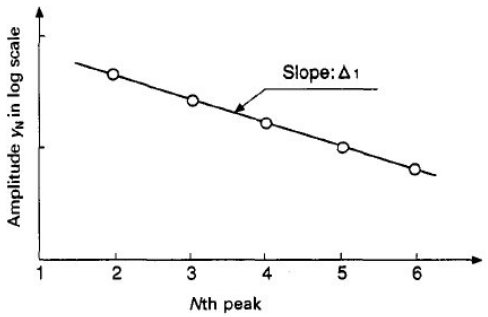

(b) Amplitude versus cycles

Figure 2.18: Method of determining the damping ratio from the free vibration phase (Ishihara, 1996)

For Figure 2.18(a), the logarithmic decreament Δ_1 is defined as,

$$\Delta_1 = log\frac{y_1}{y_2} = log\frac{y_2}{y_3} = \cdots \qquad = log\frac{y_{N-1}}{y_N} \tag{2.8}$$

where N is the number of cycles. So,

$$logy_1 = \Delta_1 + logy_2$$

$$logy_2 = \Delta_1 + logy_3 \tag{2.9}$$

...

$$logy_{N-1} = \Delta_1 + logy_N$$

From these relations,

$$\Delta_1 = \frac{1}{N-1} log\frac{y_1}{y_N} \tag{2.10}$$

As seen in Figure 2.18(b), logarithmic decreament value Δ_1 can be taken as the slope of the straight line. From the correlation of Δ_1, damping ratio D;

$$D = \frac{1}{2\pi}\Delta_1 \tag{2.11}$$

2.2.2.2 Cyclic simple shear test

Cylindrical specimen in the cyclic simple shear test is short and restrained against lateral expansion by rigid boundary platens (Cambridge-type device) , a wire-reinforced membrane (NGI-type device) or a series of stacked rings (SGI-type device). The test specimen is deformed when the cyclic horizontal shear stresses are applied. This deformation is just like the same as an element of soil subjected to vertically propagating s-waves. (Figure 2.19) However, shear stresses are only applied on the top and bottom surfaces of the specimen so the moment caused by horizontal shear stresses on the vertical sides must be balanced by non-uniformly distributed shear and normal stresses. (Kramer, 1996) NGI-type cyclic simple shear apparatus can be seen in Figure 2.20.

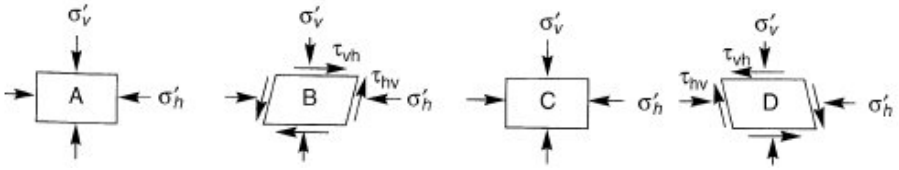

Figure 2.19: Stress and strain conditions imposed on element of soil below level ground surface by vertically propagating shear waves at four different times (Kramer, 1996)

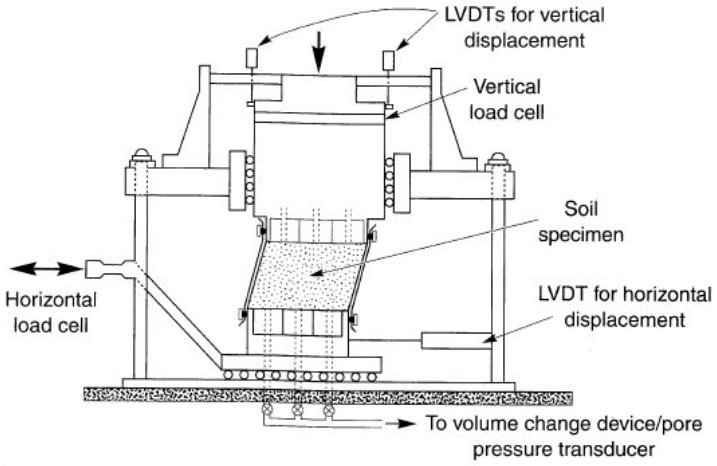

Figure 2.20: NGI-type cyclic simple shear apparatus. Soil specimen is contained within wire-reinforced rubber membrane (After Airey and Wood, 1987) (Kramer, 1996)

2.2.2.3 Cyclic triaxial test

Dynamic triaxial test is one of the most used laboratory tests for measuring dynamic soil properties at high strain levels. The liquefaction potential, the dynamic deformation modulus and damping and the resilient modulus can be determined by

triaxial test. For determination of dynamic deformation modulus and damping, saturated samples (both remoulded and unaltered) must be used in load controlled or axial deformation-control tests. In load controlled test, usually a sinusoidal cyclic load is applied and the evolution of the induced deformations are the results. Knowing the necessary number of cycles to get material failure and a determined level of deformation for different stress ratios or different confinement pressures are the main objectives of these tests. In an axial deformation controlled test, the analysis of the change in the soil mechanical properties during the load application is the main purpose by changing the deformation in a predetermined way. Necessary load or the stress to obtain the prescribed deformation in each cycle are the results. (Houbrechts et al., 2011) The damping ratio is calculated by hysteresis loops. In Figure 2.21, triaxial test apparatus is shown.

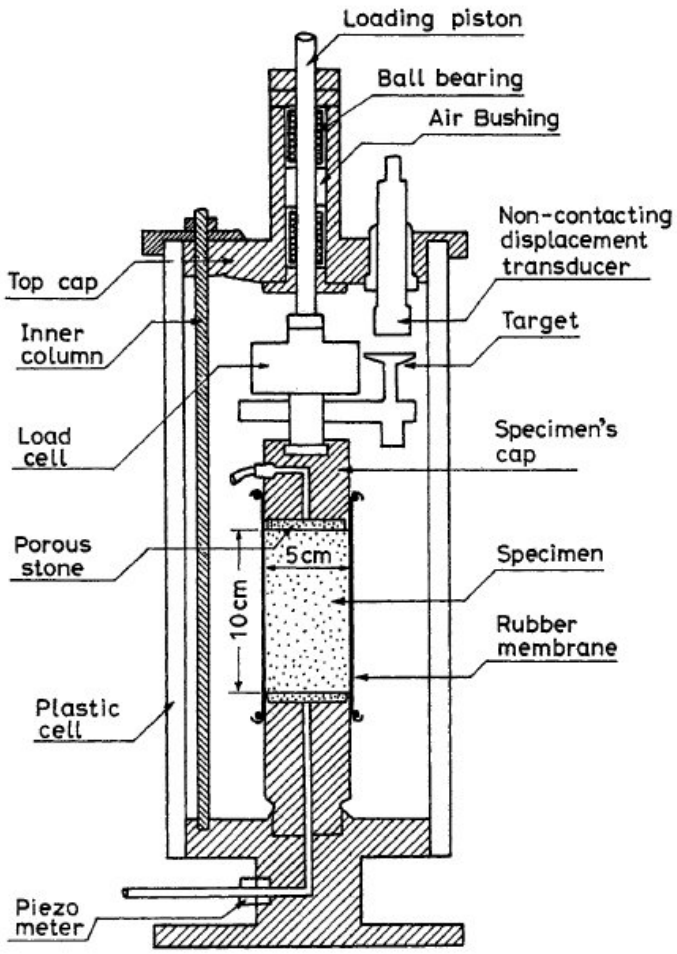

Figure 2.21: Triaxial test apparatus (Ishihara, 1996)

2.2.2.4 Cyclic torsional shear test

Cyclic torsional cyclic shear tests are most commonly used to measure stiffness and damping characteristics over a wide range of strain levels. Two types of cylindrical specimen can be tested in the torsional test apparatus: solid and hollow. However, in the radial direction in the horizontal plane of the sample, strain distribution is not uniform for solid specimens. So hollow cyclindrical samples are preferred because of the best uniformity and control over stresses and drainage. But the preparation of specimen can be difficult and the equipment is not widely available. (Ishihara, 1996; Kramer, 1996) Figure 2.22 shows the hollow cyclinder apparatus.

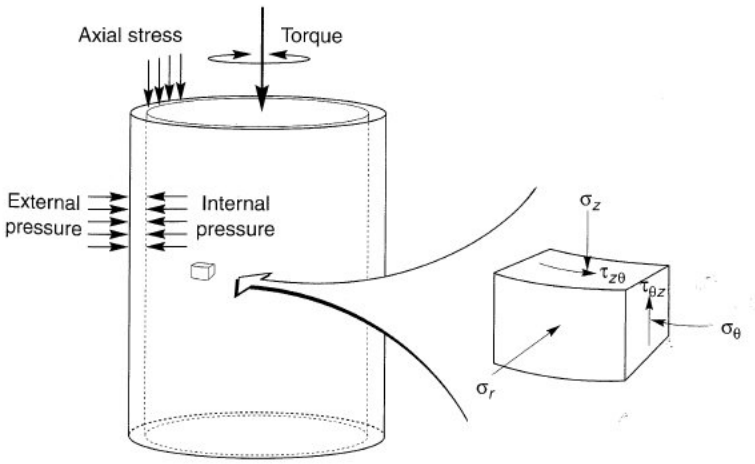

Figure 2.22: Hollow cylinder apparatus (Kramer, 1996)

3. OVERVIEW OF SOIL DAMPING

3.1 Suggested and Developed Equations for Damping Determination

As explained in the previous chapter, damping is determined by Equation (2.1) in generally. Studies on different kind of soils or different kind of situations requires a different solutions. In this manner some researchers suggested different formulation for damping determination and also some researchers developed these suggestions.

3.1.1 Ramberg-Osgood model (Ray and Woods, 1988)

Ray and Woods (1988) performed the torsional simple shear (TOSS) and resonant column (RC) tests on five different cohesionless soils to determine their modulus and damping characteristics by using a nonlinear Ramberg-Osgood stress strain model. Tested soils are 20-30 Ottowa sand, Mambucaba sand, Soil 3, crushed quartz silt and glacier way silt. The 20-30 Ottowa sand is composed of subrounded and rounded quartz grains, Mambuacha sand is a light- brown residual soil which is composed mostly of quartz with other minerals. Glacier way silt is a light-brown silt composed of subangular quartz grains with other minerals present. Grain-size distribution curves and properties of soils are shown in Figure 3.1 and Table 3.1 respectively.

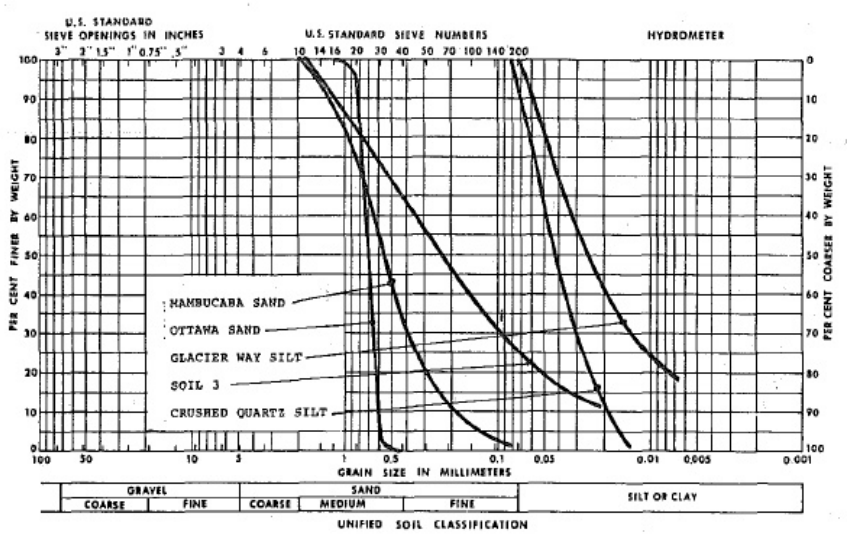

Figure 3.1: Grain-Size Curves for Soils Tested (Ray and Woods, 1988)

Table 3.1: Index and Strength Properties (Ray and Woods, 1988)

Soil (1)	G_s (2)	e_{max} (3)	e_{min} (4)	Triaxial test ϕ (deg.) (5)
Ottawa sand	2.66	0.73	0.48	30
Mambucaba sand	2.66	0.87	0.51	41
Soil 3	2.66	1.19	0.48	41
Glacier way silt	2.66	1.27	0.64	17
Quartz silt	2.66	—	—	48

Reference shear strain γ_r is a stiffness parameter of the specimen and was suggested by Hardin and Drnevich (1972). The term G_{max} is at amplitudes $\gamma \cong 10^{-4}$% in this plot. Ramberg-Osgood curve formulation is taken from Streeter et al.(1974) (Ray and Woods,1988):

$$\gamma = \frac{\sigma_o sin\emptyset_{triax}}{G_{max}} = \frac{\tau_{max}}{G_{max}} \quad \textbf{(3.1)}$$

$$\frac{G}{G_{max}} = \frac{1}{1+\alpha\left|\frac{\tau}{C_1\tau_{max}}\right|^{R-1}} \quad \textbf{(3.2)}$$

$$\frac{\gamma}{\gamma_r} = \frac{\tau}{\tau_{max}} \times \left(1 + \alpha\left|\frac{\tau}{C_1\tau_{max}}\right|^{R-1}\right) \quad \textbf{(3.3)}$$

in which α, C_1, R are the curve-fitting constants. By using Ramberg-Osgood model, Jennings (1964) computed damping ratio and rewrote his equation in terms of the variables as the following:

$$D = \frac{2\times\alpha\times C_1\times\left(\frac{R-1}{R+1}\frac{\tau}{C_1\times\tau_{max}}\right)^R}{\pi\times\frac{\gamma}{\gamma_r}} \quad \textbf{(3.4)}$$

For obtaining the damping, values of τ/τ_{max} are first selected then γ/γ_r is computed. Computed damping values of tested materials under a variety of confining pressures, void ratios and strain levels aer shown in Figures 3.2 to 3.4.

The prediction of damping value by the Ramberg-Osgood model is a fair indicator of material damping. Because it tends to predict on the high side at lower strain levels and it underpredicts damping at larger strain levels. Ramberg-Osgood parameters taken with uniform cyclic tests can be transferred to irregular loading as well.(Ray and Woods, 1988) Also it must be noted that the tested materials are dense.

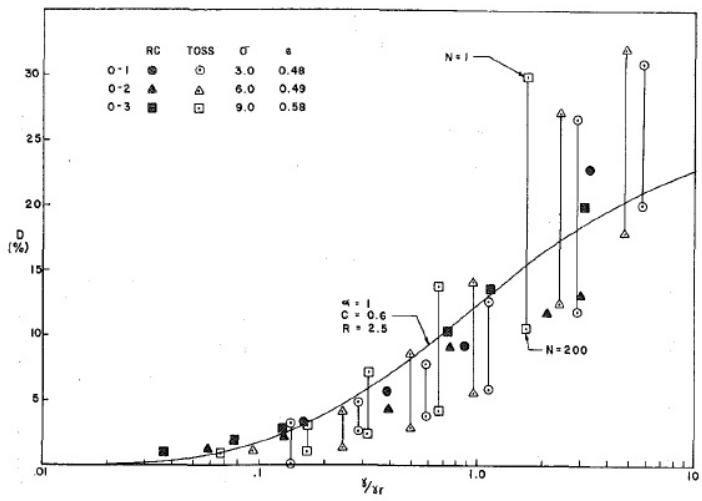

Figure 3.2: Damping vs. γ/γ_r, Ottawa Sand (Ray and Woods, 1988)

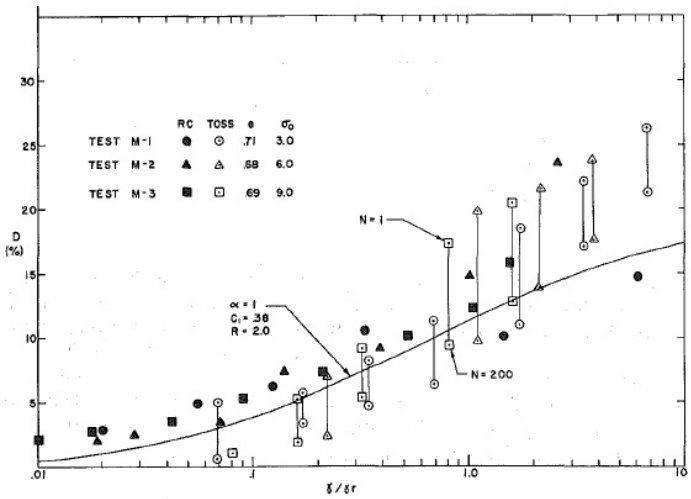

Figure 3.3: Damping vs. γ/γ_r, Mambucaba Sand (Ray and Woods, 1988)

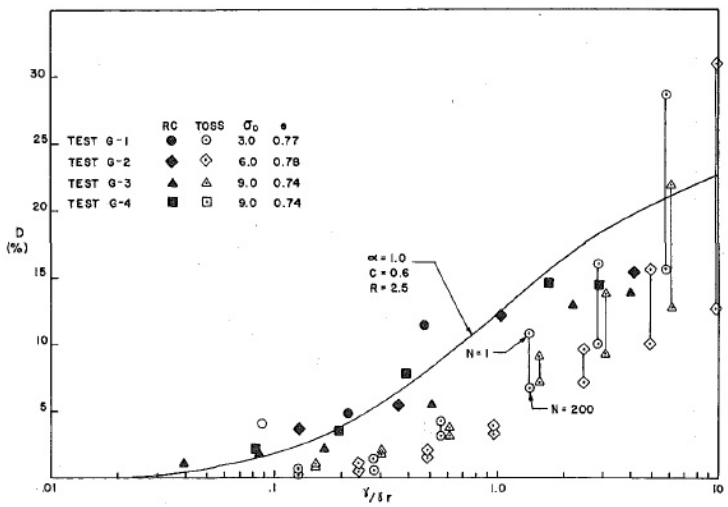

Figure 3.4: Damping vs. γ/γ_r, Glacier Way Silt (Ray and Woods, 1988)

3.1.2 Ishibashi and Zhang (1993) suggestions

3.1.2.1 Sandy soils

Hardin and Drnevich (1972) and Tatsuoka et al. (1978) suggested that the damping ratio is expressed as a function of G/G_{max}.

$$D = f\left(\frac{G}{G_{max}}\right) \tag{3.5}$$

where at $\gamma \leq 10^{-6}$

$$\frac{G}{G_{max}} = K(\gamma){\sigma_0}^{m(\gamma)-m_0} \tag{3.6}$$

$$m_o = m(\gamma \leq 10^{-6}) \tag{3.7}$$

where $K(\gamma)$ is a decreasing function of γ, σ_0 is the mean effective confining pressure and power $m(\gamma)$ is an increasing funtion of γ. Khouri(1984) analyzed and plotted the available experimental data on log G/G_{max} and log σ_0 at various levels of γ. From the slope, $m(\gamma)$-m_0 values and from the intersection at σ_0=1.0 kN/m^2 $K(\gamma)$ values were determined. Values as a function of γ for $K(\gamma)$ and $m(\gamma)$-m_0 are shown in Figures 3.5 and 3.6 respectively.

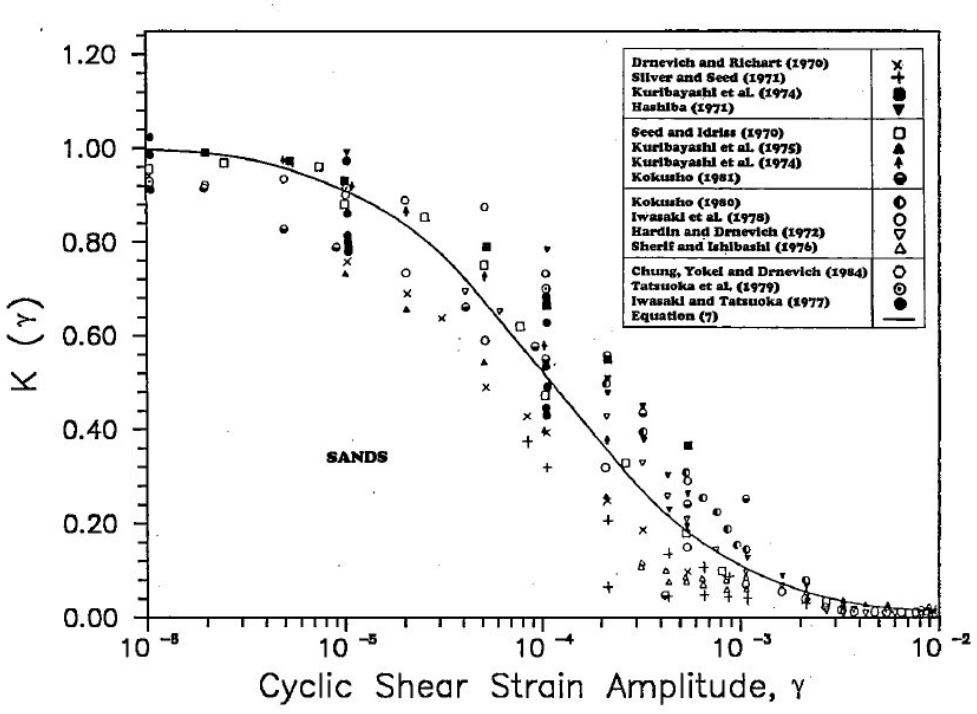

Figure 3.5: $K(\gamma)$ vs. γ for sands (Khouri, 1984) **(**Ishibashi and Zhang, 1993)

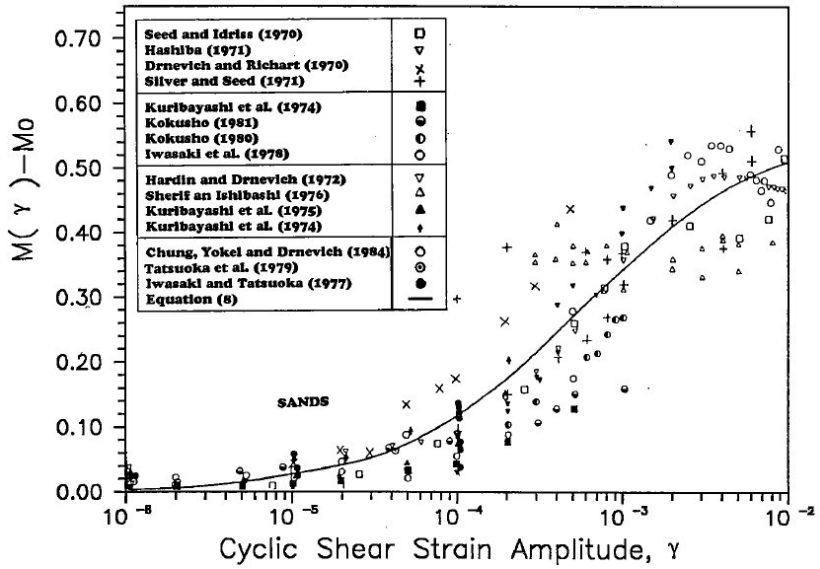

Figure 3.6: m(γ) - m_o vs. γ for sands (Khouri, 1984) **(**Ishibashi and Zhang, 1993)

Best fit data points for Figures 3.5 and 3.6, following equations were proposed respectively.

$$k(\gamma) = 0.5\left[1 + tanh\left\{\ln\left(\frac{0.000102}{\gamma}\right)^{0.492}\right\}\right] \quad \textbf{(3.8)}$$

$$m(\gamma) - m_o = 0.272\left[1 - tanh\left\{\ln\left(\frac{0.000556}{\gamma}\right)^{0.4}\right\}\right] \quad \textbf{(3.9)}$$

Damping versus G/G_{max} values for same experimental data were plotted in Figure 3.7.

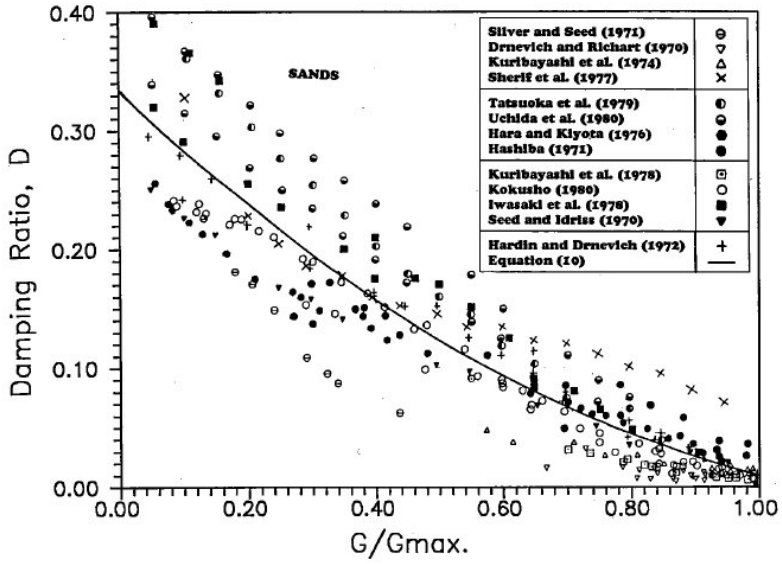

Figure 3.7: Damping Ratios vs. G/G_{max} for sands (Khouri, 1984) **(**Ishibashi and Zhang, 1993)

Damping ratio values are fitted in Figure 2.7 by:

$$D_{sand} = 0.333\left\{0.586\left(\frac{G}{G_{max}}\right)^2 - 1.547\left(\frac{G}{G_{max}}\right) + 1\right\} \quad \textbf{(3.10)}$$

As a conclusion, Ishibashi and Zhang (1993) proposed Equations (3.6), (3.7), (3.8), (3.9) for G values and Equation (3.10) for D values to cover most types of sands.

3.1.2.2 Modified equations for silts and clays (Plastic soils)

Kokusho et al. (1982) and Dobry and Vucetic (1987) stated that plasticity index of soil (I_p) affects the modulus and the damping ratio significantly. Hence, Ishibashi and Zhang (1993) modified their suggested formulas with including I_p for plastic soils:

$$\frac{G}{G_{max}} = K(\gamma, I_p)\sigma_0^{\,m(\gamma,I_p)-m_0} \quad \textbf{(3.11)}$$

$$D = D_{sand} \times A(I_p) \quad \textbf{(3.12)}$$

where $A(I_p)$ is a modification function for sands. These modifications satisfies the sand conditions at I_p=0. Figure 3.8 shows plot of $m(\gamma=10^3, I_p)$-m_0 versus I_p by using limited laboratory data.

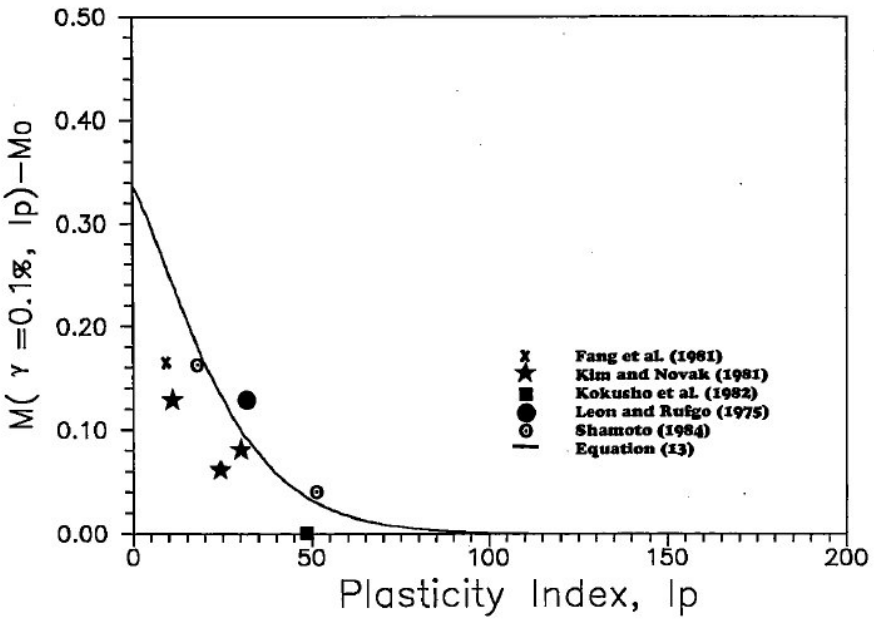

Figure 3.8: $m(\gamma=0.1\ \%, I_p)$ - m_o vs. I_p relationships (Ishibashi and Zhang, 1993)

From Figure 3.8,

$$m(\gamma = 10^{-3}, I_p) - m_0 = 0.335e^{-0.0145{I_p}^{1.3}} \quad \textbf{(3.13)}$$

was generated and by combination with Equation (3.9),

$$m(\gamma, I_p) - m_o = 0.272\left[1 - tanh\left\{\ln\left(\frac{0.000556}{\gamma}\right)^{0.4}\right\}\right] e^{-0.0145{I_p}^{1.3}} \qquad \textbf{(3.14)}$$

is obtained. With known I_p values and using experimental data of G/G_{max}, σ_0 and Equation (3.14), $K(\gamma=10^3, I_p)$ values were calculated from Equation (3.11). These values are plotted in Figure 3.9.

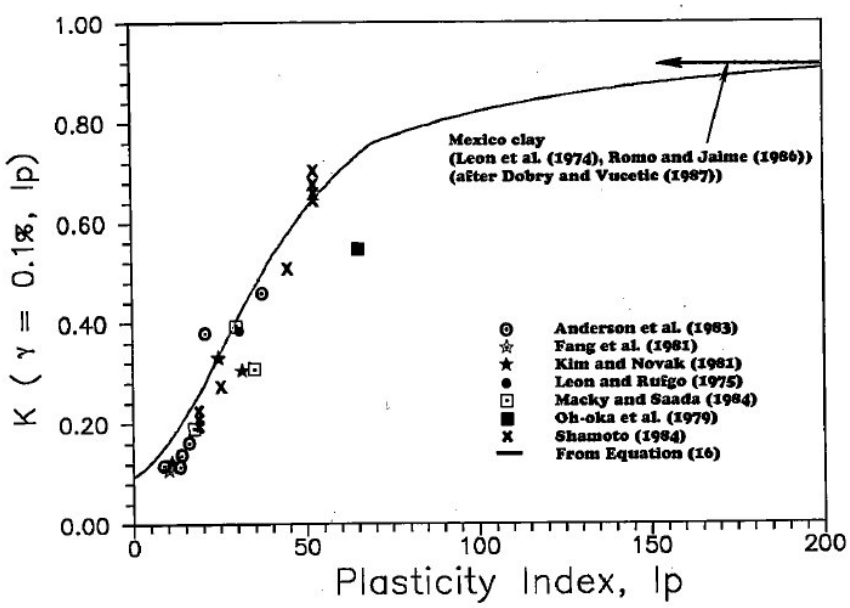

Figure 3.9: $K(\gamma=0.1\ \%, I_p)$ vs. I_p relationships (Ishibashi and Zhang, 1993)

$K(\gamma, I_p)$ is expressed as a modification of Equation (3.8) with an inclusion of $n(I_p)$ function because best fit curve was not possible as a single function.

$$k(\gamma, I_p) = 0.5\left[1 + tanh\left\{\ln\left(\frac{0.000102 + n(I_p)}{\gamma}\right)^{0.492}\right\}\right] \qquad \textbf{(3.15)}$$

where,

$$n(I_p) = \begin{cases} 0.0 & \text{for } I_p = 0 \quad \text{(sandy soils)} \\ 3.37\times10^{-6} I_p^{1.404} & \text{for } 0 < I_p \le 15 \quad \text{(low plastic soils)} \\ 7.0\times10^{-7} I_p^{1.976} & \text{for } 15 < I_p \le 70 \quad \text{(medium plastic soils)} \\ 2.7\times10^{-5} I_p^{1.115} & \text{for } I_p > 70 \quad \text{(high plastic soils)} \end{cases} \qquad \textbf{(3.16)}$$

With three different ranges of I_p, experimental data for damping ratio of non-sandy soils are plotted in Figures 3.10(a), (b) and (c).

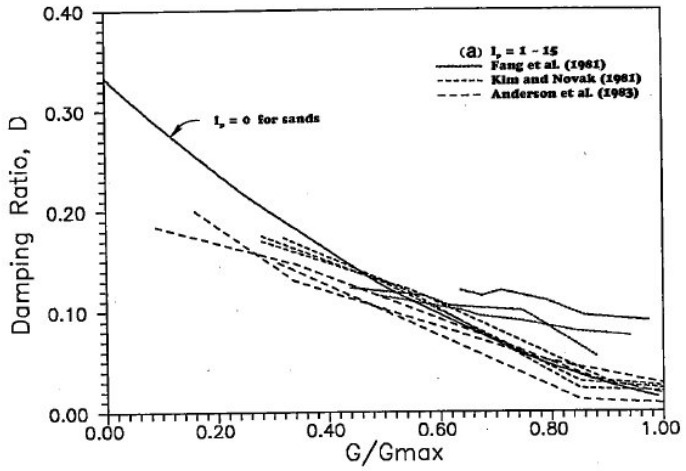

Figure 3.10(a): Damping Ratios vs. G/G_{max} for soils with I_p=1-15 (Ishibashi and Zhang, 1993)

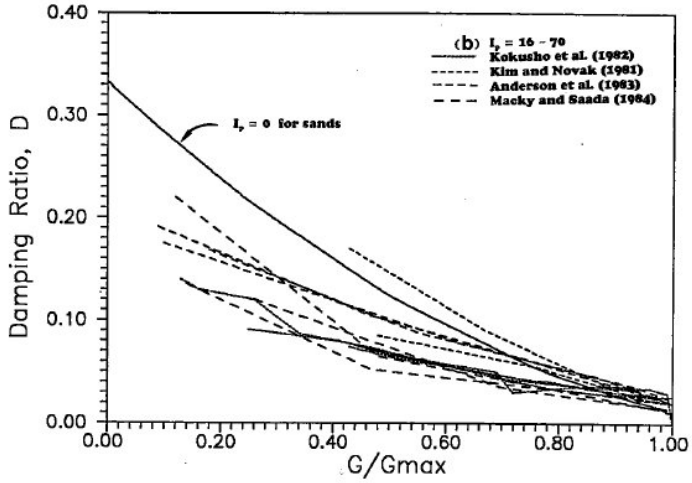

Figure 3.10(b): Damping Ratios vs. G/G_{max} for soils with I_p=16-70 (Ishibashi and Zhang, 1993)

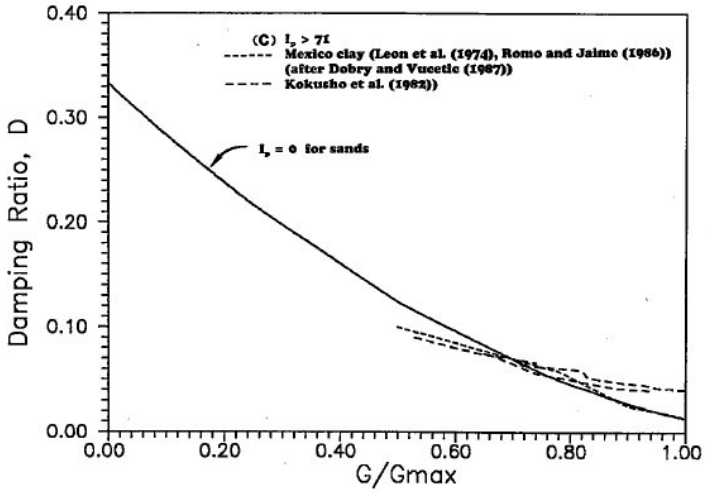

Figure 3.10(c): Damping Ratios vs. G/G_{max} for soils with I_p>71 (Ishibashi and Zhang, 1993)

For wide variety of soils, Equation (3.17) was proposed by Ishibashi and Zhang (1993) for the damping ratio.

$$D = D_{sand} \times A(I_P) = D_{sand} \times \frac{1+e^{-0.0145{I_p}^{1.3}}}{2}$$

$$D = \frac{0.333\,(1+e^{-0.0145{I_p}^{1.3}})}{2}\left\{\{0.586\left(\frac{G}{G_{max}}\right)^2 - 1.547\left(\frac{G}{G_{max}}\right) + 1\right\} \quad \textbf{(3.17)}$$

In Figure 3.11, analytical and experimental values of damping versus plasticity index at $\gamma=10^{-3}$ are compared.

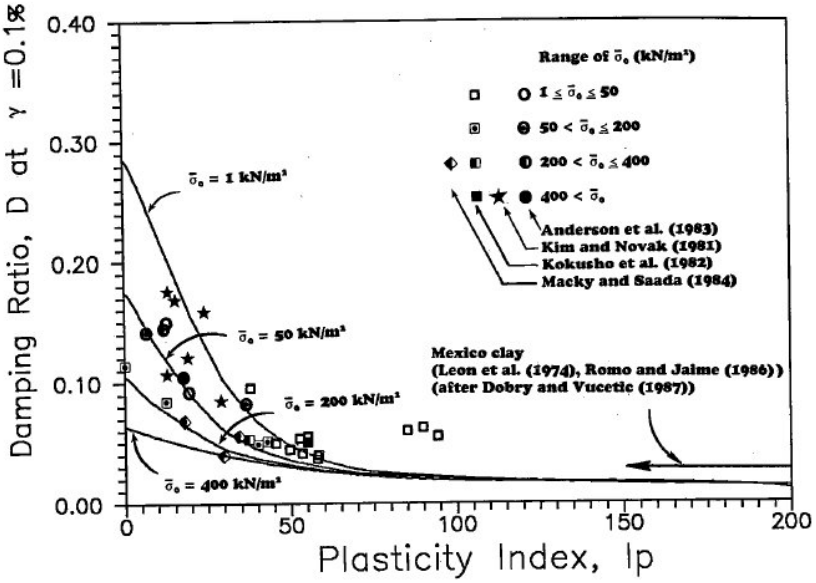

Figure 3.11: Analytical and experimantel damping ratios vs. I_p with various σ_o (Ishibashi and Zhang, 1993)

3.1.3 Equations for sinusoidal, random and impulse loading (Zhang and Aggour, 1996)

Zhang and Aggour (1996) performed sinusoidal, random and impulse loading tests on air-dry Ottowa 20-30 sand. Drnevich 'fixed-free' type resonant column device was used. All specimens were prepared with a relative density of approximetely 78%. Three confining pressures of 5, 10 and 40 psi (approx. 35, 69 and 276 kPa) were applied to each specimen. At each stage of testing, with the results of measurements of resonant frequency, amplitudes of axcitation and response at the resonant frequency, the root-mean-square (rms) of shear strain amplitude induced in the specimens and the damping ratio were determined. (Zhang and Aggour, 1996) Conventional method (Drnevich et al., 1978) for sinusoidal loading and random vibration theory for random and impulse loadings were used to determine the rms

values of shear strain amplitude. (Zhang, 1994) The damping ratio under each type of loadings was determined with The Damping Calibration Factor (DCF) method suggested by Hardin (1970).

$$D = \frac{1}{2}\frac{DCF}{\sqrt{{H_n}^2 - 2(DCF)^2}} \quad \textbf{(3.18)}$$

and,

$$DCF = 0.045 - 0.00015 \times \sigma_0 \quad \textbf{(3.19)}$$

where DCF is a calibration factor of the whole system, σ_0 is principal stress in specimens and H_n is the value of the transfer function at the resonant frequency f_n. (Zhang and Aggour, 2004)

At three confining pressures, the damping ratios under sinusoidal loading are shown in Figure 3.12.

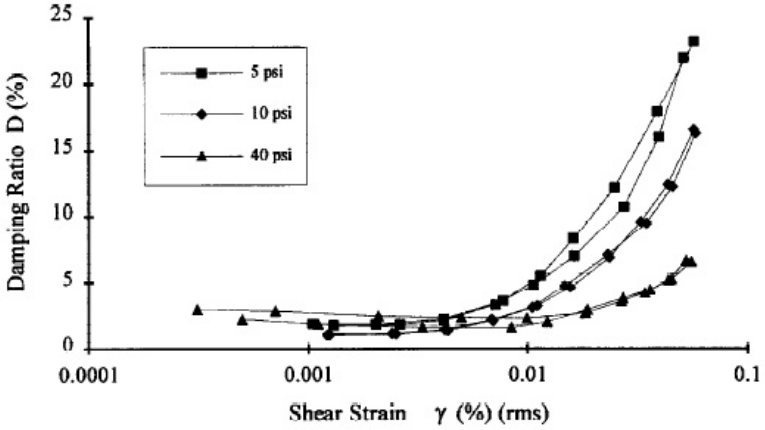

Figure 3.12: Damping ratio (%) vs. shear strain (%) at different confining pressures from sinusoidal tests (Zhang and Aggour, 1996)

At a low strain range (<0.003%), it can be seen in Figure 3.12 that the damping ratio was low and relatively constant. It was found that if a normalized scale of shear strain (γ/γ_r) was used, the damping ratio could be unified. For cohesionless specimens, reference shear strain (γ_r) was suggested by Hardin and Drnevich (1972) as;

$$\gamma_r = \frac{\sigma_0 sin\emptyset}{G_{max}} \quad \textbf{(3.20)}$$

where σ_0 is the mean principal stress, ϕ is the internal friction angle of the soil. The unified damping ratio under sinusoidal loading is shown in Figure 3.13. And also it

must be noted that the damping ratio under random and impulse loadings has a smilar trend with sinusoidal loading.

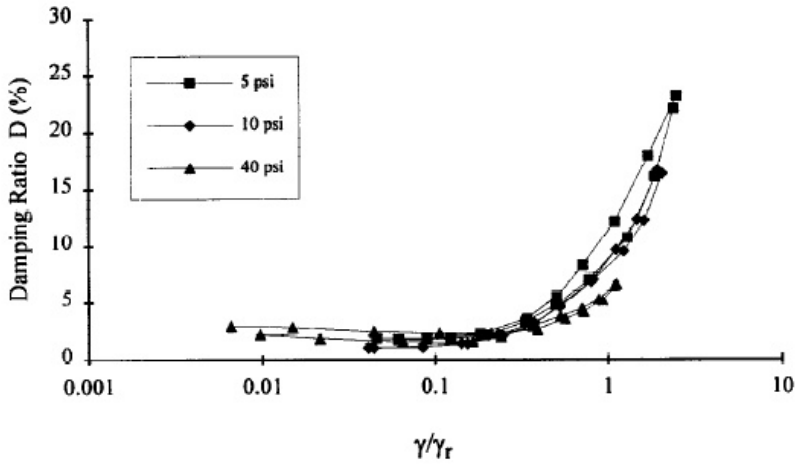

Figure 3.13: Damping ratio vs. normalized shear strain (γ/γ_r) from sinusoidal loading tests (Zhang and Aggour, 1996)

In Figure 3.14, unified damping ratios for every type of loading are shown. The damping ratio of all three loading types are relatively constant and same when the $\gamma/\gamma_r<0.1$.

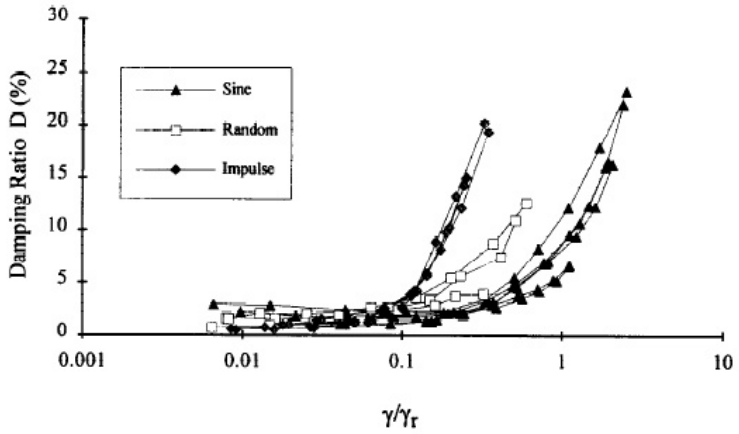

Figure 3.14: Damping Ratio vs. γ/γ_r from different loading tests (Zhang and Aggour, 1996)

As mentioned in the previous chapter, Hardin and Drnevich (1972), Tatsuoka et al. (1978) and Ishibashi (1981) proposed to express damping ratio as a function of G/G_{max}. Analyzing the test data of this research, Zhang and Aggour (1996) developed a following function.

$$D(\%) = A \times e^{-a\left(\frac{G}{G_{max}}\right)^b} \quad \textbf{(3.21)}$$

where A, a and b are regression constants. By choosing constant b, a linear relationship between log(D) and $(G/G_{max})^b$ could be obtained and from the interseption of the straight line at $G/G_{max}=0$ and 1, the constants A and a could be determined. In Figure 3.15 this relationship is shown for sinusoidal loading.

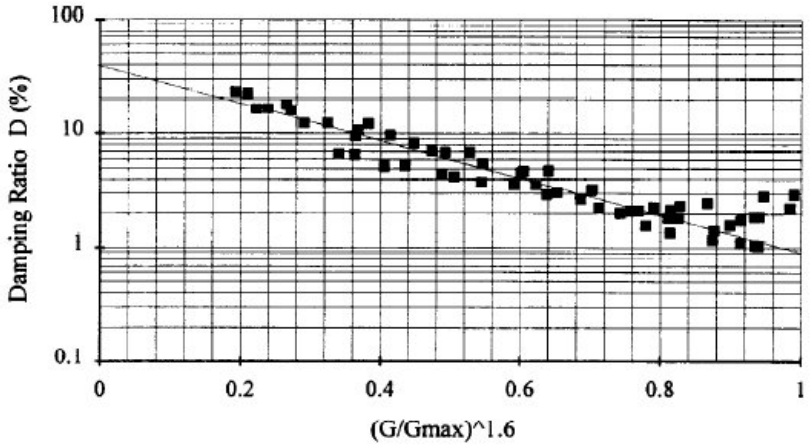

Figure 3.15: Linear relationship between log(D) and $(G/G_{max})^{1.6}$ from sinusoidal loading tests (Zhang and Aggour, 1996)

For all three types of loading, correlation equations are summarized in Table 3.2. And it was found that A=40, a=3.8 for all loading types but constant b was changing.

Table 3.2: Damping Ratio Equations (Zhang and Aggour, 1996)

Sinusoidal	Random	Impulse
$D(\%) = 40 \bullet e^{-3.8(\frac{G}{G_{max}})^{1.6}}$	$D(\%) = 40 \bullet e^{-3.8(\frac{G}{G_{max}})^{2.4}}$	$D(\%) = 40 \bullet e^{-3.8(\frac{G}{G_{max}})^{3.8}}$

3.1.4 Rollins et al. (1998) suggestion

Rollins et al. (1998) collected the data of damping ratio from available investigations to develop best-fit curve between the damping ratio and shear strain. Tested soils are mostly poorly-graded gravels and gravelly sands but there are also a few well-graded gravels. Relative densities are ranged from 27 to 97%, maximum grain size are varied from 10 to 150 mm, uniformity coefficients are ranged from 1.33 to 75 and the gravel percentage are varied from 20 to 90%. Properties of tested soils are summarized in Table 3.3. Cyclic triaxial test (CTX) and cyclic torsional simple shear tests (CTSS) are performed. Confining pressures are renged from 29 to 490 kPa for specimen consolidation. Testing equipment and testing conditions are summarized in Table 2.4.

Table 3.3: Summary of mechanical properties of gravelly soils on which cyclic shear tests were performed by 15 investigators (Rollins et al., 1998)

Reference (1)	USCS symbol (2)	Percent gravel >4.75 mm (3)	Percent fines <0.075 mm (4)	Maximum grain size (mm) (5)	Mean grain size (mm) (6)	Coefficient of uniformity (Cu) (7)	Specific gravity Gs (8)	Dry density (g/cm³) (9)	Relative density Dr (10)	Maximum void ratio e max (11)	Minimum void ratio e min (12)
This study	SP	20	0	10	0.5	36	2.65	1.57	40	0.8	0.51
	SP	40	0	10	0.5	23	2.67	1.75	40	0.62	0.4
	GP	60	0	10	4.4	17	2.68	1.87	40	0.51	0.32
Goto et al. 1994	GP	66	0.3	105	10.9	39	2.68*	2	NA	NA	NA
	SP	22	1.9	94	1.5	8.2	2.68*	1.93	NA	NA	NA
Goto et al. (1992)	GP	60	0.1	91	10	37.5	NA	2.11	69	NA	NA
	GP	55	0.5	77	6	25	NA	1.93	27	NA	NA
Hatanaka et al. (1988)	GP	55	8.5	90	5.7	60	2.69	2.027	57	0.45	0.23
	GP	65	8.5	90	10.3	13.9	2.69	2.138	69	0.4	0.2
Hatanaka and Uchida (1994)	GP*	NA	0.3	125	NA	NA	NA	2.19	NA	NA	NA
	GP*	NA	0.4	106	NA	NA	NA	2.19	NA	NA	NA
	GP*	NA	0.5	99	NA	NA	NA	1.82	NA	NA	NA
	GP*	NA	1.1	110	NA	NA	NA	2.02	NA	NA	NA
Hynes (1988)	GP	84	9	152	24	75.8	2.83	1.94–2.06	25–46	0.56	0.15
Iida et al. (1984)	GW	77	0	38.1	12.7	7.2	2.58	1.82	85	0.72	0.383
Kokusho et al. (1994)	GP	80–90	2	100	23	37	2.68*	2.1–2.2	80*	NA	NA
	SP	22	1	40	2	5	2.68*	1.9–2.1	NA	NA	NA
Konno et al. (1994)	GP	55	0–3	70–150	3–17	30	2.65	1.82–2.02	92–109	0.54–0.62	0.30–0.44
Seed et al. (1986)	GP	70	5	50.8	10	27.2	2.9	2.25–2.44	60–95	0.46	0.176
	GW	50	2	50.8	8	7.1	2.62	1.75–1.89	64–95	0.737	0.366
	GW	NA	NA	50.8	NA	NA	2.74	1.72–1.88	67–95	0.923	0.435
	GW	60	8	50.8	7.6	62.5	2.65	2.12–2.24	70–95	0.455	0.166
Shamoto et al. (1986)	SW	15	0	30	1.7	8.5	2.68*	1.95–1.97	92–100	0.64	0.36
Shibuya et al. (1990)	SP	0	0	3.3	1.85	1.33	2.68*	1.7–1.77	44–100	0.633	0.511
	GP	90	0	10	6.65	1.21	2.68*	1.73–1.74	68–89	0.676	0.49
Souto et al. (1994)	SP	44	3.7	18	2.81	25.6	2.67	2.08	NA	NA	NA
	SW	44	6	18	3.36	27.1	2.78	2.1	NA	NA	NA
Yasuda and Matsumoto (1994)	GW	83	0	63.5	16	7	2.65	1.92–2.07	70, 90	0.72	0.23
	SP	48	0	63.5	8	14.7	2.62	1.93–2.01	70, 90	0.55	0.27
	GW	52	0	63.5	10	35.7	2.68*	NA	85	NA	NA
	GW	NA	NA	63.5	NA	NA	NA	NA	NA	NA	NA
Yasuda and Matsumoto (1993)	GW	75	0	38.1	13.4	7	2.68*	1.76–1.89	50–70	NA	NA
	GP	65	0	25.4	8.4	7	2.68*	1.76–1.89	50–70	NA	NA

*Estimated value.

Table 3.4: Summary of testing equipment and testing conditions employed by 15 investigators conducting cyclic shear tests on gravelly soils (Rollins et al., 1998)

Reference (1)	Test type (2)	Sample dia./ht. (mm) (3)	Sample type (4)	G/Gmax data? (5)	D data? (6)	Number of cycles @ meas./total (7)	Loading frequency (hz) (8)	Confining pressure (kPa) (9)	Drainage conditions (10)
This study	CTX	71/150	R	Y	N	5/10	0.05	100	S/U
Goto et al. (1994)	CTX	300/600	U	Y	N	5/10	0.01	118, 127	S/U
Goto et al. (1992)	CTX	300/600	U/R	Y	Y	5/10	0.01	128, 186	S/U
Hatanaka et al. (1988)	CTX	300/600	U/R	Y	Y	3/3	0.01	294, 490	S/U
Hatanaka and Uchida (1994)	CTX	300/600	U/R	Y	Y	5/11	0.01	98–392	S/U
Hynes (1988)	CTX	381/97	R	Y	N	10/10	0.1	69–414	S/U
Iida et al. (1984)	CTX	300/600	R	Y	N	10/12	0.2	98–392	D/D
	CTX	400/800	R	Y	N	10/12	0.2	98–392	D/D
	CTSS	40 ID. 80 OD. 80 ht.	R	Y	N	10/12	0.2	98–392	D/D
Kokusho et al. (1994)	CTX	300/600	U/R	Y	Y	NA	NA	100–400	S/U
Konno et al. (1994)	CTX	300/600	U/R	Y	Y	NA	0.01	186, 392	S/U
Seed et al. (1986)	CTX	300/600	R	Y	Y	5/6	0.017	196	S/U
Shamoto et al. (1986)	CTX	300/600	U	Y	N	NA	NA	118	S/U
Shibuya et al. (1990)	CTX	75/150	R	Y	Y	10/10	0.1	29, 49, 78	D/D
	CTX	300/600	R	Y	Y	10/10	0.1	49	D/D
Souto et al. (1994)	CTX	51/100	R	Y	N	NA	NA	100	S/U
Yasuda and Matsumoto (1994)	CTX & CTSS	300/600	R	Y	N	10/12	0.2	100–400	D/D
		40 ID. 80 OD. 80 ht.	R	Y	N	10/12	0.2	100–400	D/D
Yasuda and Matsumoto (1993)	CTX & CTSS	300/600	R	Y	Y	10/12	0.2	100–400	D/D
		40 ID. 80 OD. 80 ht.	R	Y	Y	10/12	0.2	100–400	D/D

Note: R = reconstituted; U = undisturbed; U/R = undisturbed and reconstituted; S/U = saturated, undrained; D/D = dry, drained.

In Figure 3.16, G/G_{max} vs. γ data points and for comparison the range of sands data from Seed and Idriss (1970) are shown.

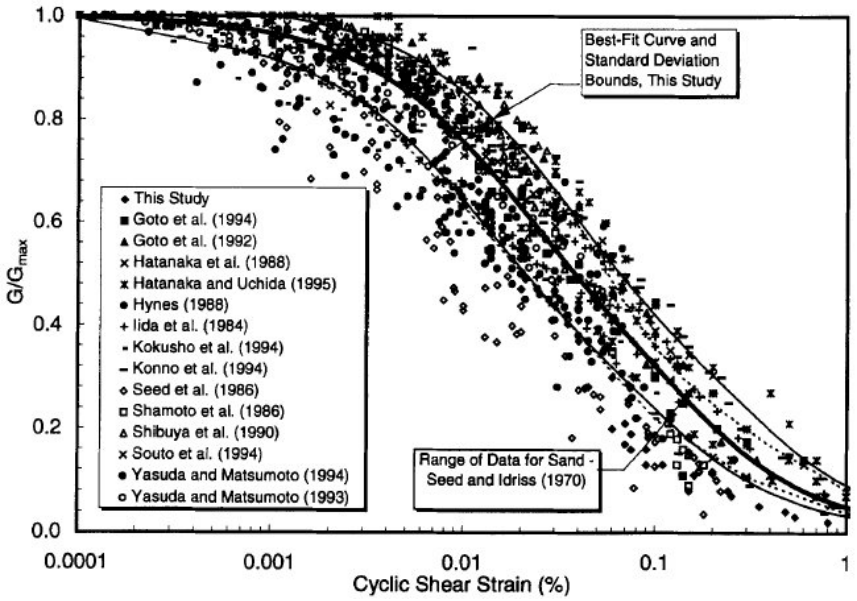

Figure 3.16: Data points defining G/G_{max} vs. γ relationships for gravelly soils based on testing by all 15 investigators along with best-fit curve and $\pm$ one standard deviation bounds for entire data set (Rollins et al., 1998)

There is also a study about drained and undrained tests for meam G/G_{max} vs. γ which are presented in Figure 3.17 with determined standart deviation bounds in this study for gravels.

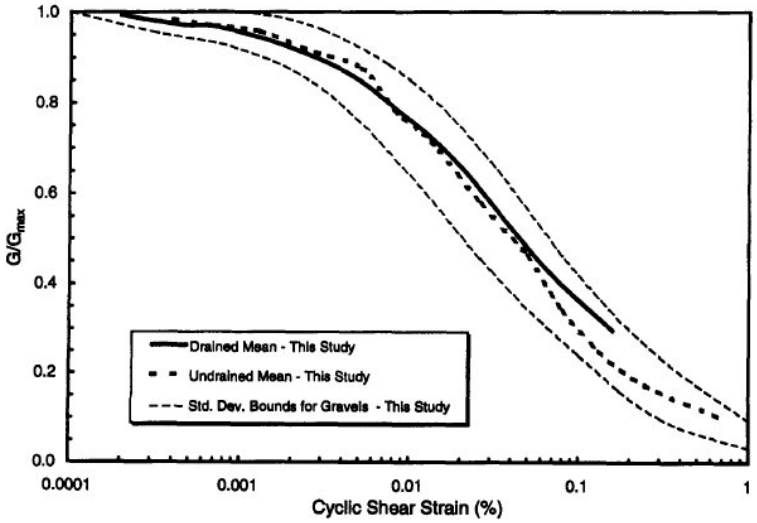

Figure 3.17: Comparison of mean G/G_{max} vs. γ curves for gravels based on undrained tests on saturated specimens and drained tests on dry specimens (Rollins et al., 1998)

It can be seen that, two curves are less than 5% apart for γ less than 0.05%; however at larger shear strain amplitudes, the drained curve diverges above the undrained curve. But there is not sufficient data to define the drained curve shape above 0.2% shear strain. (Rollins et al., 1998)

Damping ratio data points are shown in Figure 3.18 for gravelly soils. And also for comparison the range of sands and gravels data from Seed et al. (1986) is shown. It should be noted that determined data range in this study falls toward the bottom of the curve defined by Seed et al. (1986).

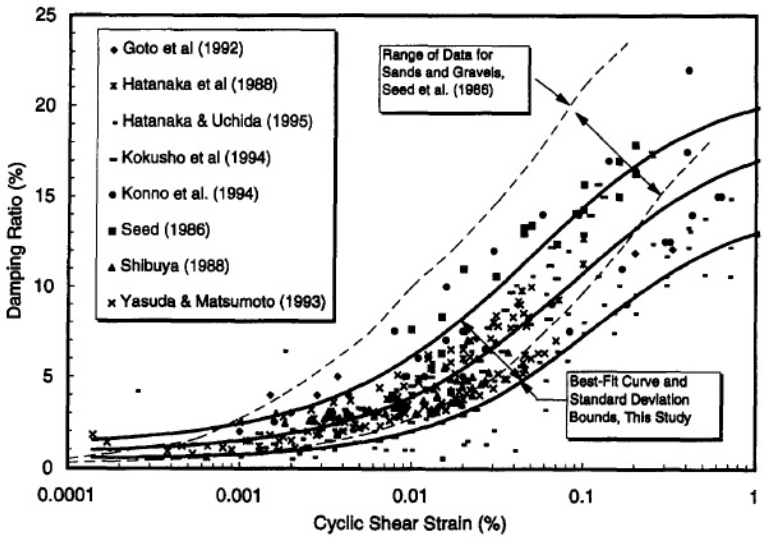

Figure 3.18: Data points defining D vs. γ relationships for gravelly soils based on testing by eight investigators along with best-fit curve and standard deviation bounds for data set (Rollins et al., 1998)

For the best-fit curve Rollins et al. (1998) suggested following equation:

$$D = 0.8 + 18(1 + 0.15\gamma^{-0.9})^{-0.75} \qquad \textbf{(3.22)}$$

But this equation should not be used at shear strain above 1% because it could be erroneus. (Rollins et al., 1998)

3.1.5 Kelvin-Voight model (Michaels, 1998)

For the prediction of the seismic behaviour of foundations and soil embankment structures, determination of in situ dynamic soil properties is important. Dynamic soils properties calculations are done under a constitutive model with the corresponding differential equations. For computational analysis, both elastic (stiffness) and inelastic (damping) values are required. But there is no elastic constitutive model for a soil damping value. Thus, if viscous damping is presented, it will be erroneous because of the calculation of shear modulus from wave velocity. Since some portion of the SH-wave velocity will be incorrectly attributed to stiffness in an elastic model. (Michaels, 1998)

Kelvin-Voight model is used for engineering practice such as consolidation and soil dynamics. Laboratory measurements by resonant column techniques (Hardin, 1965) and also computation programs SHAKE (Schnabel et al., 1972) and DESRA2 (Lee and Finn, 1982) are invoke the Kelvin-Voight soil model. The spring-mass dashpot analog model is shown in Figure 3.19. The spring provides the stiffness (force proportional to displacement) and the dashpot represents the viscous damping (force proportional to particle velocity). (Michaels, 1998)

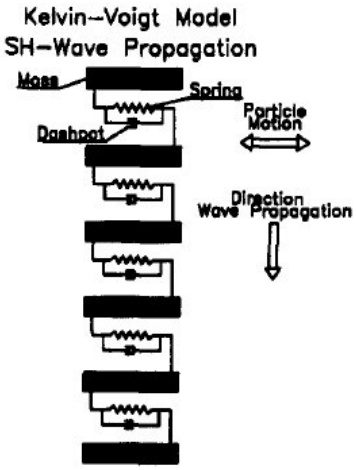

Figure 3.19: Discrete realization of Kelvin-Voigt soil model, consisting of a chain of spring, dashpot and mass elements (Michaels, 1998)

If the spring-mass-dashpot elements are considered as the multiple-degree-of-freedom chain, the moment of all elements are assumed as identical and by summing the stiffness and damping forces, the finite difference equation of motion is found. Thus, for the *j*th element in the chain,

$$\frac{\partial v_j}{\partial t} = \frac{\partial u_j}{\partial t} \cong \left(\frac{\Delta x^2 k}{m}\right)\left(\frac{\Delta^2 u_j}{\Delta x^2}\right) + \left(\frac{\Delta x^2 d}{m}\right)\left(\frac{\Delta^2 v_j}{\Delta x^2}\right) \qquad \textbf{(3.23)}$$

where u_j and v_j are the particle displacement and particle velocity (measured in meters) for the *j*th mass, respectively. *k* is the spring constant, *d* is the dashpot and Δx is the element spacing. (Michaels, 1998)

In the limit of a continuum, Equation (3.23) becomes,

$$\frac{\partial^2 u}{\partial t^2} = C_1 \frac{\partial^2 u}{\partial x^2} + C_1 \frac{\partial^3 u}{\partial t \partial x^2} \qquad \textbf{(3.24)}$$

where u is particle displacement, x is the spatial coordinate and t is time. Contant

$C_1$is the stiffness coefficient and C_2 is the viscous damping coefficient. The ratio of C_2 (m^2/s) to C_1 (m^2/s^2) is the relaxation time in seconds. (Michaels, 1998)

The coefficients are given in terms of shear modulus (G), mass density (ρ) and absolute viscosity (η) of the soil model. The mapping between Equations (3.23) and (3.24) coefficients are:

$$\left(\frac{\Delta x^2 k}{m}\right) \rightarrow \left(\frac{G}{\rho}\right) = C_1 \quad \textbf{(3.25)}$$

$$\left(\frac{\Delta x^2 d}{m}\right) \rightarrow \left(\frac{\eta}{\rho}\right) = C_2 \quad \textbf{(3.26)}$$

To express viscous damping, a number of forms have been chosen by using the Kelvin-Voigt model. These forms include complex modulus, loss tangent, loss angle and damping ratio. Shear modulus is expressed as a complex quantity by some authors (Kramer, 1996; Schnabel et al., 1972; Stoll, 1985);

$$G^* = G_R + iG_\iota \quad \textbf{(3.27)}$$

where i^2=-1 . G_R is the real part and G_I is the complex part. And this is related to the wave equations coefficient by;

$$C_1 = \frac{G_R}{\rho} \; ; \;\; C_2 = \frac{G_\iota}{\omega\rho} \quad \textbf{(3.28)}$$

where ω is frequency. in the Kelvin-Voigt model, the complex shear modulus, G*, varies as a funtion of frequency. The variation is linear. (Michaels, 1998)

Loss tangent can be computed from the complex shear modulus and it is given by;

$$tan(\delta) = \frac{G_I}{G_R} \quad \textbf{(3.29)}$$

where δ is the loss angle. It follows,

$$tan(\delta) = \omega\left(\frac{C_2}{C_1}\right) = \omega T_r \quad \textbf{(3.30)}$$

where T_r is the relaxation time. (Michaels, 1998)

The concept of damping ratio is often employed by resonant column workers (Drnevich, 1978). Finally, D_T (the ratio between any value of damping to critical damping) is given by;

$$D_T = \frac{C_2 \omega_0 \rho}{2G_R} \quad \textbf{(3.31)}$$

where ω_o is the resonant frequency. The resonant frequency is given by the root of the ratio of the equivalent spring constant to polar moment of inertia in a resonant column experiment (Drnevich et al. 1978). (Michaels, 1998)

Table 3.5 is prepared for summarization of all suggested and developed equations for damping determination.

Table 3.5: Summarization of suggested and developed equations for damping determination

REFERENCE	SOIL TYPE	EQUATIONS	NOTES
Seed and Idriss, 1970	All soil types	$D = \frac{W_D}{4\pi W_S} = \frac{1}{2\pi} \times \frac{A_{loop}}{G\gamma^2}$	where, $G = \tau/\gamma$
Jennings, 1964 Ray and Woods, 1988	Cohesionless Soils	$D = \frac{2 \times \alpha \times C_1 \times \left(\frac{R-1}{R+1}\frac{\tau}{C_1 \times \tau_{max}}\right)^R}{\pi \times \frac{\gamma}{\gamma_r}}$	C_1, R, and α, are given to generate a curve of damping versus γ/γ_r, values for τ/τ_{max} are first selected, γ/γ_r is then computed, and the value for damping is obtained.
Hardin and Drnevich, 1972 Tatsuoka et al., 1978 Ishibashi and Zhang, 1993	Sandy Soils	$D = f\left(\frac{G}{G_{max}}\right)$ $D_{sand} = 0.333\left\{0.586\left(\frac{G}{G_{max}}\right)^2 - 1.547\left(\frac{G}{G_{max}}\right) + 1\right\}$	where at $\gamma \leq 10^{-6}$, $\frac{G}{G_{max}} = K(\gamma){\sigma_0}^{m(\gamma)-m_0}$ $m_o = m(\gamma \leq 10^{-6})$ $k(\gamma) = 0.5\left[1 + tanh\left\{\ln\left(\frac{0.000102}{\gamma}\right)^{0.492}\right\}\right]$ $m(\gamma) - m_o = 0.272\left[1 - tanh\left\{\ln\left(\frac{0.000556}{\gamma}\right)^{0.4}\right\}\right]$
Zhang and Aggour, 1996	Sands	$D(\%) = A \times e^{-a\left(\frac{G}{G_{max}}\right)^b}$	where, A=40, a=3.8 for all type of loadings b=1.6 for sinusoidal loading b=2.4 for random loading b=3.8 for impulse loading
Rollins et al., 1998	Gravelly Soils	$D = 0.8 + 18(1 + 0.15\gamma^{-0.9})^{-0.75}$	

Table 3.5: Summarization of suggested and developed equations for damping determination (Continued)

REFERENCE	SOIL TYPE	EQUATIONS	NOTES
Kokusho et al., 1982 Dobry and Vucetic, 1987 Ishibashi and Zhang, 1993	Plastic Soils	$D = D_{sand} \times A(I_p)$ $D = D_{sand} \times \frac{1 + e^{-0.0145{I_p}^{1.3}}}{2}$ $D = \frac{0.333\ (1 + e^{-0.0145{I_p}^{1.3}})}{2} \left\{ \{0.586 \left(\frac{G}{G_{max}}\right)^2 - 1.547 \left(\frac{G}{G_{max}}\right) + 1 \right\}$	where, $\frac{G}{G_{max}} = K(\gamma, I_p){\sigma_0}^{m(\gamma, I_p) - m_0}$ $m(\gamma, I_p) - m_o = 0.272 \left[1 - tanh\left\{\ln\left(\frac{0.000556}{\gamma}\right)^{0.4}\right\}\right] e^{-0.0145{I_p}^{1.3}}$ $k(\gamma, I_p) = 0.5 \left[1 + tanh\left\{\ln\left(\frac{0.000102 + n(I_p)}{\gamma}\right)^{0.492}\right\}\right]$ $n(I_p) = 0.0$ for $I_p = 0$ (sandy soils) $= 3.37\ x\ 10^{-6}{I_p}^{1.404}$ for $0 < I_p \leq 15$ (low plastic soils) $= 7.0\ x\ 10^{-7}{I_p}^{1.976}$ for $15 < I_p \leq 70$ (medium plastic soils) $= 2.7\ x\ 10^{-5}{I_p}^{1.115}$ for $I_p > 70$ (high plastic soils)
Hardin, 1970	Sands	$D = \frac{1}{2} \frac{DCF}{\sqrt{{H_n}^2 - 2(DCF)^2}}$	where, $DCF = 0.045 - 0.00015 \times \sigma_0$
Drnevich, 1978 Michaels, 1998		$D_T = \frac{C_2 \omega_0 \rho}{2G_R}$	$\frac{\partial^2 u}{\partial t^2} = C_1 \frac{\partial^2 u}{\partial x^2} + C_2 \frac{\partial^3 u}{\partial t \partial x^2}$ $C_1 = \left(\frac{G}{\rho}\right)\ and\ C_2 = \left(\frac{\eta}{\rho}\right)$ $G^* = G_R + iG_I$ $C_1 = \left(\frac{G_R}{\rho}\right)\ and\ C_2 = \left(\frac{G_I}{\omega\rho}\right)$ $\tan(\delta) = \frac{G_I}{G_R} \rightarrow \tan(\delta) = \omega\left(\frac{C_1}{C_2}\right)$

3.2 General Curves of Damping

3.2.1 Gravelly soils and sands

Seed and Idriss (1970) considered the potential scatter of test data for damping ratios to determine an average damping ratio versus shear strain relationship for sands. To be more accurate, same investigators' works was considered even if they used the same test procedure. In Figure 3.20, approximate upper and lower bound relationships for sands can be seen by the dashed lines. These curves also provide a basis evaluation between damping ratio and strain for sands.

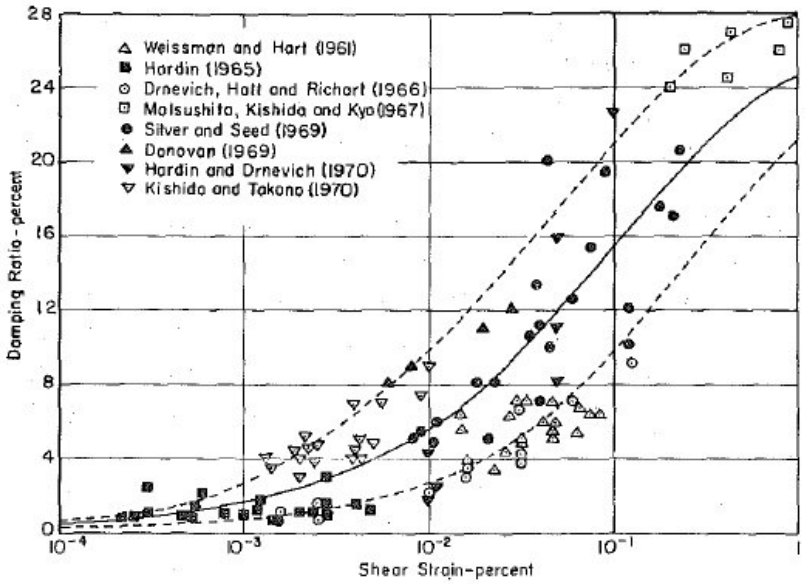

Figure 3.20: Damping ratios for sands (Seed et al., 1986)

Seed et al. (1986) review available information on the damping ratio for sands and present new data for gravels to provide a useful guide for analysis purposes. The tested soils are the Oroville gravel which was prepared from the shell material used for the Oroville Dam, Pyramid gravel which was rockfill material for the shell section of the Pyramid Dam in Southern California, the Venado sandstone which was obtained from a medium to thick-bedded sandstone in the Upper Cretaceous Venado formation and the Livermore natural gravel deposit which was obtained from the flood plain of Livermore Valley. In Figure 3.21, grain size distribution curves of tested soils are shown and in Table 3.6, properties of tested soils are summarized.

Table 3.6: Specific gravities and maximum and minumum void ratios of soils tested(Seed et. al., 1986)

Name (1)	Size (2)	Specific gravity (3)	e_{max} (4)	e_{min} (5)
Oroville Dam material	1-1/2 in. to 3/4 in.	2.94	0.81	0.52
Oroville Dam material	2 in. to -No. 200	2.90	0.46	0.176
Pyramid Dam material	2 in. to -No. 200	2.62	0.737	0.366
Venado sandstone	2 in. to -No. 200	2.74	0.923	0.435
Livermore natural deposit	2 in. to -No. 200	2.65	0.455	0.166

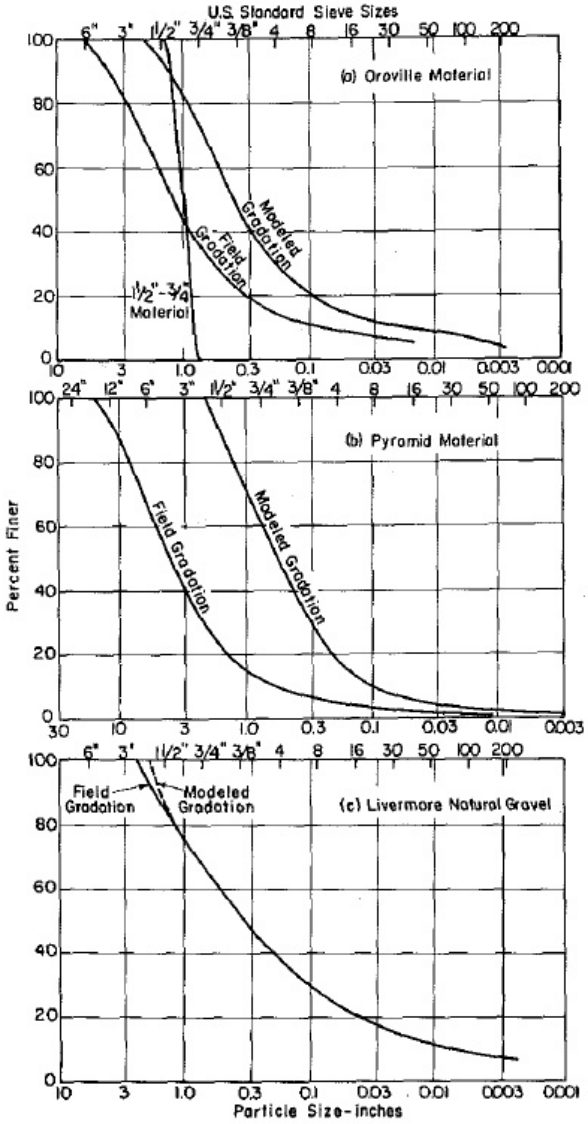

Figure 3.21: Grain size distribution curves for field and modeled gradations (Seed et. al., 1986)

Cyclic undrained triaxial test method was used and the hysteretic stress-strain relationships were used to determine the damping characteristics of soils. For

evaluate the damping ratios, fifth cycle of the hysteresis loops were used. Measured values at a relative density of 80% for all materials are shown in Figure 3.22.

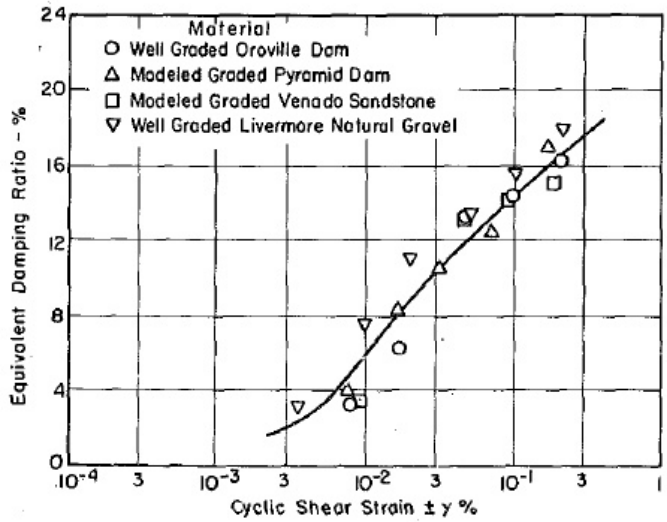

Figure 3.22: Equivalent Damping Ratios for Gravelly Soils at D_r = 80%(Seed et al., 1986)

All measured values of damping ratio for four tested gravels are shown in Figure 3.23. For comparison, the range of values for sands shown in Figure 3.17 is also shown.

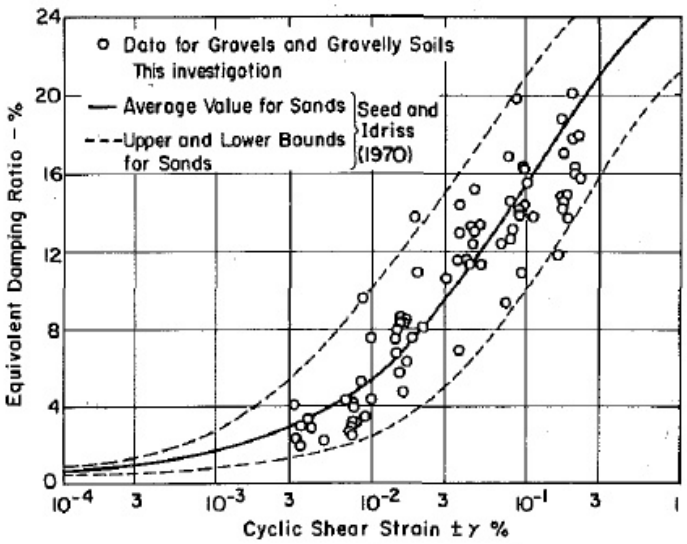

Figure 3.23: Comparison of Damping Ratios for Gravelly Soils and Sands (Seed et. al., 1986)

As a conclusion of Figures 3.20 and 3.23 damping ratios for gravels and sands are very similar. And these curves can be used as a guide for cohesionless soils.

3.2.2 Plastic soils

To refine the trends between PI (Plasticiy index) and damping ratio curves, Vucetic and Dobry(1991) analyzed the several additional data with the data presented in 1987 paper (Dobry and Vucetic, 1987) to present a ready-to-use charts. Considered 16 investigations are summarized in Figure 3.24 and these studies include normally and overconsolidated soils (OCR=1-15) as well as sands. In Figure 3.25, main results of this study are represented. And it should be noted that PI=0 curves in Figure 3.25, satisfy the curves by Seed and Idriss(1970), Seed et al. (1986) which are shown in Figures 3.20 and 3.23.

Symbols Used in Figs. 4 & 5	Type of Cyclic Test	Overconsolidation Ratio OCR	Number of Cycles N	Reference
(1)	(2)	(3)	(4)	(5)
▽	-	-	-	Nishigaki (1970)
↕	Different	-	-	Seed & Idriss (1970)
▨	-	-	-	Leon et al. (1974) Romo and Jaime (1986)
●	Resonant Column	-	1000	Anderson and Richart (1976)
×	-	-	-	Zen et al. (1978)
◇	Resonant Column, Triaxial	1,2,4,8	– 10	Koutsoftas & Fischer (1980)
△	Resonant Column	1,2,3,7	1000	Kim & Novak (1981)
▯	Resonant Column	-	-	Andreasson (1981)
■	-	-	-	Lodde & Stokoe (1982)
○	Triaxial	1,5,10,15	10	Kokusho et al. (1982)
▲	Simple Shear	1,4	1	Andersen (1983)
□	Resonant Column, Triaxial, Simple Shear	-	-	Anderson et al. (1983)
↕	Triaxial	-	5	Seed et al. (1986)
◆	Simple Shear	1,2,4	1-64	Vucetic & Dobry (1986)
▭	Resonant Column, Triaxial	-	-	Romo et al. (1988)
⬡	Simple Shear	1,2,4	1-20	Vucetic & Tan (1989)

Figure 3.24: Summary of studies considered (Vucetic and Dobry, 1991)

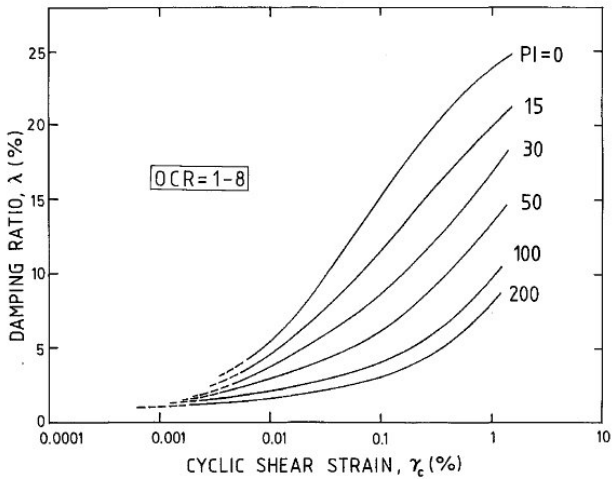

Figure 3.25: Relations λ vs. γ_c, Curves and Soil Plasticity for Normally and Overconsolidated Soils (Vucetic & Dobry, 1991)

Figure 3.25 shows the trends between PI and damping ratio and it can be used as a ready-to-use chart for plastic soils.

3.3 Factors Affecting Soil Damping

3.3.1 Relative density

As explained in chapter 3.2.1, Seed et al.(1986) made tests on gravelly soils. Soil properties can be seen on Table 3.6 and grain-size distribution curves can be seen in Figure 3.21. In Figure 3.22, measured damping values for all materials at a relative density of 80% are shown. Average damping ratios at relative densities of 65%, 80% and 100% for the four gravelly soils was plotted to comprehend the effect of relative density on the damping ratio in Figure 3.26.

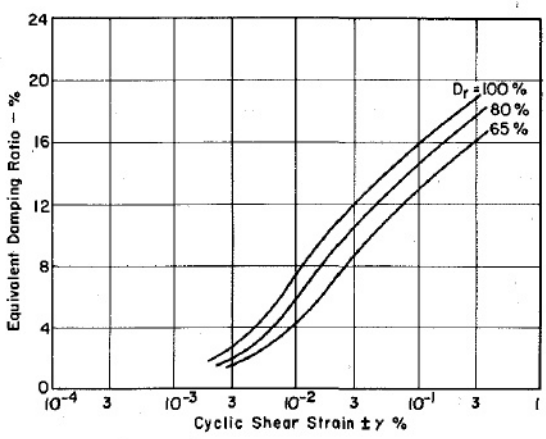

Figure 3.26: Effect of Relative Density on the Damping Ratio versus Strain Relationship for Gravelly Soils (Seed et. al., 1986)

As a conclusion, relative density affect the damping ratios for sands and gravels slightly and positively. (Seed et al.,1986)

3.3.2 Number of cycles (N)

In chapter 3.1.1, performed tests from Ray and Woods(1988) on sands and silts was explained. In Fig 3.1 and Table 3.1, tested soil properties are shown. Based on Figures 3.2, 3.3 and 3.4, damping capacity reduces with N for both sands and silts. Even after 200 cycles, damping ratios can drop to 50% their initial value. (Ray and Woods, 1988)

3.3.3 Plasticity index (PI)

As mentioned in chapter 3.2.2, to refine the trends between PI (Plasticiy index) and damping ratio curves, Vucetic and Dobry(1991) analyzed the several additional data with the data presented in 1987 paper (Dobry and Vucetic, 1987) which were summarized in Figure 3.24. Correlations between damping ratio and plasticity index for these investigations are plotted in Figure 3.27.

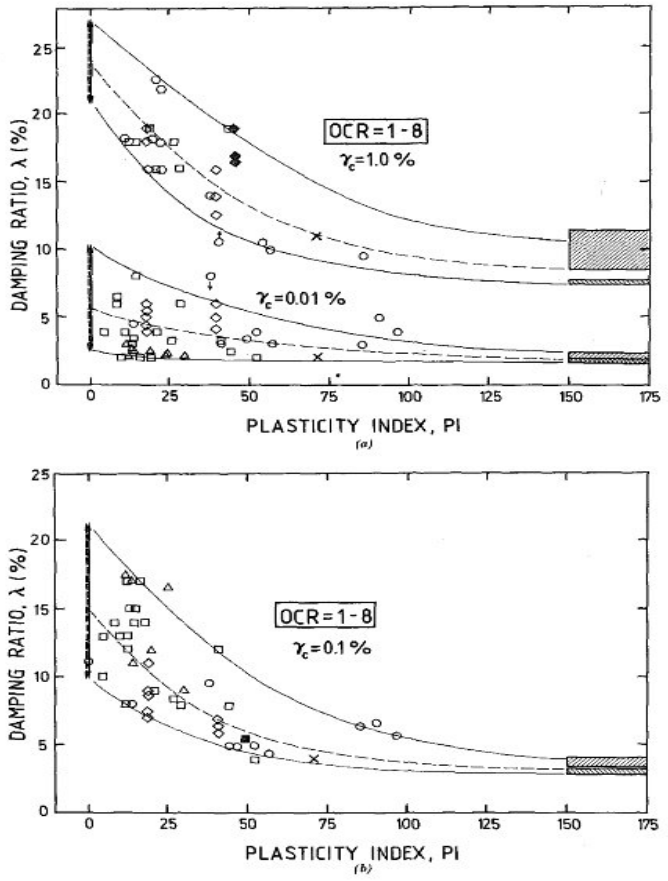

Figure 3.27: Correlations between Damping λ and Plasticity Index PI for Normally and Overconsolidated Soils (Vucetic & Dobry, 1991)

Developed curve from Figure 3.27 can be seen as Figure 3.25. These figures show that damping ratio decreases when the plasticity index increases.

3.3.4 Overconsolidation ratio (OCR)

Vucetic et al. (1998) perform tests on five different soils at small strains with a new testing apparatus which is called the double specimen direct simple shear (DSDSS) device. Details about the device can be found in Doroudian and Vucetic (1993,1995). Soils were tested with this apparatus in the approximate range $\gamma_c \approx 0.001$ - 0.004%. Five soils include two sands with different silt contents and three clays with different plasticity. Grain size distribution curves of two sands are shown in Figure 3.28. And also soil properties and testing program are summarized in Table 3.7 and 3.8 respectively.

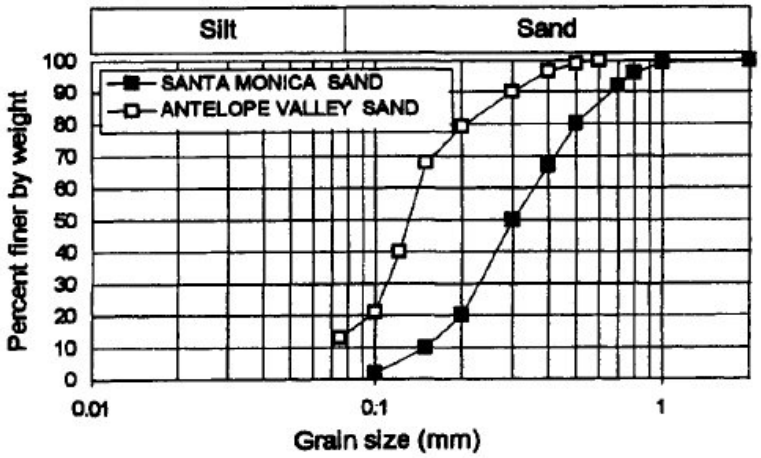

Figure 3.28: Grain Size Distribution Curves of Two Sands Tested (Vucetic et al., 1998)

Table 3.7: Relevant Physical Properties and Classification Characteristics of Soils Tested (Vucetic et al., 1998)

Soil (1)	Initial water content w_0 (%) (2)	Initial void ratio e_0 (3)	Liquid limit W_L (4)	Plastic limit W_P (5)	Plasticity index PI (6)	Initial liquidity index LI (7)	Silt content (%) (8)
Santa Monica sand (SM sand)	~0[a]	0.549	—	—	0[b]	—	0
Antelope Valley sand (AV sand)	~0[a]	0.886	—	—	0[b]	—	13
Clay A	48.0	1.382	52	30	22	0.82	Not tested
Clay B	58.4	1.570	66	28	38	0.80	Not tested
Clay C	63.0	1.729	125	50	75	0.17	Not tested

[a]Dry at room temperature.
[b]Nonplastic.

Table 3.8: Summary Of Testing Program (Vucetic et al., 1998)

Soil (1)	Vertical load sequence (2)	Effective vertical consolidation stress σ'_{vc} (kPa) (3)	Void ratio e (4)	Liquidity index LI (5)	Over-consolidation ratio OCR (6)
Santa Monica sand (SM sand)	Loading	30	0.548	—	1
		80	0.546	—	1
		150	0.544	—	1
	Unloading	80	0.544	—	1.9
		30	0.545	—	5
	Reloading	200	0.540	—	1
		300	—[a]	—	1
Antelope Valley sand (AV sand)	Loading	30	0.885	—	1
		80	0.875	—	1
		150	0.861	—	1
	Unloading	80	—[a]	—	1.9
		30	—[a]	—	5
Clay A	Loading	30	1.361	0.81	3.3
		80	1.326	0.78	1.25
		150	1.249	0.70	1
		284	1.166	0.59	1
	Unloading	150	1.166	0.59	1.89
		80	1.169	0.60	3.55
		30	1.173	0.61	9.46
Clay B	Loading	30	1.561	0.78	4.33
		80	1.545	0.77	1.63
		150	1.509	0.73	1
		284	1.404	0.63	1
	Unloading	150	1.454	0.68	1.89
		80	1.469	0.69	3.55
		30	1.477	0.70	9.46
Clay C	Loading	~30	1.711	0.16	Unknown
		~80	1.660	0.14	Unknown

[a]Not measured.

3.3.4.1 Results for sands

In Figure 3.29 and 3.30, OCR effect can be seen on damping ratio for Santa Monica (SM) sand and Antelope Valley (AV) sand, respectively.

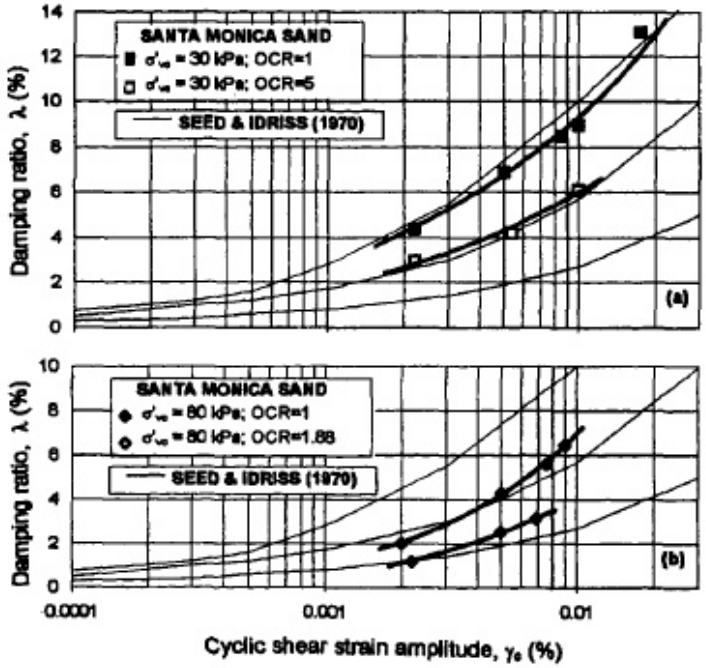

Figure 3.29: Effect of OCR on λ for Santa Monica (SM) Sand (Vucetic et al., 1998)

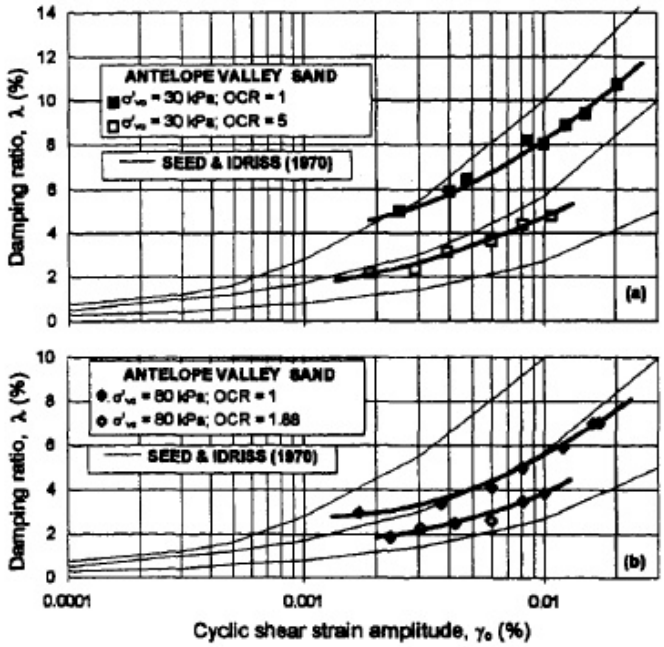

Figure 3.30: Effect of OCR on λ for Antelope Valley (AV) Sand (Vucetic et al., 1998)

Damping ratio significantly decreases when OCR increases for both sands.

3.3.4.2 Results for clays

In Figures 3.31 and 3.32, OCR effect can be seen on damping ratio for Clay A and Clay B, respectively.

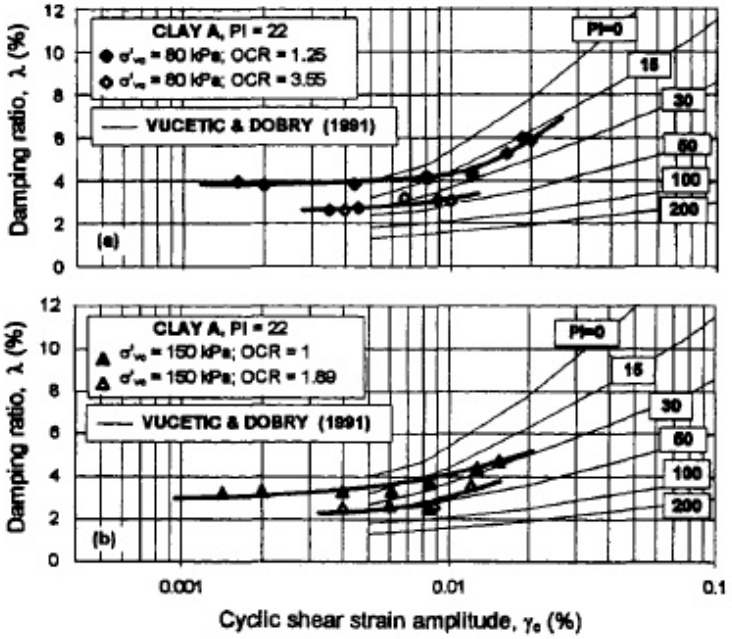

Figure 3.31: Effect of OCR on λ for Clay A (Vucetic et al., 1998)

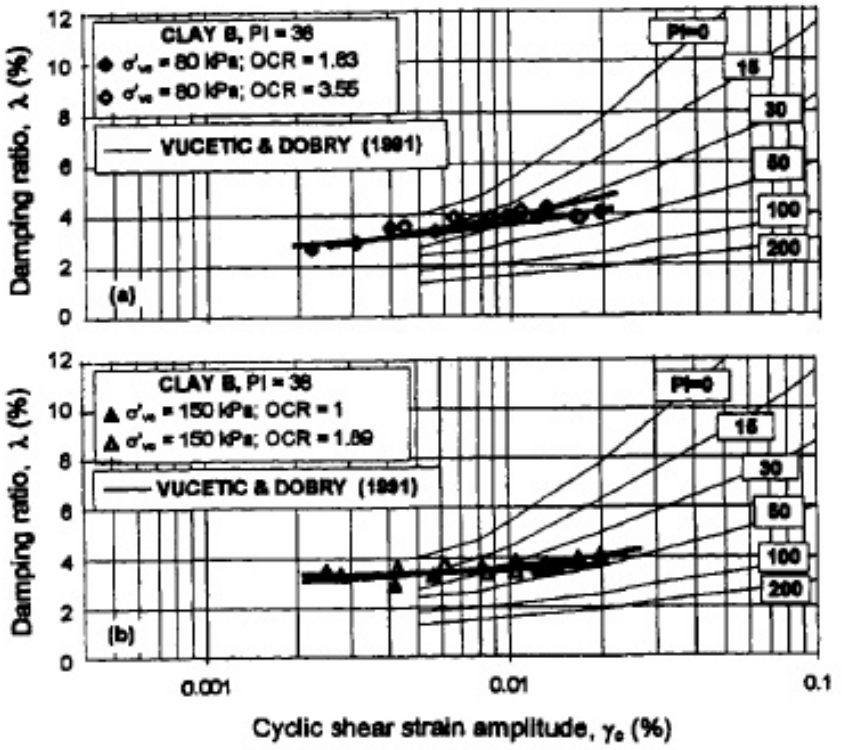

Figure 3.32: Effect of OCR on λ for Clay B (Vucetic et al., 1998)

The OCR effect is different for Clay A and Clay B because of different plasticity index of clays. Clay A has a lower PI=22 and Clay B has a larger PI=38. For Clay A, damping ratio significantly decreases when OCR increases but the effect is still less for sands (PI=0). For Clay B, OCR has no effect on damping ratio. So it can be said that, OCR affects the damping less as PI increases. (Vucetic et al., 1998)

3.3.5 Effective consolidation stress (σ'_{vc})

Vucetic et al. (1998) tests are explained in Chapter 3.3.5. Soil properties are shown in Figure 3.28 and Table 3.7 and test procedures are shown in Table 3.8.

3.3.5.1 Effects on sands

In Figure 3.33, effective consolidation stress effect can be seen on damping ratio for Santa Monica (SM) sand and Antelope Valley (AV) sand. Damping ratio decreases as the effective consolidation stress increases. But the effect is smaller in the range of large σ'_{vc}. (Vucetic et al., 1998)

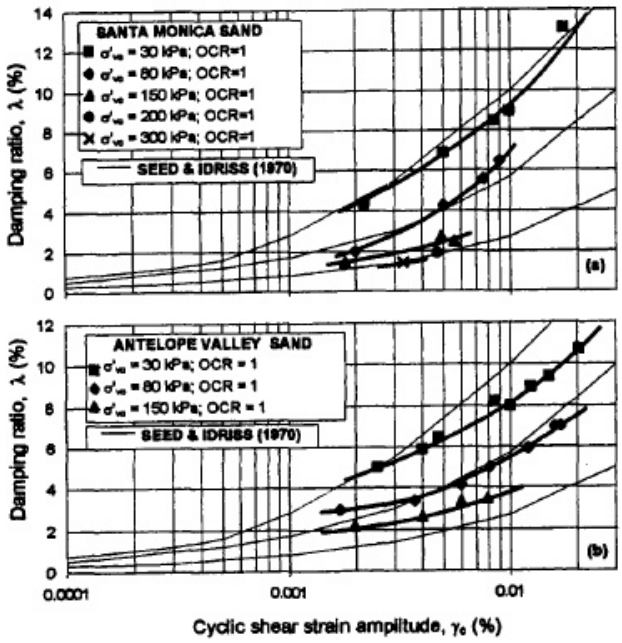

Figure 3.33: Effect of σ'_{vc} on λ for: (a) Santa Monica (SM) Sand; (b) Antelope Valley (AV) Sand (Vucetic et al., 1998)

3.3.5.1 Effects on clays

In Figures 3.34 and 3.35, effective consolidation stress effect can be seen on damping ratio for Clay A and Clay B, respectively.

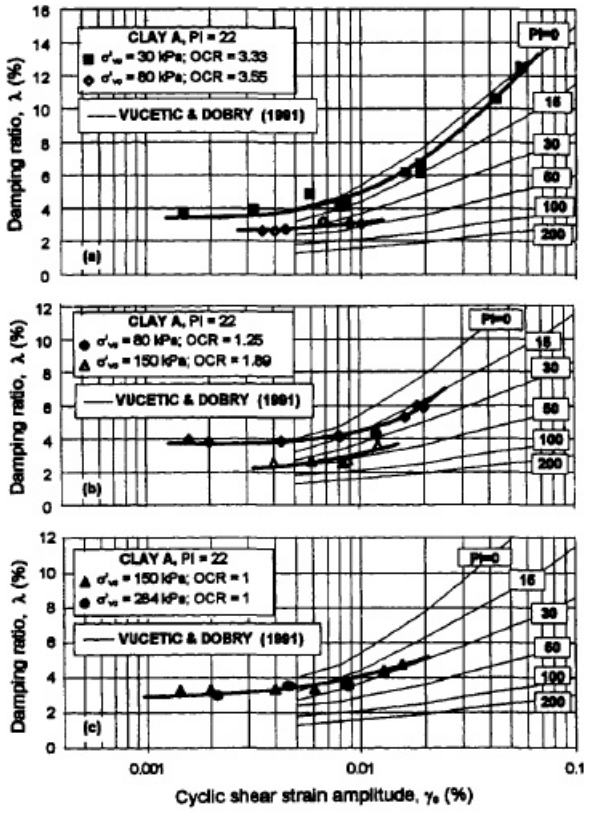

Figure 3.34: Effect of σ'_{vc} on λ for Clay A (Vucetic et al., 1998)

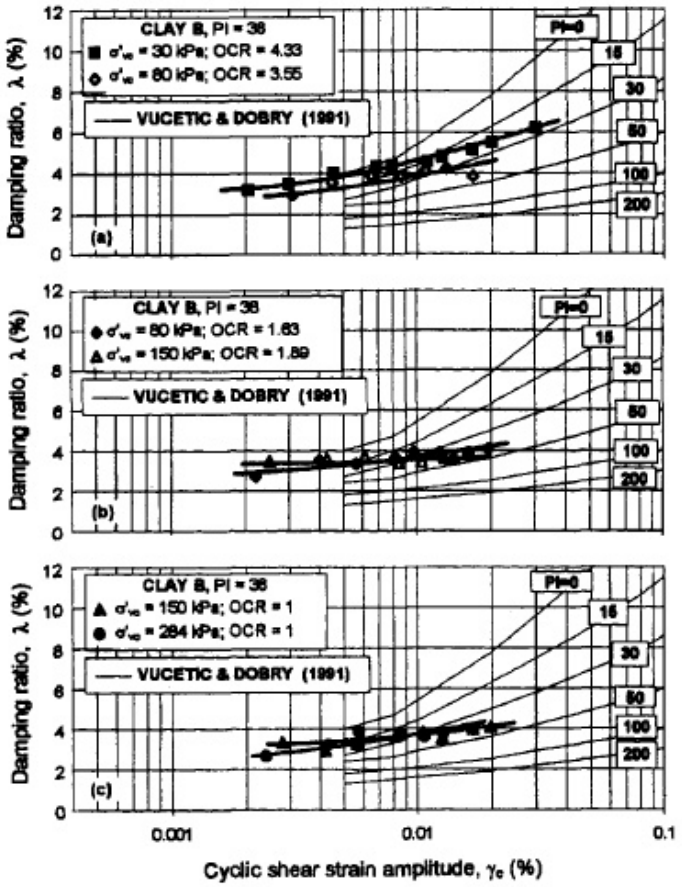

Figure 3.35: Effect of σ'_{vc} on λ for Clay B (Vucetic et al., 1998)

Damping ratio decreases as the σ'_{vc} increases below 150 kPa. And the effect is greater for Clay A than for Clay B because of their PI. And the effect of σ'_{vc} on damping cannot be observed above 150 kPa. (Vucetic et al., 1998)

3.3.6 Silt content

Again Vucetic et al. (1998) paper is used to explain the silt content effect on damping. Soil properties are already shown in Figure 3.28 and Table 3.7 and test procedures are shown in Table 3.8. Silt content effect is shown in Figure 3.36.

Damping values are generally higher for clean SM sand than the silty AV sand above $\gamma_c \approx 0.005\%$ except the case where σ'_{vc}=150 kPa and OCR=1. But below $\gamma_c \approx 0.005\%$, damping values are higher for silty AV than the clean SM sand except the case where σ'_{vc}=30 kPa and OCR=5. (Vucetic et al., 1998)

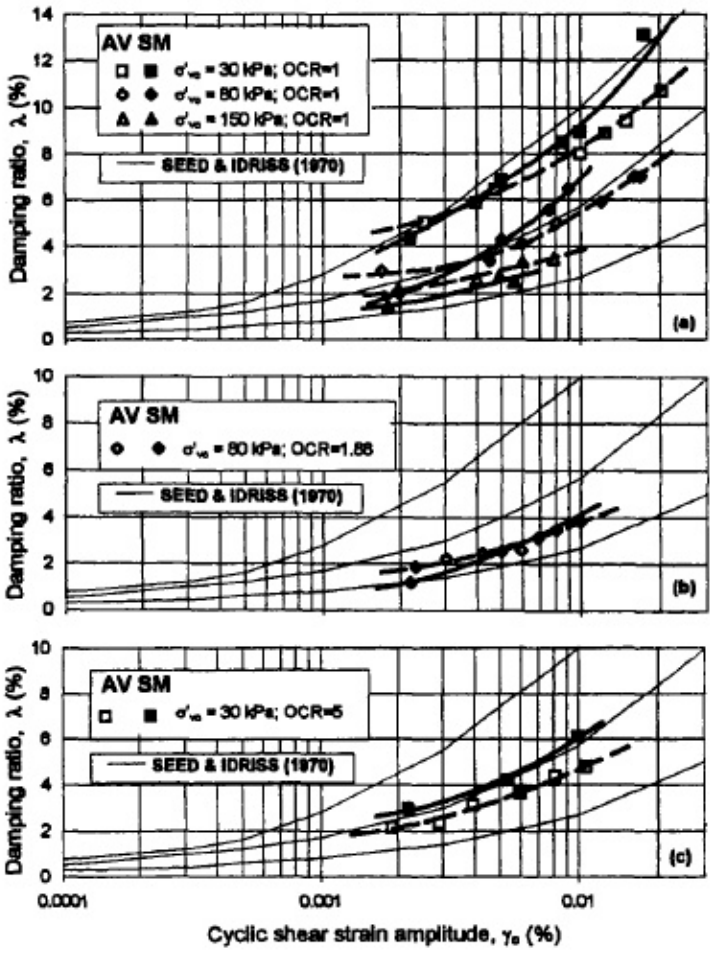

Figure 3.36: Effect of Silt Content on λ (Vucetic et al., 1998)

3.3.7 Loading type effect

As mentioned in Chapter 3.1.3, Zhang and Aggour (1996) performed sinusoidal, random and impulse loading tests on air-dry Ottowa 20-30 sand. Comparison of three type loading on damping ratio can be seen in Figure 3.37.

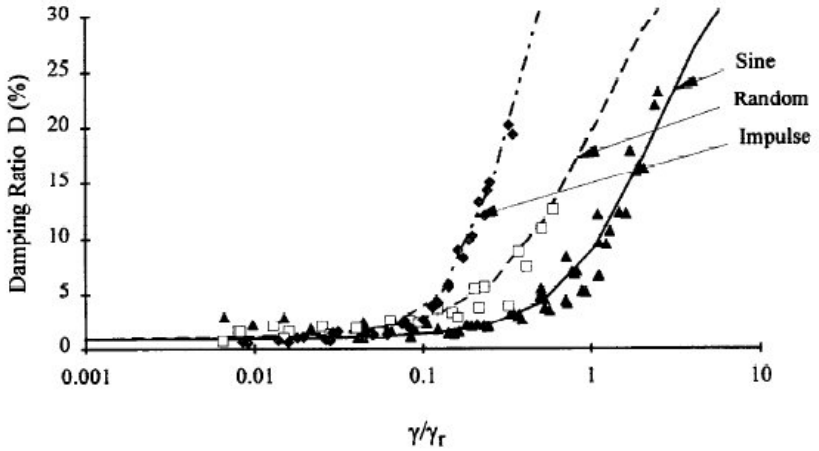

Figure 3.37: Damping Ratio vs. γ/γ_r from different loading tests (Zhang & Aggour, 1996)

Damping ratios are relatively constant and low at low strain levels ($\gamma/\gamma_r<0.1$) for all type of loadings. But at higher strain levels ($\gamma/\gamma_r>0.1$), loading types affect the damping ratio significantly. The damping ratio is highest under impulse loading and the lowest under sinusoidal loading for sands. (Zhang & Aggour, 1996)

3.3.8 Comparison of seismic centrifuge test and resonant column test on damping

To determine the damping parameters, many researchers have used the cyclic triaxial or resonant column tests. Dynamic centrifuge test is an alternative technique and Rayhani and El Naggar (2008) compared the seismic centrifuge tests and the resonant column tests on soft clay and loose sand. In Figure 3.38, centrifuge models configuration can be seen in prototype scale. To apply a one dimensional prescribed base input motion, an electro-hydraulic earthquke simulator (EQS) was attached on the centrifuge. Equivalent shear beam model container (ESB) has 0.73 m lenght, 0.3 m width and 0.57 m height. Prototype of soil in depth 30 m is simulated with the soil model at 80 g. With extensive horizontal and vertical arrays of accelerometers and transformers (LVDT), the model were instrumented.

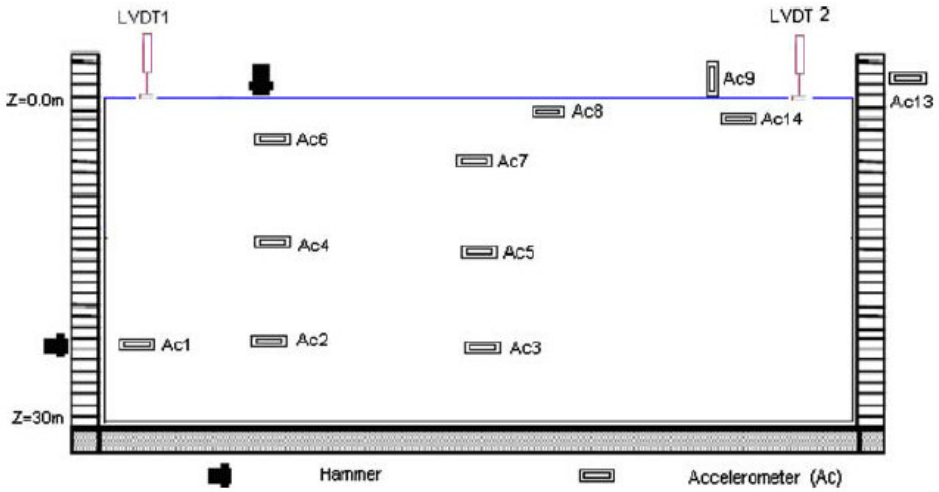

Figure 3.38: Centrifuge models configuration in prototype scale (Rayhani and El Naggar, 2008)

Glyben is a mixture of sodium bentonite powder and glycerin and was used to simulate soft clay behaviour in tests. Well graded Al white silica was used for sand soil. The material properties are summarized in Table 3.9.

Table 3.9: Soil properties used in experimental tests (Rayhani and El Naggar, 2008)

	Dry sand	Clay (Glyben)
Specification	A1 Standard sand	Bentonite + Glycerin
Pore fluid	None	Glycerin
Density (kg/m3)	1,422	1,575
Void ratio (e)	0.90	1.23
Moisture content	Dry	45%
D_{50} (μm)	289	5
Average Vs (m/s)	149	73
Plasticity index	0	10.5

To measure the shear wave velocity at depth 20 m, horizontal blow tests were performed. Shear wave velocities are shown in Table 3.10.

Table 3.10: Shear wave velocity of soil in centrifuge container (Rayhani and El Naggar, 2008)

Gravity	Confining pressure (kPa)	Shear wave velocity (m/s)	
		Clay	Sand
10	35	50	125
20	70	55	131
30	106	65	139
40	142	70	143
50	177	80	156
60	213	85	161
70	248	90	167
80	283	92	172

6 earthquake-like shaking events which were scaled versions of artificial west Canada eathquake (Seid-Karbasi, 2003) and the Port Island ground motion during the 1995 Kobe earthquake subjected to each model. In Table 3.11, earthquake input motions are listed.

Table 3.11: Earthquake inputmotion in centrifuge tests (Rayhani and El Naggar, 2008)

Event	Description	Prototype		Centrifuge (scale 1:80)	
		Peak acc. (g)	Frequency at peak (Hz)	Peak acc. (g)	Frequency at peak (Hz)
WCL	West Canada	0.1	0.93	8	75
WCM	West Canada	0.2	0.93	16	75
WCH	West Canada	0.39	0.93	31	75
KL	Kobe (1995)	0.07	2.19	5.5	175
KM	Kobe (1995)	0.22	2.19	17.6	175
KH	Kobe (1995)	0.49	2.19	39	175

Representative acceleration during moderate event is shown in Figure 3.39 for clay and sand.

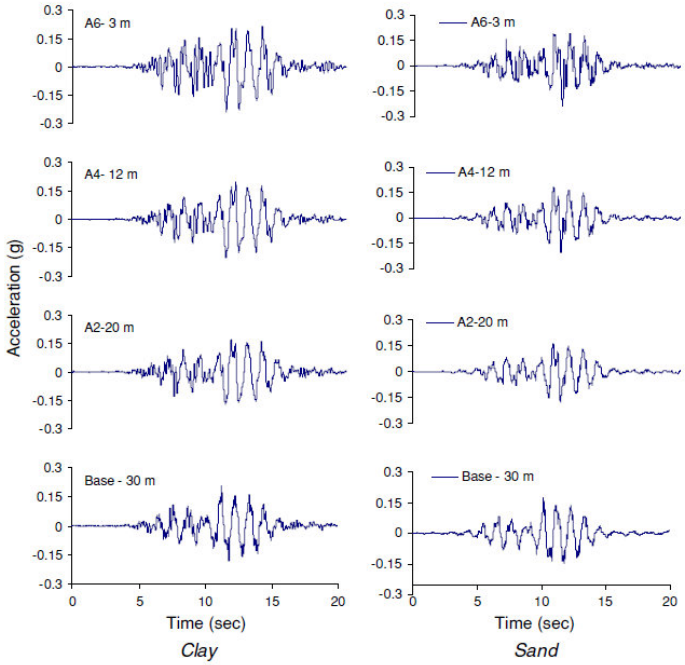

Figure 3.39: Representative acceleration during WCM event in clay and sand (Rayhani and El Naggar, 2008)

For the clay model, the shear stress-strain histories at depths 3 m, 12 m and 20 m during WCM (moderate) shaking event are shown in Figure 3.40. For the sand model, the shear stress-strain histories at different depths during WCL (weak), WCM (moderate) and WCH (strong) events are shown in Figure 3.41.

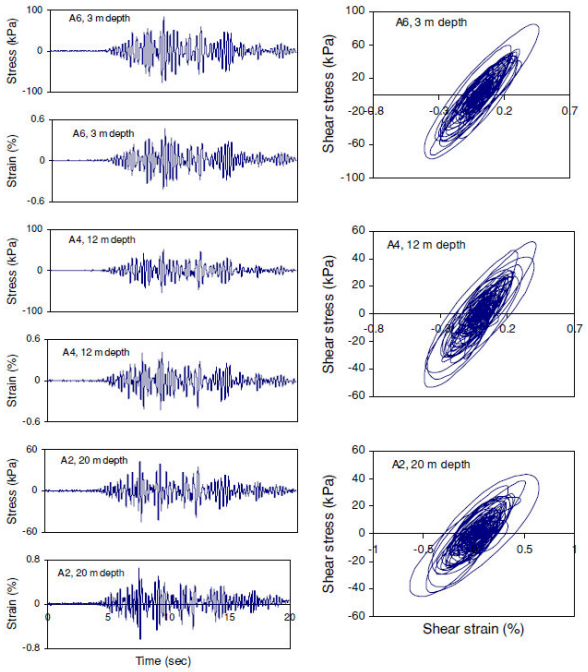

Figure 3.40: Shear stress–strain histories at different depths during WCM event in clay (Rayhani and El Naggar, 2008)

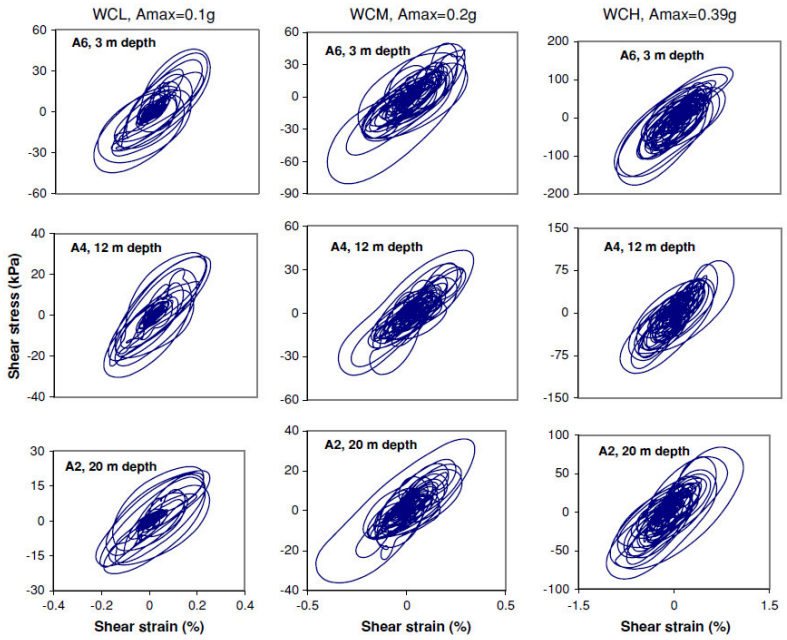

Figure 3.41: Shear stress–strain histories at different depths during all shaking events in sand (Rayhani and El Naggar, 2008)

Shear strain level increases with the stronger shaking events. And with the depth of accelerometer, the hysteresis loop slope increases. That means the soil damping increases as the strain increases and decreases as the depth increases. (Rayhani and El Naggar, 2008)

3.3.8.1 Soft clay

In Figure 3.42, identified and emperical damping relationships for glyben clay are shown.

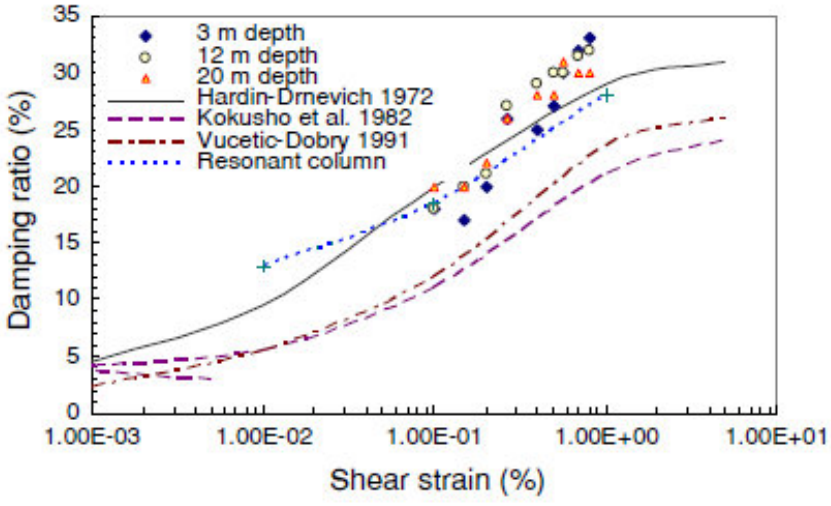

Figure 3.42: Identified damping and empirical relationships for glyben clay (Rayhani & El Naggar, 2008)

The estimated centrifuge damping ratio data is in aggreement with the resonant column results and the corresponding Hardin and Drnevich (1972) curves at shear strain smaller than 0.5%. However, the damping ratio data is slightly higher at shear strain larger than 0.5%. And also the centrifuge data are noticeably far from the design curves suggested by Kokusho et al. (1982) and Vucetic and Dobry (1991) for fine grained soils. (Rayhani and El Naggar, 2008)

3.3.8.2 Dry sand

In Figure 3.43, identified and emperical damping relationships for dry sand are shown.

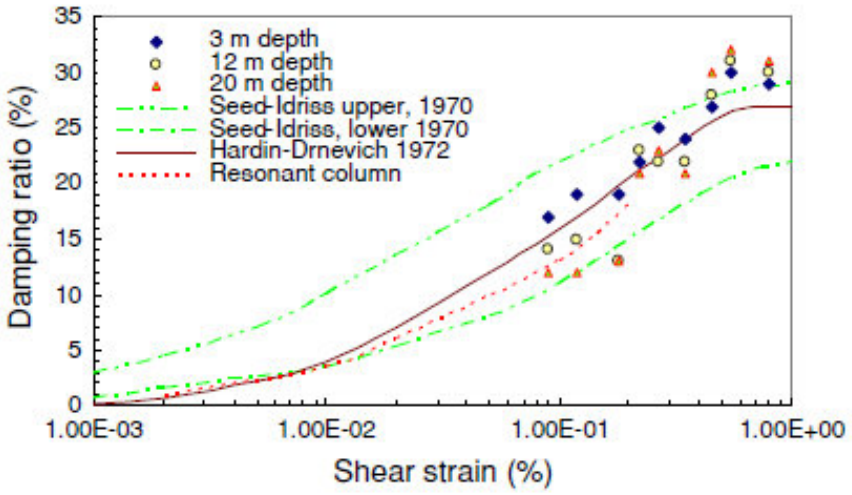

Figure 3.43: Calculated damping and empirical relationships for dry sand (Rayhani and El Naggar, 2008)

Like soft clay, at shear strain smaller than 0.5%, the damping ratios show a reasonable agreement with the emperical curves of Hardin and Drnevich (1972), Seed and Idriss (1970) and resonant column results for dry sand. However, the damping ratio data is slightly higher at shear strain larger than 0.5%. (Rayhani and El Naggar, 2008)

3.3.9 Compaction energy

Wu et al. (2008) performed resonant column (RC) tests on saturated compacted soils which are classified as SM, ML and CL. These soils were taken from the borrow areas of planned earth dam. Physical properties of the compacted soils are summarized in Table 3.12.

Table 3.12: Physical Properties of the Compacted Soils (Wu et al., 2008)

		Classification (USCS)		
		SM	ML	CL
Specific gravity G_s		2.71	2.69	2.74
Fines content (%)		17.03	78.56	93.52
Liquid limit LL (%)		NA	20.89	34.84
Plasticity limit PL (%)		NA	17.13	20.89
Plasticity index PI (%)		NA	3.75	13.95
Standard Proctor	γ_{dmax} (kN/m^3)	19.50	19.01	17.25
(ASTM D698)	O.M.C. (%)	11.59	12.64	19.03
Modified Proctor	γ_{dmax} (kN/m^3)	20.48	20.38	19.21
(ASTM D1557 C)	O.M.C. (%)	8.19	9.39	10.33

Soils were consolidated at the isotropic pressures of 49, 98, 196 and 294 kPa. For compacted soils, the required degree of saturation can not be achievable with traditional saturation procedures because it takes too long time. Therefore, this paper proposed vacuum-saturation concept which is explained in Figure 3.44.

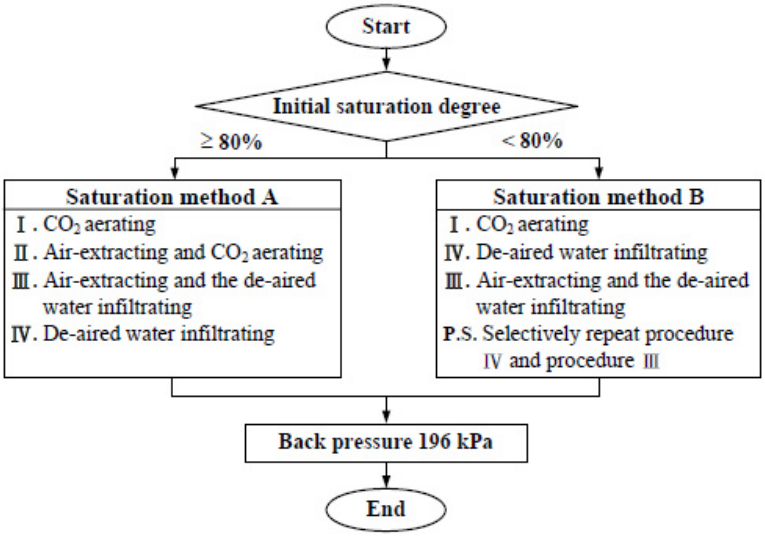

Figure 3.44: Flowchart of the Proposed Saturation Methods (Wu et al., 2008)

Saturation A method was used for ML specimen, saturation B method was used for SM and CL specimens. Both methods implemented that Skepton coefficient B was greater than 0.95 for all specimens. In Figure 3.45, damping ratio curves are shown and compared with other investigations. Figure 3.45 shows that, confining pressure effect can not be observed for ML and CL soils except SM soil. Because of the compaction, the deformation levels are low and the damping ratio values are small. Also the compaction energy type does not affect the damping ratio significantly.

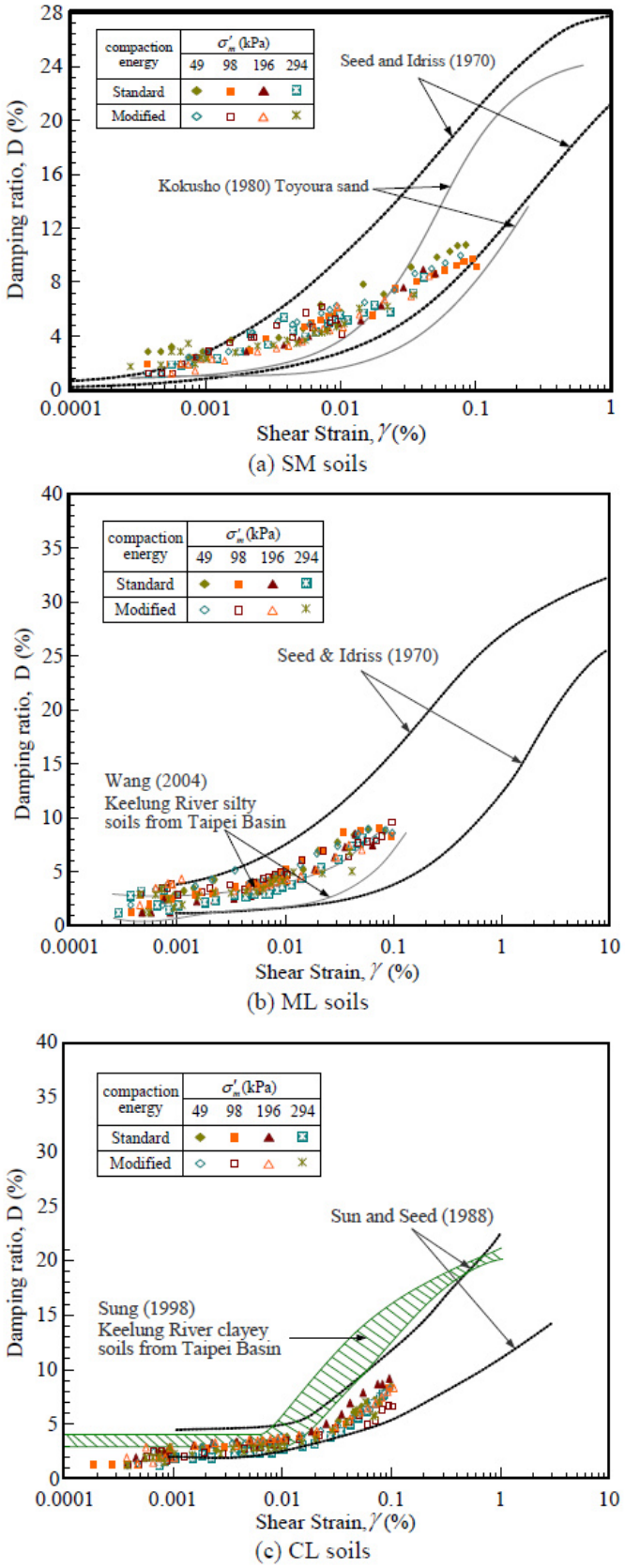

Figure 3.45: Comparison of damping ratio curves of saturated compacted soils with those of other soils in previous investigations (Wu et al., 2008)

3.3.10 Saturation

To investigate the effect of saturation, Jajarzadeh and Sadeghi (2011) performed 64 tests on medium Babolsar sand and Toyoura sand. Drained and undrained tests were carried out with a servo-controlled pneumatic cyclic simple shear device. Shape of loading was approximetely sinusoidal and the frequency was 0.5 Hz. In Figure 3.46, gradation curves are shown for tested materials. Physical properties are summarized in Table 3.13.

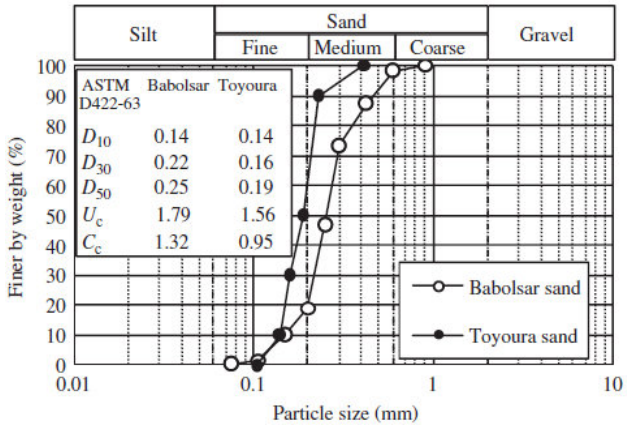

Figure 3.46: Gradation curves of tested soils (Jajarzadeh and Sadeghi, 2011)

Table 3.13: Physical properties of test materials (Jajarzadeh and Sadeghi, 2011)

Soil type	Specific gravity	e_{max}	e_{min}
Babolsar sand	2.753	0.777	0.549
Toyoura sand	2.645	0.973	0.609
Standard designation	ASTM D854-02	ASTM D4254-00	ASTM D4253-00

For undrained conditions, saturated samples are used because experiences shows that under an earthquake excitement, pore water in saturated medium to fine-grained sands does not have enough time to be drained. For drained conditions, unsaturated samples are used because under cyclic loading, unsaturated layer settles immediately. (Jajarzadeh and Sadeghi, 2011)

For a proper evaluation of the saturation of a specimen consolidated under K_0 condition, instead of Skempton's pore pressure parameter, B-value, $\Delta u/\Delta\sigma_1$ value is used; where Δu is the change in pore water pressure and $\Delta\sigma_1$ is the change in principal stress. And this parameter can be calculated as;

$$\frac{\Delta u}{\Delta \sigma_1} = \frac{1}{\left(1+\frac{nC_p}{(C_c(1+K_0))}\right)} \quad \textbf{(3.1)}$$

where n is the porosity, C_p is the compressibility of pore water and C_c is the compressibility of soil skeleton. (Jajarzadeh and Sadeghi, 2011)

Table 3.14 summarizes the measured pore water pressure parameter, relative density, total vertical stress, back pressure and effective vertical stress for 16 undrained tests.

Table 3.14: Measured pore pressure, $\Delta u/\Delta \sigma_1$, in undrained tests (Jajarzadeh and Sadeghi, 2011)

Test no.	Relative density, D_r (%)	Total vertical stress, σ_v (kPa)	Back pressure (kPa)	Effective vertical stress, σ'_v (kPa)	$\Delta u/\Delta \sigma_1$
25–B[a]	31	175	125	50	0.90
26–B	35	175	125	50	0.88
27–B	71	205	155	50	0.88
28–B	67	205	155	50	0.88
29–B	32	275	125	150	0.89
30–B	30	275	125	150	0.87
31–B	74	305	155	150	0.90
32–B	71	305	155	150	0.89
57–T[b]	32	175	125	50	0.91
58–T	33	175	125	50	0.90
59–T	71	205	155	50	0.88
60–T	70	205	155	50	0.85
61–T	28	275	125	150	0.86
62–T	39	275	125	150	0.91
63–T	68	305	155	150	0.82
64–T	70	305	155	150	0.83

[a] B: Babolsar sand.
[b] T: Toyoura sand.

Degree of saturation for drained tests were selected as 25%, 50% and 75% and for undrained tests, fully saturated specimens were assumed to have 100% degree of saturation. 30% and 70% post-consolidation relative densities represent loose and medium dense conditions, respectively. In the range of 1% and 1.5% shear strain amplitudes, seismic loads mainly occur. So these values were selected for all tests which were shear strain controlled. In Table 3.15, general conditions of testing at the beginning.

Table 3.15: Conditions of cyclic simple shear tests conducted on sandy samples at the beginning of cyclic loading stage (Jajarzadeh and Sadeghi, 2011)

Test no.	Sand tested	Degree of saturation, S_r (%)	Relative density, D_r (%)	Shear strain amplitude, γ_c (%)	Total vertical stress, σ_v (kPa)	Back pressure (kPa)
1, 2, 3, 4	Babolsar	24.9, 24.8, 24.4, 24.8	29, 31, 70, 69	1.0, 1.5, 1.0, 1.5	50	–
5, 6, 7, 8	Babolsar	24.8, 24.6, 24.4, 24.0	27, 30, 69, 69	1.0, 1.5, 1.0, 1.5	150	–
9, 10, 11, 12	Babolsar	49.7, 49.9, 48.2, 51.0	29, 29, 70, 72	1.0, 1.5, 1.0, 1.5	50	–
13, 14, 15, 16	Babolsar	50.2, 50.0, 49.1, 49.1	31, 30, 72, 70	1.0, 1.5, 1.0, 1.5	150	–
17, 18, 19, 20	Babolsar	75.3, 73.0, 75.2, 74.7	32, 29, 70, 69	1.0, 1.5, 1.0, 1.5	50	–
21, 22, 23, 24	Babolsar	72.9, 75.3, 75.1, 74.5	29, 31, 69, 68	1.0, 1.5, 1.0, 1.5	150	–
25, 26, 27, 28	Babolsar	100	31, 35, 71, 67	1.0, 1.5, 1.0, 1.5	175, 175, 205, 205	125, 125, 155, 155
29, 30, 31, 32	Babolsar	100	32, 30, 74, 71	1.0, 1.5, 1.0, 1.5	275, 275, 305, 305	125, 125, 155, 155
33, 34, 35, 36	Toyoura	25.2, 25.6, 24.5, 24.6	31, 30, 70, 70	1.0, 1.5, 1.0, 1.5	50	–
37, 38, 39, 40	Toyoura	25.0, 25.5, 24.6, 25.3	29, 30, 69, 70	1.0, 1.5, 1.0, 1.5	150	–
41, 42, 43, 44	Toyoura	50.9, 50.5, 50.6, 50.0	31, 30, 71, 71	1.0, 1.5, 1.0, 1.5	50	–
45, 46, 47, 48	Toyoura	50.0, 50.2, 50.3, 50.2	29, 30, 70, 70	1.0, 1.5, 1.0, 1.5	150	–
49, 50, 51, 52	Toyoura	74.1, 69.0, 74.6, 74.2	28, 29, 69, 70	1.0, 1.5, 1.0, 1.5	50	–
53, 54, 55, 56	Toyoura	72.1, 75.0, 74.5, 74.9	26, 29, 69, 69	1.0, 1.5, 1.0, 1.5	150	–
57, 58, 59, 60	Toyoura	100	32, 33, 71, 70	1.0, 1.5, 1.0, 1.5	175, 175, 205, 205	125, 125, 155, 155
61, 62, 63, 64	Toyoura	100	28, 39, 68, 70	1.0, 1.5, 1.0, 1.5	275, 275, 305, 305	125, 125, 155, 155

The variation of damping values with degree of saturation at 10th cycle is shown for Babolsar and Toyoura sand in Figure 3.47.

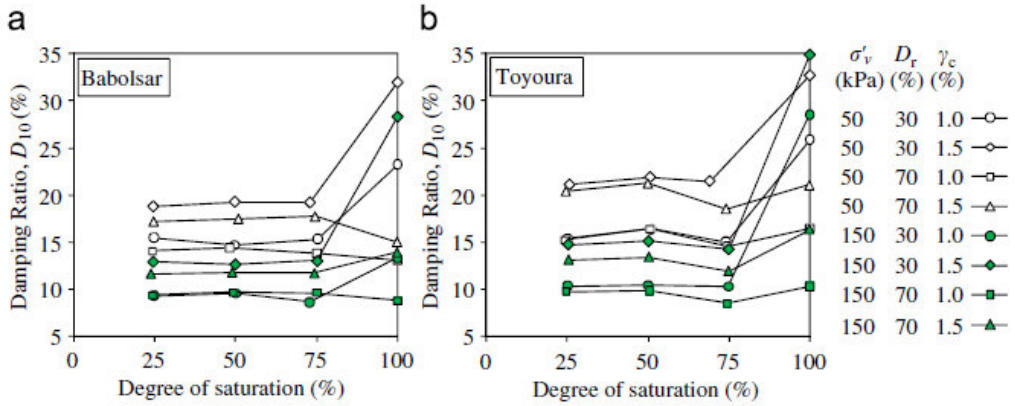

Figure 3.47: Effect of saturation on damping of (a) Babolsar sand (b) Toyoura sand at 10th cycle (Jajarzadeh and Sadeghi, 2011)

Figure 3.47 shows that between 25% and 75% degree of saturation, effect saturation degree is negligible. And also, if the liquefaction state is far for saturated specimen, the damping values of saturated and unsaturated samples have no difference. (Jajarzadeh and Sadeghi, 2011)

In Figure 3.48, the variation of damping values for undrained tests at cycle of initial liquefaction were compared with the corresponding values of drained tests.

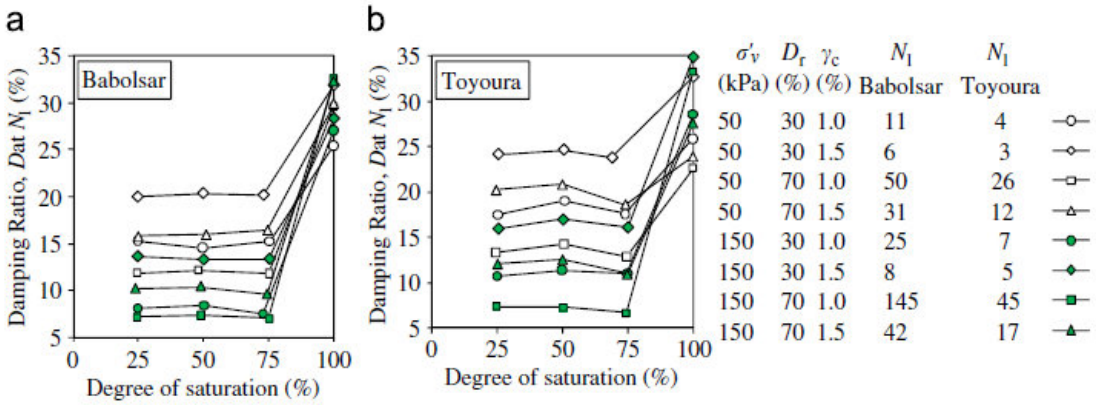

Figure 3.48: Effect of saturation on damping of (a) Babolsar sand (b) Toyoura sand at cycle of initial liquefaction (Jajarzadeh and Sadeghi, 2011)

Figure 3.48 shows that the behaviour between 25% and 75% degree of saturation is the same even though the number of cycles are different. However, saturated samples have considerably higher damping values than the unsaturated samples.

In Figure 3.49, the variation of damping values with the number of cycles for undrained conditions are shown.

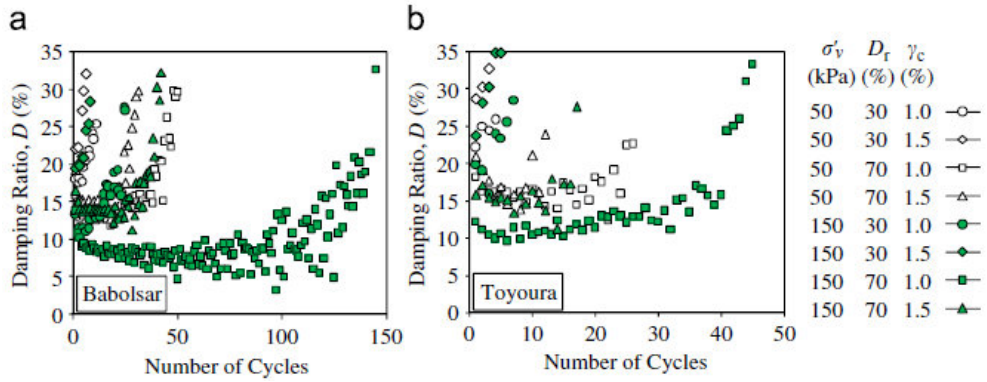

Figure 3.49: Variations in damping ratio with the number of cycles for saturated (a) Babolsar sand (b) Toyoura sand under drained condition (Jajarzadeh and Sadeghi, 2011)

It can be said that, damping values increase in the last 10 cycle to the cycle of initial liquefaction. While increase of damping values start from cycle 1 for loose samples, there is no significant change until 10 cycles for dense samples. (Jajarzadeh and Sadeghi, 2011)

Madhusudhan and Kumar (2013) also performed resonant column tests to investigate the effect of saturation on the sand which was collected from the bank of the Cauvery River (India). Three different sand mixture were prepared from the collected sand. Fine sand mixture retained entirely on 75-μm-sieve size, medium sand mixture retained on 425-μm-sieve size and coarse sand mixture retained on 2.0-mm. (ASTM 2009) Five different relative densities, D_r, (40, 50, 60, 70, 80%) were used for damping tests. Partly and fully saturated samples for a chosen relative density were prepared with the procedure described in Kumar and Madhusudhan (2011). For all three sands, the variation of the damping ratio (D_0) depending on saturation (S_r), relative density and confining pressure (σ'_3) are presented in Figures 3.50, 3.51 and 3.52. And also minimum values of damping ratio are provided in Table 3.16.

Figures show that as D_r increases, damping ratio decreases and optimum degree of saturaion inceases marginally. σ'_3 does not affect the optimum degree of saturation but when σ'_3 increases, damping ratio decreases. Regardless of the grain size, damping ratio reaches the maximum value for fully saturated sands. The maximum change in the damping ratio is generally between 0.5 and 1% for near dry to fully saturated state. This implies that, if the dynamic behavior of sand has to be modeled, saturation may not be necessary to be considered for the damping variations. (Madhusudhan and Kumar, 2013)

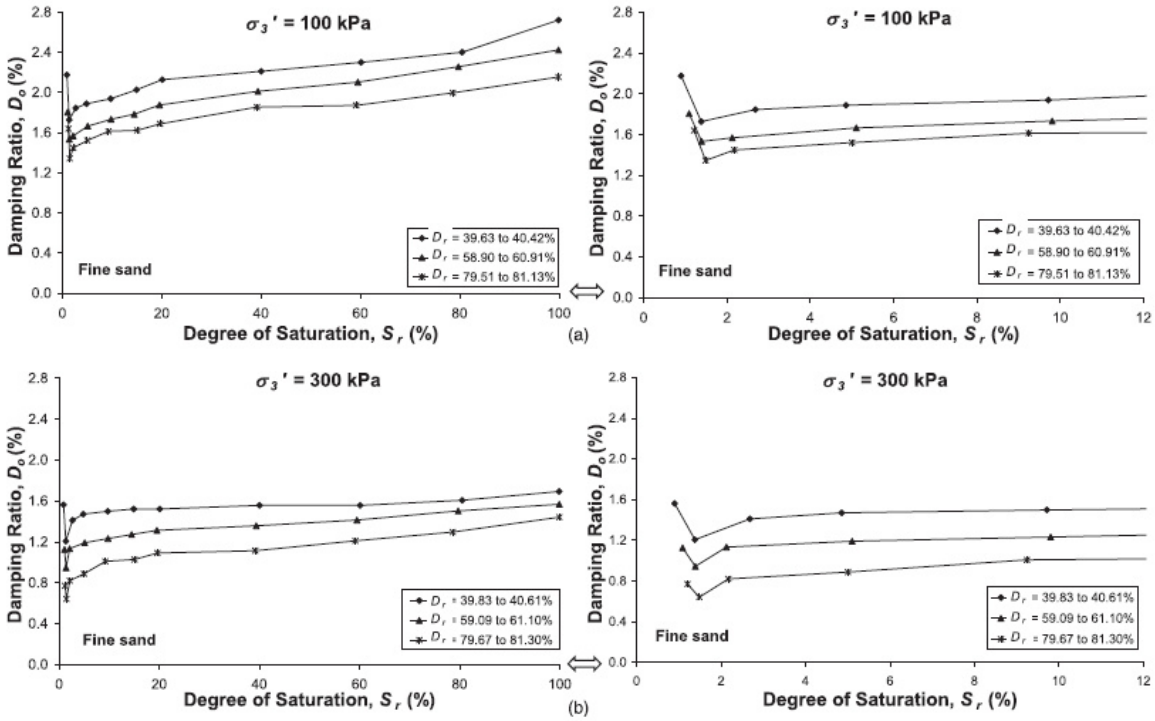

Figure 3.50: Variation of the damping ratio with S_r for fine sand at different relative densities for (a) σ'_3 =100 kPa; (b) σ'_3 = 300 kPa (Madhusudhan and Kumar, 2013)

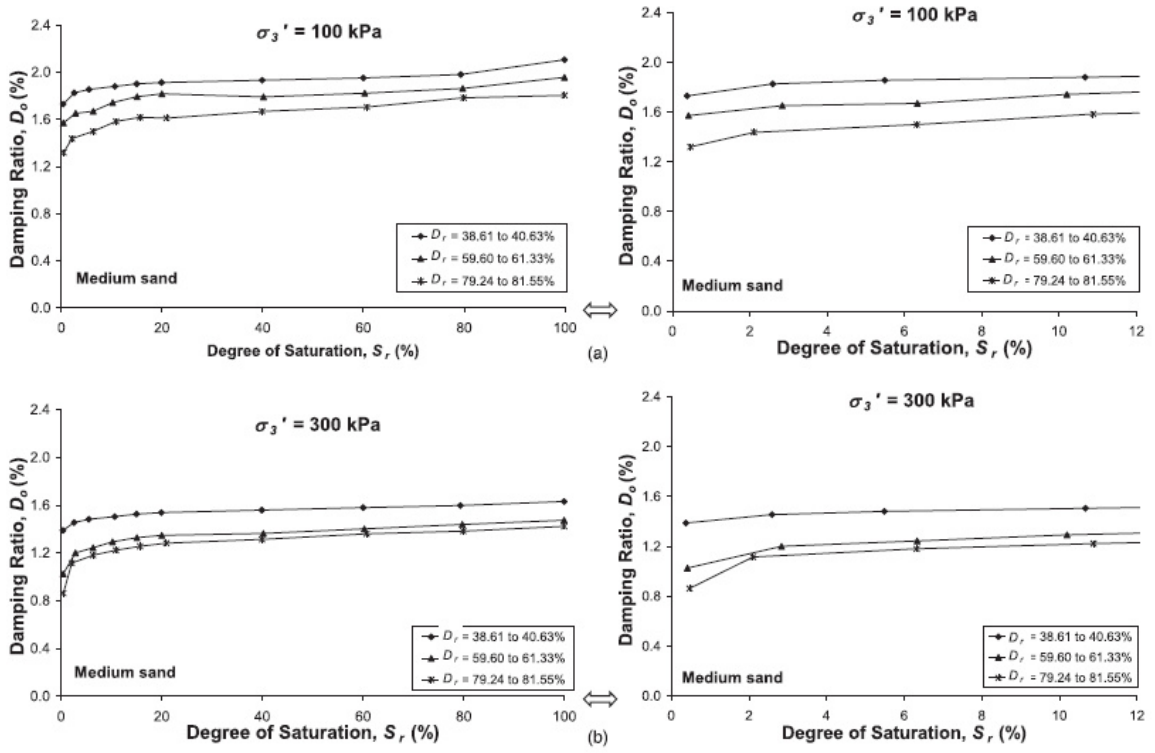

Figure 3.51: Variation of the damping ratio with S_r for medium sand at different relative densities for (a) σ'_3 =100 kPa; (b) σ'_3 = 300 kPa (Madhusudhan and Kumar, 2013)

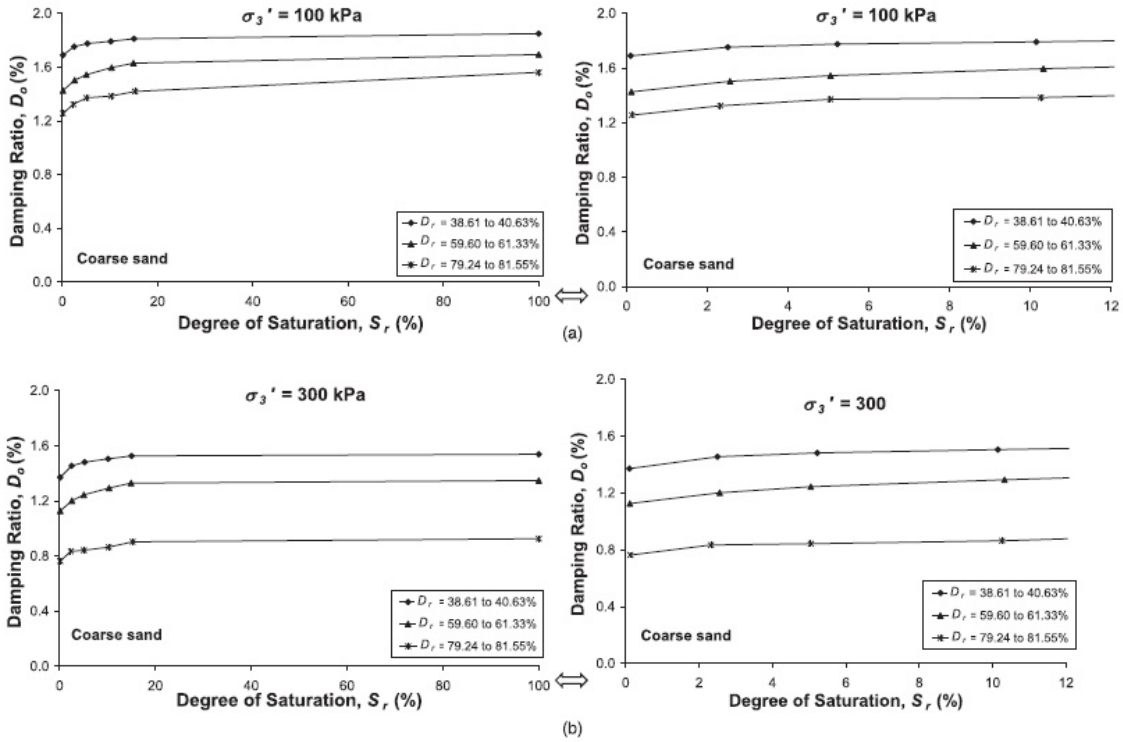

Figure 3.52: Variation of the damping ratio with S_r for coarse sand at different relative densities for (a) σ'_3 =100 kPa; (b) σ'_3 = 300 kPa (Madhusudhan and Kumar, 2013)

Table 3.16: Minimum Values of D_O and the Associated Degree of Saturation for Different Values of Relative Density (D_r) and Effective Confining Pressure (σ'_3) (Madhusudhan and Kumar, 2013)

		Fine sand		Medium sand		Coarse sand	
σ'_3 (kPa)	Relative density, D_r (%)	Optimum degree of saturation (%)	$D_{o\text{-opt}}$ (%)	Optimum degree of saturation (%)	$D_{o\text{-opt}}$ (%)	Optimum degree of saturation (%)	$D_{o\text{-opt}}$ (%)
100	40	1.38	1.72	0.38	1.73	0.10	1.70
	50	1.38	1.64	0.39	1.65	0.11	1.57
	60	1.40	1.53	0.42	1.57	0.12	1.43
	70	1.43	1.48	0.44	1.47	0.12	1.35
	80	1.49	1.34	0.47	1.32	0.13	1.26
300	40	1.38	1.20	0.38	1.39	0.10	1.37
	50	1.38	1.06	0.39	1.25	0.11	1.26
	60	1.40	0.94	0.42	1.03	0.12	1.13
	70	1.43	0.77	0.44	0.94	0.12	0.96
	80	1.49	0.64	0.47	0.86	0.13	0.76
500	40	1.38	0.88	0.38	1.12	0.10	1.15
	50	1.38	0.78	0.39	1.09	0.11	0.99
	60	1.40	0.57	0.42	0.90	0.12	0.83
	70	1.43	0.53	0.44	0.76	0.12	0.73
	80	1.49	0.43	0.47	0.52	0.13	0.50

3.3.11 Mean grain size and uniformity coefficient effect on damping

Witchmann and Triantafyllidis (2013) performed approximetely 280 resonant column tests on 27 clean quartz sands which were obtained from sand pit near Dorsten, Germany. The grain size distribution curves are linear in the semilogarithmic scale and shown in Figure 3.53. Tested materials are summarized with d_{50} and C_u values and also minimum and maximum void ratios in Table 3.17.

Materials from L1 to L8 were used to d_{50} influence and from L10 to L26 were used to C_u influence.

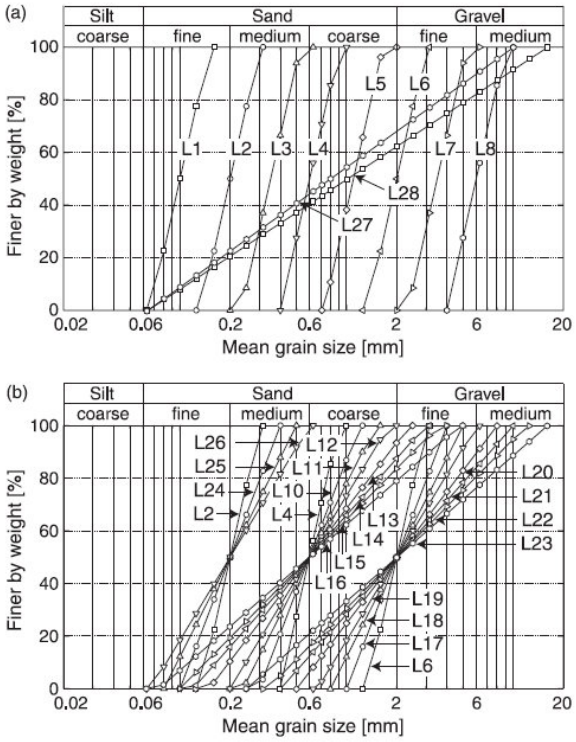

Figure 3.53: Tested grain size distribution curves (adapted from Wichtmann and Triantafyllidis, 2009) (Wichtmann and Triantafyllidis, 2013)

Table 3.17: Parameters d_{50}, C_u, e_{min}, and e_{max} (Determined according to German Standard Code DIN 18126) of the tested grain size distribution curves and range of tested initial relative densities D_{r0} (Witchmann andTriantafyllidis, 2013)

Material	d_{50} (mm)	C_u	e_{min}	e_{max}	Range of tested D_{r0}
L1	0.1	1.5	0.634	1.127	0.46–0.78
L2	0.2	1.5	0.596	0.994	0.45–0.94
L3	0.35	1.5	0.591	0.931	0.42–0.98
L4	0.6	1.5	0.571	0.891	0.43–1.05
L5	1.1	1.5	0.580	0.879	0.46–1.02
L6	2	1.5	0.591	0.877	0.48–0.95
L7	3.5	1.5	0.626	0.817	0.49–0.99
L8	6	1.5	0.634	0.799	0.38–1.10
L10	0.6	2	0.541	0.864	0.43–1.02
L11	0.6	2.5	0.495	0.856	0.46–1.00
L12	0.6	3	0.474	0.829	0.45–0.93
L13	0.6	4	0.414	0.791	0.47–0.87
L14	0.6	5	0.394	0.749	0.46–0.84
L15	0.6	6	0.387	0.719	0.54–0.86
L16	0.6	8	0.356	0.673	0.51–0.87
L17	2	2	0.555	0.827	0.50–0.98
L18	2	2.5	0.513	0.810	0.54–0.99
L19	2	3	0.491	0.783	0.64–1.00
L20	2	4	0.439	0.728	0.65–1.00
L21	2	5	0.401	0.703	0.61–0.99
L22	2	6	0.401	0.553	0.39–1.04
L23	2	8	0.398	0.521	0.45–1.04
L24	0.2	2	0.559	0.958	0.52–0.93
L25	0.2	2.5	0.545	0.937	0.61–0.95
L26	0.2	3	0.540	0.920	0.64–0.93
L27	0.79	12.6	0.327	0.564	0.66–0.94
L28	1.0	15.9	0.300	0.460	0.54–0.96

Curves of D(γ) were measured at the mean pressure, p=50, 100, 200 and 400 kPa. In Figure 3.54, d_{50} and C_u effect on damping ratio can be seen.

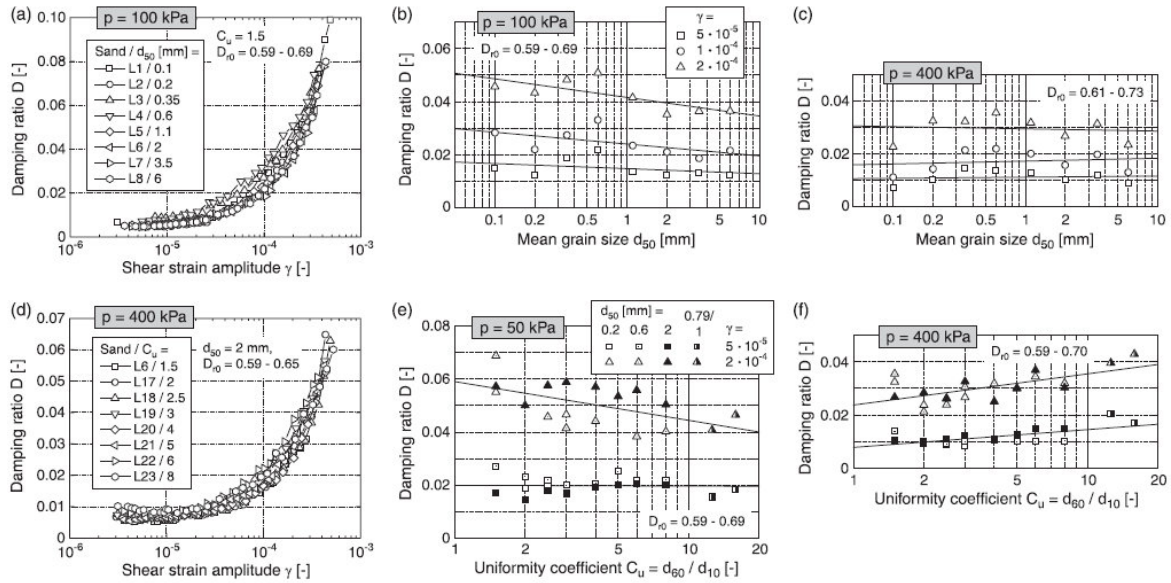

Figure 3.54: Dependence of damping ratio D on (a-c) mean grain size d_{50} and (d-f) uniformity coefficient C_u (Witchmann andTriantafyllidis, 2013)

Figure 3.54(a) shows that the damping ratio is not significantly affected by the mean grain size. For a closer inspection, in Figure 3.54(b and c) damping ratio is plotted as a function of mean grain size. For p=100 kPa, damping ratio slightly decreases when the mean grain size increases. For p=400 kPa, damping ratio is nearly independent of d_{50}.

Figure 3.54(d) shows that the damping ratio is hardly affected by uniformity of coefficient. And also Figure 3.54(e and f) reveals that, for p=50 kPa, damping ratio decreases when C_u increases, but for p=400 kPa, damping ratio increases when C_u increases. With reference to Figures 3.54(a) and 3.54(d), for practical purposes d_{50} and C_u can be neglected in emperical formulas. (Witchmann and Triantafyllidis, 2013)

Summarization of factors affecting soil damping is in Table 3.18.

Table 3.18: Summarization of factors affecting soil damping

Reference	Increasing Factor	Soil Type	Damping
Seed et al., 1986	Relative density (D_r)	Gravelly soils	Increase with D_r
Ray and Woods, 1988	Number of cycles (N)	Sands and silts	Decrease with N
Vucetic and Dobry, 1991	Plasticity index (PI)	Normally and oversonsolidated soils	Decrease with PI
Vucetic et al., 1998	Overconsolidation ratio (OCR)	Silty sands and clays	Decrease with OCR for sands and clays. However as the PI increases OCR affect decreases.
Vucetic et al., 1998	Effective consolidation stress (σ'_{vc})	Silty sands and clays	For sands decreases with σ'_{vc} for sands but the effect is smaller for large $\sigma'_{vc.}$ For clays decreases when σ'_{vc}<150 kPa. σ'_{vc}>150, the effect cannot be observed.
Vucetic et al., 1998	Silt content	Silty sands	Above $\gamma c \approx 0.005\%$, generally decreases with silt content. Below $\gamma c \approx 0.005\%$, generally increases with silt content.
Zhang and Aggour, 1996	Loading type	Sands	Impulse loading has highest damping and sinusoidal loading has lowest damping.
Wu et al., 2008	Compaction energy	Silty sands, silts and lean clays	Damping values are small and deformation levels are low. Confining pressure effect cannot be observed. Compaction energy type does not affect damping ratio significantly.
Jajarzadeh and Sadeghi, 2011	Saturation	Sands	For 25 to 75% degree of saturation, the effect is negligible. However for 100% degree of saturation, damping values are higher at the initial liquefaction cycle.
Witchmann and Triantafyllidis, 2013	Mean grain size (d_{50}) and uniformity coefficient (C_u)	Sands	Effect can be neglected for practical purposes.

4. SOILS MIXED WITH GRANULATED RUBBER AND FIBER

The application of recycled tires in engineered fills, paving projects and other earthworks are increasing. They are usually mixed with soil or asphalt according to engineering applications needs. For example, they are used as asphalt-rubber hot mix, rubber-modified asphalt surface/interlayer treatments in asphalt paving or in surface/interlayer treathments (Liang and Lee, 1996; Maupin, 1996; Eleazer and Barlaz, 1992). Recycled tires are also used in geotechnical engineering such as lightweight fills, backfill materials, highway embankments, soil reinforcements and soil-retaining walls (Humphrey et al., 1993; Upton and Machan, 1993; Ahmed and Lovell, 1993; Lee et al., 1999). (Zheng-Yi and Sutter, 2000) In developing countries, extra waste tires are generated because of the increasing traffic. And due to its lightweight and high capacity in damping energy, rubber can be used for seismic forces reduction and absorption of earthquake vibration. (Nakhaei et al., 2012)

In prehistoric times fiber was being used as a reinforcement in contruction materials. For example in Mesopotamia, straw was adding to mud bricks to provide integrity, control the growth of cracks and improve soil properties. In 1986, Freitag examined compacted cohesive soils with fiber inclusion. As a result, inclusion of fiber increases strength and toughness. Also Akbulut et al. (2007) mixed recycled short monofilament fibers in clayey soil which showed increase in compressive and shear strength of clay. (Amir-Faryar and Aggour, 2012)

4.1 Characteristics of Granulated Rubber

Tire rubber has extremely high elasticity and good fatique properties so it has high damping capacity according to Beatty (1981). Tire rubber has different characteristics than soil materials such as the elastic deformability of tire rubber is orders of magniture greater, the strength and modulus of the solid particles is much lower, there is no yield point in the stress-strain curve and when the stress is removed tire rubber can be recovered from large deformation. Temperature, aging/relaxation and environmental factors also affect the engineering properties of rubber.

Depending on packing and rubber/soil mixing ratio, rubber/soil mixture compressibility can be relatively high. (Edil and Bosscher, 1994) But due to Poisson's ratio of rubber which is nearly 0.5, its volumetric compressibility is quite small. (Beaty, 1981) Depending on metal content, the specific gravity of shredded tire generally ranges from 1.00 to 1.36. (Edil and Bosscher, 1994; Lee et al., 1999) (Zheng-Yi and Sutter, 2000)

4.2 Investigations about Rubber/Soil Mixtures

To investigate the damping ratio of granulated rubber/sand mixtures, Zheng-Yi and Sutter (2000) made tests on Ottowa sand constructed different percentages of granulated rubber. The Ottawa sand was sieved to pass the No.20 and retained on the No.30, the granulated rubber was sieved to pass the No.4 and retained on No.10. So the granular rubber has a uniform gradation. The specific gravity of Ottawa sand is 2.67 and the specific gravity of the granulated rubber is 1.1 at a temperature 20°C. The samples were prepared by two method 'undercompaction' and 'handspooning'. Since the undercompaction (UC) samples were much more uniform than the handspooning (HS) samples, most of the HS samples could not be considered to give valid results. (Zheng-Yi and Sutter, 2000) In Table 4.1, tested sample data are given. A torsional resonant device was used and the isotrophic confining pressures were 69, 207, 345 and 483 kPa (10, 30, 50 and 70 psi respectively).

Table 4.1: Samples tested (Zheng-Yi and Sutter, 2000)

% Rubber by Volume	Initial Void Ratio at 69 kPa	Preparation Method[a]
29	0.45	UC
45	0.39	UC
49	0.40	UC
76	0.46	UC
100	0.35	UC
0	0.52	HS
27	0.49	HS
42	0.49	HS
49	0.45	HS
73	0.45	HS
0	0.57	HS

[a] UC = undercompaction. HS = hand-spooning.

A torsional resonant device was used and the isotrophic confining pressures were 69, 207, 345 and 483 kPa (10, 30, 50 and 70 psi respectively). Damping ratios for specimens with the granulated rubber contents of 29, 49, 76 and 100% are shown in

Figures 4.1 to 4.4, respectively, under different confining pressures. And in Figure 4.5, damping ratios for the different percentages of rubber at 345 kPa are shown.

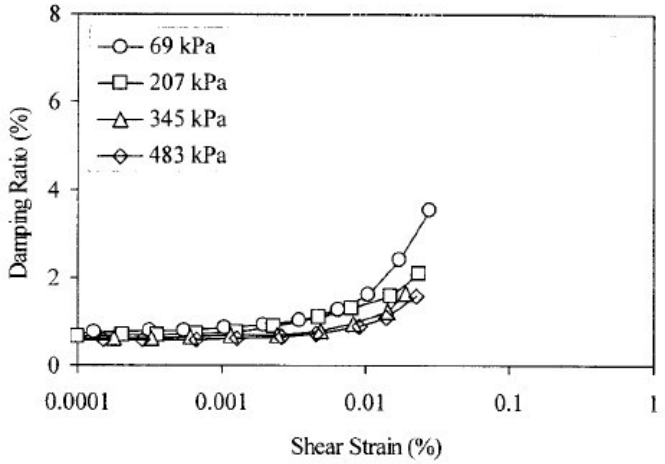

Figure 4.1: Damping behavior for 29% rubber by volume prepared using undercompaction (Zheng-Yi and Sutter, 2000)

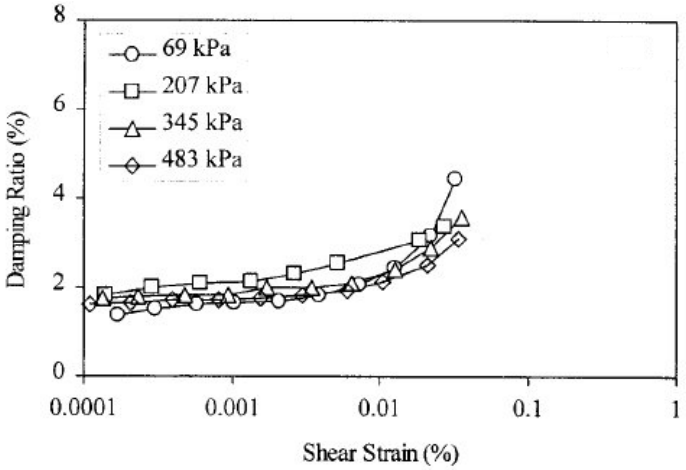

Figure 4.2: Damping behavior for 49% rubber by volume prepared using undercompaction (Zheng-Yi and Sutter, 2000)

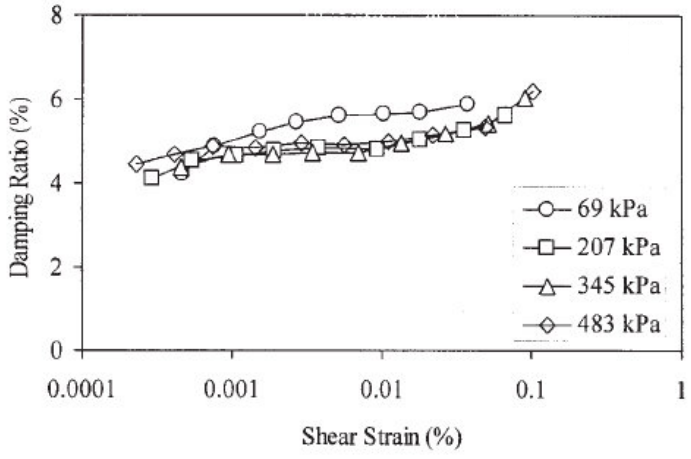

Figure 4.3: Damping behavior for 76% rubber by volume prepared using undercompaction (Zheng-Yi and Sutter, 2000)

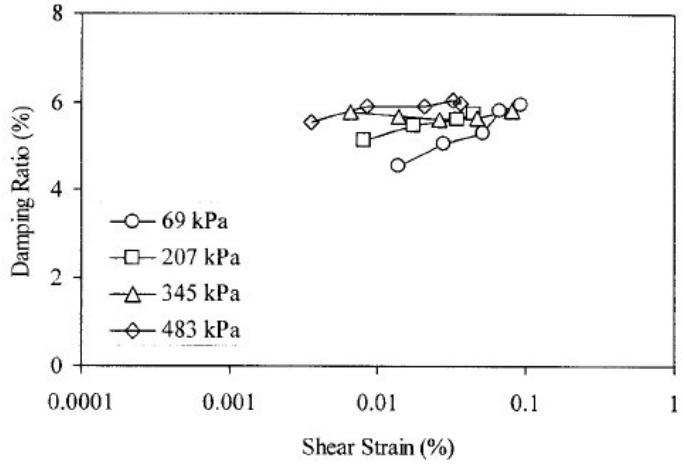

Figure 4.4: Damping behavior for 100% rubber by volume prepared using undercompaction (Zheng-Yi and Sutter, 2000)

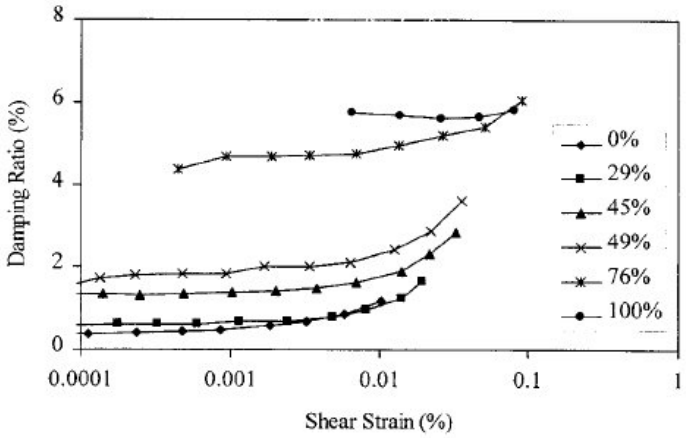

Figure 4.5: Damping behavior for the different percentages of rubber at 345 kPa, prepared using undercompaction (Zheng-Yi and Sutter, 2000)

The sand particles dissipate very little energy in particle deformation because they are very stiff. On the other hand, the rubber consumes much energy for deformation of rubber particles. For higher percentages of rubber; when the confining pressure increases, the damping ratio slightly increases which is an opposite behaviour for typical soils and this can be seen in Figure 4.4 clearly for 100% rubber sample. In Figure 4.5 shows that the damping ratio increases when the rubber content increases. (Zheng-Yi and Sutter, 2000)

Nakhaei et al. (2012) made also a research about dynamic properties of granular soils mixed with granulated rubber. A series of large-scale consolidated undrained cylindrical triaxial tests were carried out on the granular soils which were mixed with different percentages of rubber. The soil was excavated from a huge mine situated in Ekhtiar Abbad Kerman site, south-east of Iran. The granulated rubber was supplied

from Behzist Factory located in Orumieh City, north-west of Iran. Specific gravity of granulated rubber is 1.1 and granulated rubber particles have nonspherical shapes. The particle size distribution curves for soil and rubber are shown in Figure 4.6.

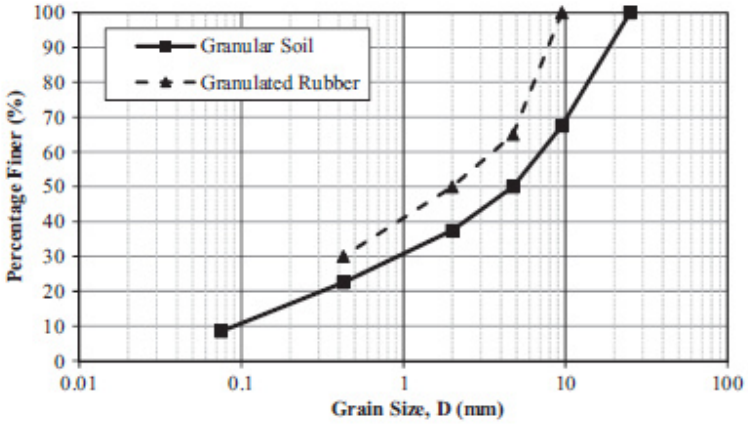

Figure 4.6: The particle size distribution for granular soil and granulated rubber (Nakhaei et al., 2012)

The tested soil was well graded gravel with clay based on Unified Soil Classification System. Properties of soil are summarized in Table 4.2.

Table 4.2: The properties of tested soil (Nakhaei et al., 2012)

	Coeficient of uniformity (c_u)	Coeficient of curvature (c_c)	Passed seive no. 200 (%)	Sand equivalent (%)	Plasticity index (%)	Unified classification	Specific gravity
Soil	77.77	1.29	8.5	51	4	GW–GC	2.65

Soil samples contained 0, 8, 10 and 14% granulated rubber by weight. Some properties of the mixtures and prepared specimen are shown in Table 4.3 and 4.4, respectively.

Table 4.3: The optimum water content, maximum and minimum dry unit weights, and specific gravites of the mixtures (Nakhaei et al., 2012)

Granulated rubber (%)	Optimum water content (%)	Maximum dry unit weight (kN/m^3)	Minimum dry unit weight (kN/m^3)	Mixture specific gravity
0.0	6.6	21.68	13.63	2.65
8.0	7.8	19.42	12.85	2.38
10.0	8.4	19.03	11.38	2.32
14.0	9.2	18.05	10.98	2.21

Table 4.4: The prepared specimen properties (Nakhaei et al., 2012)

Granulated rubber (%)	Moisture unit weight (kN/m^3)	Dry unit weight (kN/m^3)	Void ratio	Relative density D_r(%)
0.0	22.00	20.64	0.259	91.47
8.0	20.14	18.68	0.250	92.25
10.0	19.47	17.96	0.266	91.14
14.0	18.67	17.10	0.267	91.37

The samples have a 15 cm diameters and 30 cm heights. Each samples were saturated and then consolidated isotrophically under 50, 100, 200 and 300 kPa pressures. The testing program is summarized in Table 4.5.

Table 4.5: The testing program procedure (Nakhaei et al., 2012)

	σ_3(kPa)	50	100	200	300
Series 1	σ_d(kPa)	10, 20, 30, 40	20, 30, 40, 50, 60, 70, 80	50, 60, 70, 80, 90, 100, 110, 120, 130, 140, 150, 160, 170, 180	100, 120, 140, 160, 180, 200, 220, 240, 260, 280
	σ_3(kPa)	50	100	200	300
Series 2	σ_d(kPa)	15, 25, 35	25, 35, 45, 55, 65, 75, 85	55, 65, 75, 85, 95, 105, 115, 125	110, 130, 150, 170, 190

Damping ratio curves for rubber/soil mixtures variation of granulated rubber percentages and variation of confining pressures are presented in Figure 4.7 and 4.8, respectively.

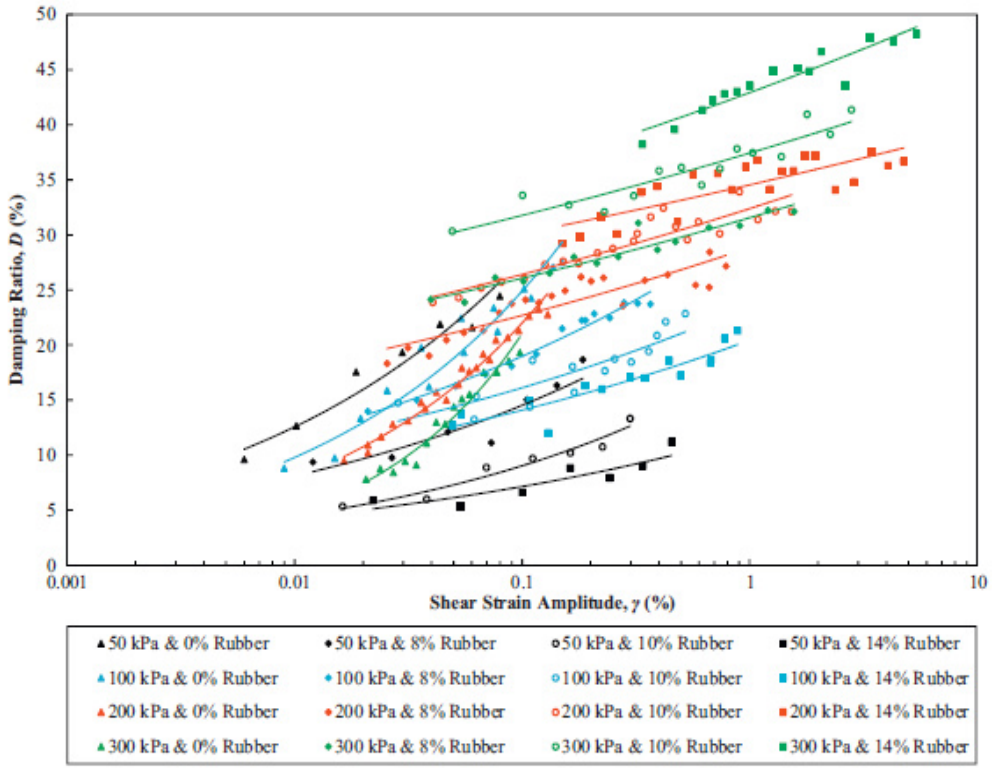

Figure 4.7: Damping ratio versus shear strain amplitude for the confining pressures of 50, 100, 200 and 300 kPa and the variation of granulated rubber percentages (Nakhaei et al., 2012)

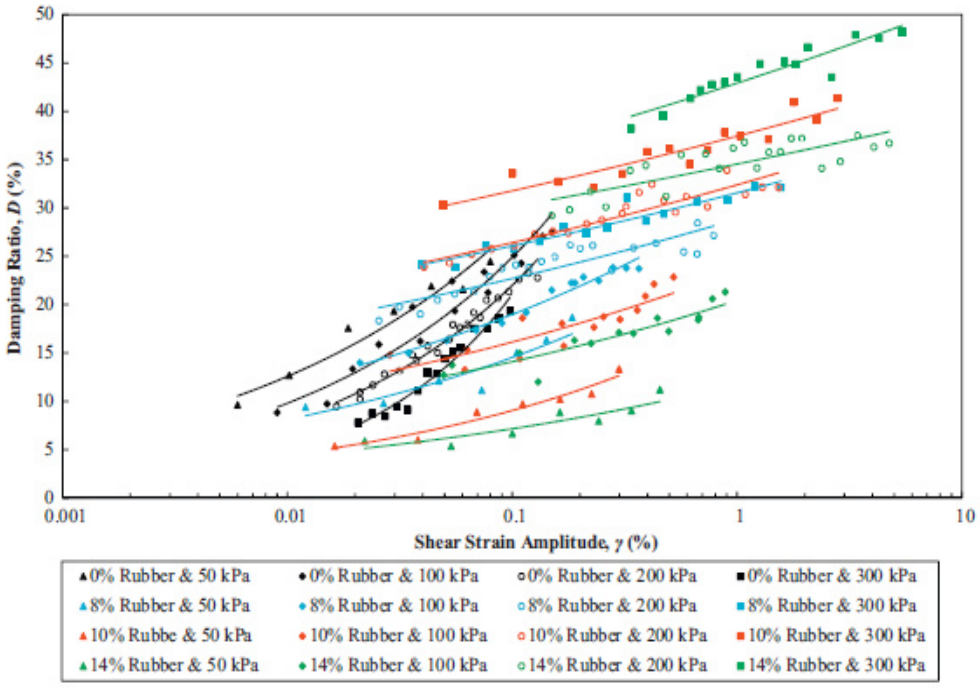

Figure 4.8: Damping ratio versus shear strain amplitude for 0.0, 8, 10 and 14% granulated rubber and the variation of confining pressures. (Nakhaei et al., 2012)

Figure 4.7 shows that for 50 and 100 kPa, damping ratio decreases with an increase of rubber content. However, for 200 and 300 kPa, this trend is opposite. This behaviour can be explained that; for low confining pressures (50 and 100 kPa), elastic strain increases with an increase of rubber content due to its high elastic deformation capacity so it causes to decrease in damping ratio. On the other hand for high confining pressures (200 and 300 kPa); during the application of deviator stress, relative displacement increases because of the inflexibility of rubber grains which were pressed so it causes to increase in both plastic strain and damping ratio. (Nakhaei et al., 2012)

Figure 4.8 shows that for soil without rubber content, the damping ratio decreases with an increase of confining pressure. However, damping ratio increases with an increase of confining pressure for the soils with granulated rubber inclusion. This behaviour may be explained that, increasing confining pressure causes to compression of granulated rubber which becomes inflexible. As mentioned before; during the application of deviator stress, slippage of the soil grains on each other increases so it causes to increase in both plastic strain and damping ratio. (Nakhaei et al., 2012)

Also the effect of confining pressure on damping increases as the rubber content increases because at high confining pressures, the mixture has more plastic strain and at low confining pressures, the mixture has more elastic strain. (Nakhaei et al., 2012)

Senetakis et al.(2011) have a research about the dynamic properties of dry sand/rubber (SRM) and gravel/rubber (GRM) mixturesin a wide strain range of shear strains. High-amplitude resonant column tests were performed on the dry mixtures with high relative densities. Specimens have 71.1 mm diameter and 142.2 mm height and the rubber contents are ranging from 0% to 35%. Fluvial sand of sub-rounded to rounded particles are named as C2D03, C3D06, C2D1 and quarry sandy gravel of sub-angular to angular particles are named as C2D3, C6D3, C13D3 and C1D8. Also uniform rubber materials are named as R03, R06, R2 and R3. The mean grain size (D_{50}) of solids and rubbers is in a range of 0.30-8.0 mm and 0.30-3.0 mm, respectively. And the uniformity coefficient (C_u) for solids and rubbers is approximetely in a range of 1.0-13 and 2.0-3.0, respectively. 'Parent' materials used for tested mixtures are summarized in Table 4.6 and 4.7.

Table 4.6: Parent sandy and gravelly soils used as physical part of the mixtures(G_s=2.67 g/cm^3) (Senetakis et al., 2011)

No.	Code name of material	Initial soil	Classification[a]	Gravel content (%)	D_{max} (mm)	D_{50}(mm)	C_u[b]	C_c[c]
1	C2D03	Fluvial sand[d]	SP	0	0.25–0.43	0.27	1.58	0.93
2	C3D06	Fluvial sand	SP	0	0.85–2.00	0.56	2.76	1.23
3	C2D1	Fluvial sand	SP	0	0.85–2.00	1.33	2.13	1.01
4	C2D3	Quarry sandy gravel[e]	SP	15	4.75–6.35	3.00	2.45	1.10
5	C1D8	Quarry sandy gravel	GP	100	6.35–9.53	7.80	1.22	0.94
6	C6D3	Quarry sandy gravel	SP-SW	30	6.35–9.53	2.90	5.95	1.19
7	C13D3	Quarry sandy gravel	SP-SW	40	6.35–9.53	3.00	12.50	0.94

[a] [39].
[b] $C_u = D_{60}/D_{10}$.
[c] $C_c = D_{30}^2/(D_{60} \times D_{10})$.
[d] Sub-rounded to rounded particles.
[e] Sub-angular to angular particles.

Table 4.7: Parent rubber materials used as synthetic part of the mixtures (G_s=1.10 g/cm^3) (Senetakis et al., 2011)

No.	Code name of material	Classification[a]	D_{max} (mm)	D_{50} (mm)	C_u[b]	C_c[c]
1	R03	Granulated rubber	0.85–2.00	0.34	1.95	0.87
2	R06	Granulated rubber	2.00–4.75	0.40	2.65	0.85
3	R2	Granulated rubber	2.00–4.75	1.50	1.81	0.96
4	R3	Granulated rubber	4.75–6.35	2.80	2.29	1.18

[a] [40].
[b] $C_u = D_{60}/D_{10}$.
[c] $C_c = D_{30}^2/(D_{60} \times D_{10})$.

The grain size distribution curves of the 'parent' materials are shown in Figures 4.9 and 4.10.

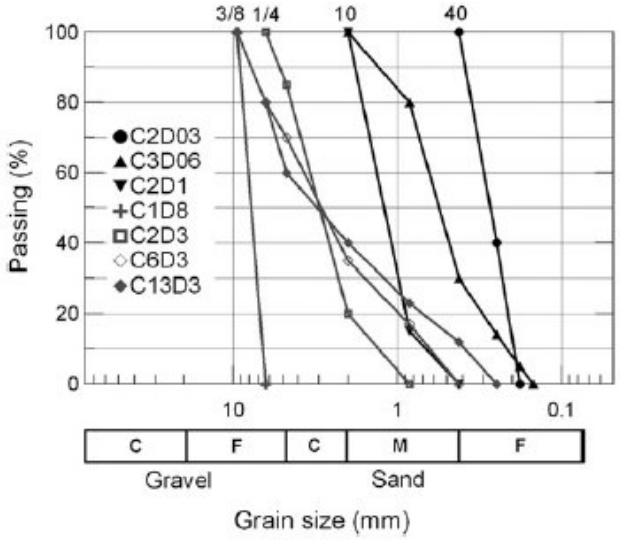

Figure 4.9: Grain size distribution curves of 'parent' sandy and gravelly soils (Senetakis et al., 2011)

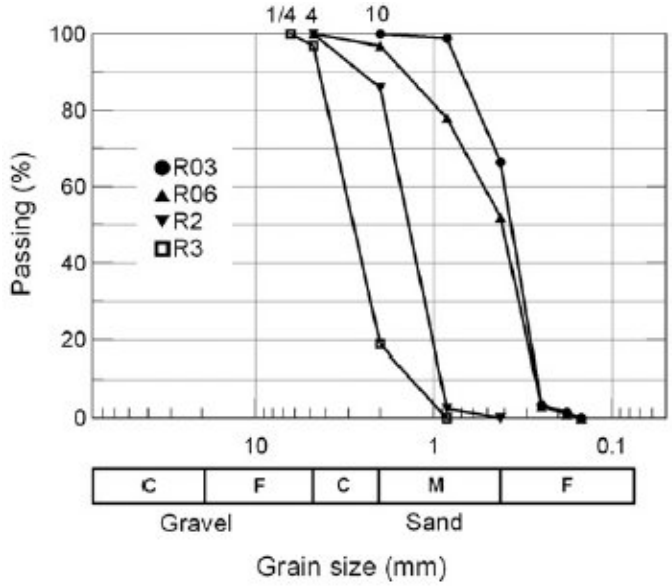

Figure 4.10: Grain size distribution curves of 'parent' granulated rubber materials(Senetakis et al., 2011)

Torsional resonant column tests were applied of fourty-one dry specimens. Shear strain amplitudes (γ) are ranging from $2x10^{-4}$ % to $3x10^{-1}$%, mean confining pressures (σ'_m) are ranging from 25 to 400 kPa and rubber contents are ranging from 0% to 35%. It must be noted that, rubber content of 35% by weight corresponds to rubber content about 55-60% by mixture volume. Testing programs are summarized in Table 4.8 and 4.9.

Table 4.8: High-amplitude torsional RC testing program (Senetakis et al., 2011)

No.	Mixture group	$D_{50,s}/D_{50,r}$[a]	Rubber content by mixture weight (%)					
			0	5	10	15	25	35
1	C2D03-R3[b]	1:10	●	●	●	●	●	●
2	C2D03-R03	1:1		●		●	●	
3	C3D06-R3	1:5	●	●	●	●	●	●
4	C2D1-R3	1:2	●			●	●	●
5	C2D3-R3	1:1	●	●	●	●	●	●
6	C2D3-R06	5:1		●		●	●	
7	C1D8-R2	5:1	●	●		●	●	
8	C6D3-R3	1:1	●	●		●		●
9	C13D3-R3	1:1	●	●		●	●	●

[a] Ratio of mean grain size of soil versus rubber solids.
[b] 'Parent' soil: C2D03, 'Parent' rubber: R3.

Table 4.9: High-amplitude torsional RC testing program: code names and data of dry 71.1 x 142.2 mm specimens (Senetakis et al., 2011)

No.	Specimen code	Rubber content[a] (%)	γ_d[b] (kN/m^3)	σ_m'[c] (kPa)	γ_{tA}[d] (%)
1	C2D03[f]	0	15.8	50, 100, 200	4.8×10^{-4}–5.2×10^{-4}
2	C2D03-R3-95/5[g]	5	15.4	50, 100, 200, 400	4.3×10^{-4}–6.7×10^{-4}
3	C2D03-R3-90/10	10	14.8	50, 100, 200	8.1×10^{-4}–9.2×10^{-4}
4	C2D03-R3-85/15	15	14.2	50, 100, 200, 400	6.9×10^{-4}–8.1×10^{-4}
5	C2D03-R3-75/25	25	13.4	50, 100, 200	1.5×10^{-3}–1.6×10^{-3}
6	C2D03-R3-65/35	35	12.4	25, 50, 100	1.8×10^{-3}–2.2×10^{-3}
7	C2D03-R03-95/5	5	14.6	50, 100, 200	5.4×10^{-4}–6.7×10^{-4}
8	C2D03-R03-85/15	15	13.1	50, 100	7.9×10^{-4}–2.1×10^{-3}
9	C2D03-R03-75/25	25	11.3	25, 50, 100	2.4×10^{-3}–3.4×10^{-3}
10	C3D06[f]	0	16.5	25, 50, 100, 200	4.8×10^{-4}–7.0×10^{-4}
11	C3D06-R3-95/5	5	16.4	50, 100, 200	6.2×10^{-4}–7.1×10^{-4}
12	C3D06-R3-90/10	10	15.3	50, 100, 200, 400	1.8×10^{-4}–5.0×10^{-4}
13	C3D06-R3-85/15	15	14.9	50, 100, 200, 400	3.2×10^{-4}–4.3×10^{-4}
14	C3D06-R3-75/25	25	13.9	50, 100, 200, 400	6.9×10^{-4}–9.1×10^{-4}
15	C3D06-R3-65/35	35	12.6	50, 100, 200	1.1×10^{-3}–1.3×10^{-3}
16	C2D1[f]	0	16.8	50, 100, 200	4.2×10^{-4}–5.6×10^{-4}
17	C2D1-R3-85/15	15	14.3	50, 100, 200	6.1×10^{-4}–7.8×10^{-4}
18	C2D1-R3-75/25	25	13.0	50, 100, 200	2.3×10^{-3}–2.5×10^{-3}
19	C2D1-R3-65/35	35	12.4	50, 100, 200, 400	5.2×10^{-3}–5.5×10^{-3}
20	C2D3[f]	0	16.3	50, 100	4.0×10^{-4}–4.1×10^{-4}
21	C2D3-R3-95/5	5	15.4	100, 200	4.0×10^{-4}–4.2×10^{-4}
22	C2D3-R3-90/10	10	14.5	50, 100, 200, 400	6.0×10^{-4}–6.8×10^{-4}
23	C2D3-R3-85/15	15	13.7	50, 100, 200	5.2×10^{-4}–8.6×10^{-4}
24	C2D3-R3-75/25	25	12.6	50, 100, 200, 400	1.4×10^{-3}–1.8×10^{-3}
25	C2D3-R3-65/35	35	12.1	50, 100, 200	2.5×10^{-3}–2.7×10^{-3}
26	C2D3-R06-95/5	5	16.4	50, 100, 200	1.9×10^{-4}–2.5×10^{-4}
27	C2D3-R06-85/15	15	15.4	50, 100	4.8×10^{-4}–4.8×10^{-4}
28	C2D3-R06-75/25	25	14.2	50, 100	1.0×10^{-3}–1.4×10^{-3}
29	C1D8[f]	0	15.4	25, 50, 100, 200	3.5×10^{-4}–7.2×10^{-4}
30	C1D8-R2-95/5	5	15.6	25, 50, 100, 200	7.4×10^{-4}–9.3×10^{-4}
31	C1D8-R2-85/15	15	14.9	25, 50, 100	6.2×10^{-4}–7.3×10^{-4}
32	C1D8-R2-75/25	25	13.8	50, 100, 200	1.5×10^{-3}–1.6×10^{-3}
33	C6D3[f]	0	17.7	50, 100, 200	2.8×10^{-4}–3.5×10^{-4}
34	C6D3-R3-95/5	5	16.6	50, 100, 200	2.5×10^{-4}–2.8×10^{-4}
35	C6D3-R3-85/15	15	14.3	100, 200, 400	4.4×10^{-4}–4.6×10^{-4}
36	C6D3-R3-65/35	35	12.0	100, 200	1.4×10^{-3}–1.5×10^{-3}
37	C13D3[f]	0	18.1	50, 100, 200	1.4×10^{-4}–4.4×10^{-4}
38	C13D3-R3-95/5	5	16.9	50, 100, 200	4.4×10^{-4}–5.3×10^{-4}
39	C13D3-R3-85/15	15	15.3	50, 100, 200	1.1×10^{-3}–1.2×10^{-3}
40	C13D3-R3-75/25	25	13.7	50, 100	8.5×10^{-4}–2.0×10^{-3}
41	C13D3-R3-65/35	35	12.7	50, 100	3.8×10^{-3}–4.0×10^{-3}

[a] By mixture weight.
[b] Initial dry unit weight at $\sigma_m'=25$ kPa.
[c] Mean confining pressure where high-amplitude tests were performed.
[d] Shearing strain amplitude where G_O and DT_O are defined in this study.
[e] Relative papers where representative results or analytical relationships have been presented.
[f] Specimens of clean soils.
[g] Mixture composed of the sand C2D03 and the rubber R3 with 5% rubber content.

Equation (4.1) is given for the small-strain damping ratio ($DT_{o,mix}$) of SRM and GRM and it is a function of confining pressure (σ'_m) and the corresponding initial damping ratio of the mixture at σ'_m=100 kPa ($DT_{o,mix,100}$). Equation (4.2) is given for the correlation of $DT_{o,mix,100}$ with the corresponding small-strain damping ratio of the soil which has 0% rubber content at σ'_m=100 kPa ($DT_{o,soil,100}$) and a linear function of

the rubber content ($F(pr_d)$) which is also given as Eq. (4.3). The constant values of Equations (4.1) and (4.3) are given in Tables 4.10 and 4.11, respectively.

$$DT_{O,mix} = DT_{O,mix,100} \times A_D \times (\sigma'_m)^{n_D} \quad \textbf{(4.1)}$$

$$DT_{O,mix,100} = DT_{O,soil,100} \times F(pr_d) \quad \textbf{(4.2)}$$

$$F(pr_d) = A_6 \times (pr) + A_7 \quad \textbf{(4.3)}$$

Table 4.10: Parameters for the estimation of the small-strain damping ratio of the SRM and GRM (Senetakis et al., 2011)

No.	Mixture group	A_D	n_D
1	$C_{u,s} < 5$	1.750	−0.12
2	$C_{u,s} > 5$	2.749	−0.21

Table 4.11: Parameters for the estimation of the function $F(pr_d)$ (Senetakis et al., 2011)

No.	Mixture group	A_6	A_7
1	$D_{50,s} \ll D_{50,r}$	0.1004	1
2	$D_{50,s} \approx D_{50,r}$	0.1487	1
3	$D_{50,s} \gg D_{50,r}$	0.3683	1

Figure 4.11 presents the damping values of clean sandy and gravelly soils while Figure 4.12 presents the all experimental data of SRM and GRM. In both figures, curves proposed by Menq (2003) for clean sands and gravels are plotted as a comparison. Menq (2003) indicates that with increasing confining pressure and decreasing coefficient of uniformity, DT-logγ curves of granular soils become more linear.

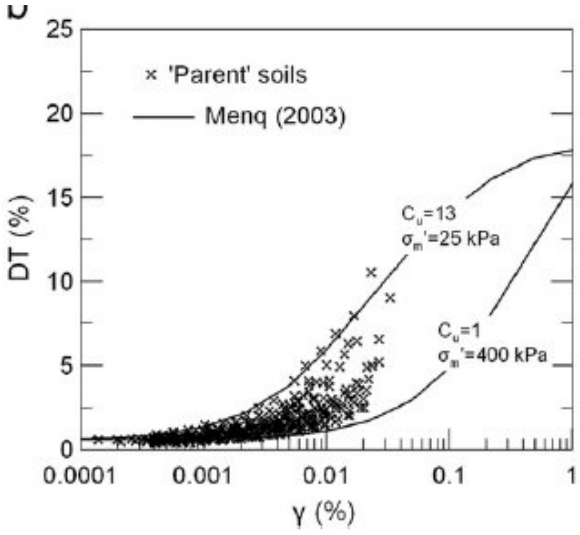

Figure 4.11: Synopsis of the experimental DT-logγ values of the tested clean sandy and gravelly soils (Senetakis et al., 2011)

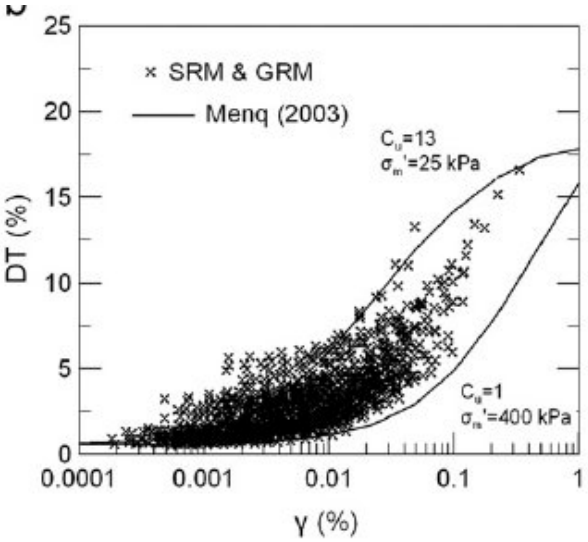

Figure 4.12: Synopsis of the experimental DT-logγ values of the tested SRM and GRM (Senetakis et al., 2011)

To examine the shear strain amplitude and the mean confining pressure effect on the DT values, the results of three specimens of mixture group C1D8-R2 with rubber content of 0%, 15% and 25% by mixture weight are presented in Figures 4.13, 4.14 and 4.15, respectively. Also curves for sands proposed by Seed et al. (1986) are shown in the same figures. As expected, the increase of shear strain amplitude increases the damping. As the mean confining pressure increases DT values are slightly decrease and at the same shear strain amplitude, increasing of σ'_m leads to more 'linear' behaviour. (Senetakis et al., 2011)

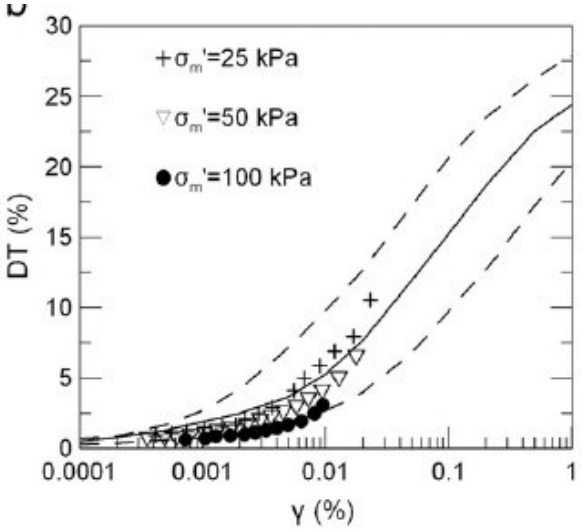

Figure 4.13: Effect of shear strain amplitude, γ, and confining pressure, σ'_m, on DT of clean gravel C1D8 (Senetakis et al., 2011)

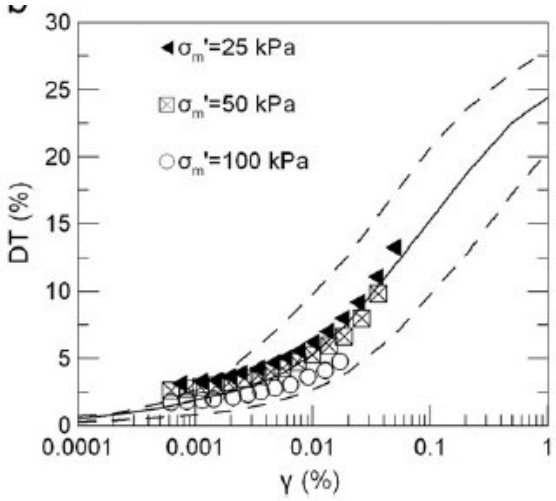

Figure 4.14: Effect of shear strain amplitude, γ, and confining pressure, σ'_m, on DT of GRM C1D8-R2-85/15 having 15% rubber content by mixture weight (Senetakis et al., 2011)

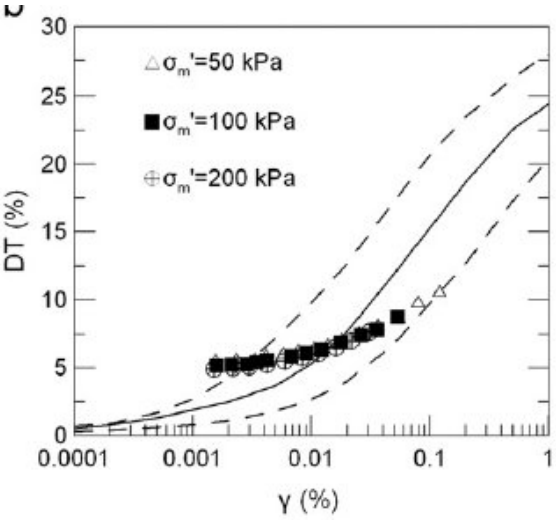

Figure 4.15: Effect of shear strain amplitude, γ, and confining pressure, σ'_m, on DT of GRM C1D8-R2-75/25 having 25% rubber content by mixture weight (Senetakis et al., 2011)

To examine the rubber content effect on the DT values which are normalized (DT-DT_O) to eliminate the effect of DT_O ; in Figure 4.16 and 4.17, the mixture groups C1D8-R2 and C6D3-R3 at σ'_m=100 kPa and in Figure 4.18, the mixture group C2D03-R03 at σ'_m=50 kPa are presented.

With increasing of rubber content, DT-logγ curves are more linear shape especially for rubber content equal or higher than 15% by mixture weight. It can be also said that the effect of σ'_m on DT-logγ curves decreases as the rubber content increases for SRM and GRM. (Senetakis et al., 2011)

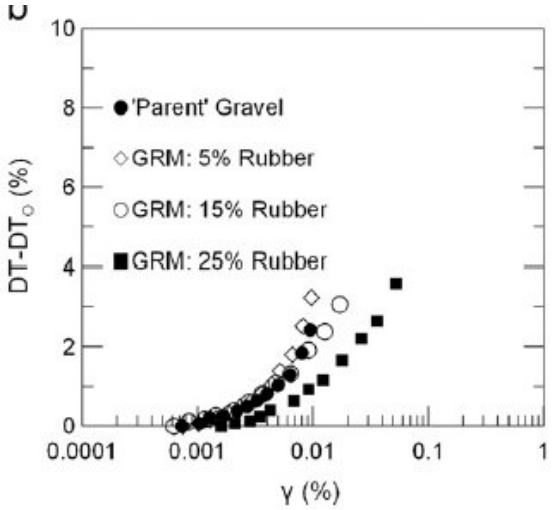

Figure 4.16: Effect of rubber content on DT-logγ curves mixture group C1D8-R2 at σ'_m=100 kPa (Senetakis et al., 2011)

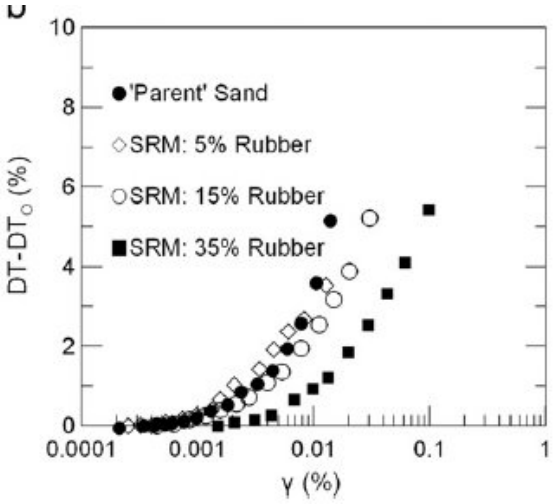

Figure 4.17: Effect of rubber content on DT-logγ curves mixture group C6D3-R3 at σ'_m=100 kPa (Senetakis et al., 2011)

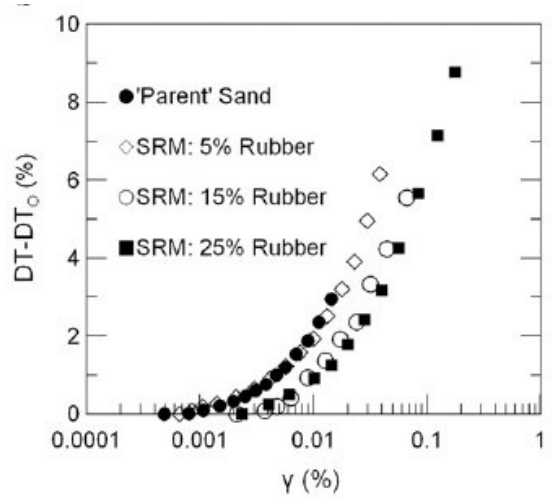

Figure 4.18: Effect of rubber content on DT-logγ curves mixture group C2D03-R03 at σ'_m=50 kPa (Senetakis et al., 2011)

Previous study of Senetakis et al. (2012) additionally examines fully saturated specimens. Dry soil and rubber materials, the range of rubber content and mean confining pressure are exactly the same with Senetakis et al. (2011). Summarization of these materials can be seen in Tables 4.6 to 4.9 and in Figures 4.9 and 4.10. Also for Senetakis et al. (2012), testing program on dry and saturated specimens is shown in Table 4.12. DT-logγ curves of the mixture groups C2D03-R2 and C3D06-R06 with rubber contents between 0% and 15% at σ'_m=100 kPa are presented in Figure 4.19. Seed et al. (1986) curves for sandy soils are also plotted.

Table 4.12: High-amplitude torsional resonant column testing program on dry and saturated specimens (Senetakis et al., 2012)

	Specimen Code	Rubber Content (%)[a]	γ_d (kN/m^3)[b]	σ'_m (kPa)[c]	γ_{LA} to γ_{HA} (%)[d]
Dry, 71.1 × 142.2	C2D03-D01[e]	0	15.8	50, 100, 200	4.8×10^{-4} to 2.1×10^{-2}
	C2D03-R3-95/5-D01[f]	5	15.4	50, 100, 200, 400	4.3×10^{-4} to 1.8×10^{-2}
	C2D03-R3-90/10-D01	10	14.8	50, 100, 200	8.1×10^{-4} to 4.2×10^{-2}
	C2D03-R3-85/15-D01	15	14.2	50, 100, 200, 400	6.9×10^{-4} to 5.5×10^{-2}
	C2D03-R3-75/25-D01	25	13.3	50, 100, 200	1.5×10^{-3} to 7.4×10^{-2}
	C2D03-R3-65/35-D01	35	12.3	25, 50, 100	1.8×10^{-3} to 1.3×10^{-1}
	C3D06-D01[e]	0	16.5	25, 50, 100, 200	4.8×10^{-4} to 3.3×10^{-2}
	C3D06-R3-95/5-D01	5	16.4	50, 100, 200	6.2×10^{-4} to 1.9×10^{-2}
	C3D06-R3-90/10-D01	10	15.3	50, 100, 200, 400	4.3×10^{-4} to 2.1×10^{-2}
	C3D06-R3-85/15-D01	15	14.9	50, 100, 200, 400	3.2×10^{-4} to 4.0×10^{-2}
	C3D06-R3-75/25-D01	25	13.9	50, 100, 200, 400	6.9×10^{-4} to 2.8×10^{-2}
	C3D06-R3-65/35-D01	35	12.5	50, 100, 200	1.1×10^{-3} to 8.3×10^{-2}
Saturated, 35.7 × 82.2	C2D03-S11[e]	0	15.7	100	1.8×10^{-3} to 7.6×10^{-2}
	C2D03-R2-95/5-S11	5	15.3	100	3.2×10^{-3} to 1.6×10^{-1}
	C2D03-R2-90/10-S11	10	14.3	100	2.3×10^{-3} to 4.6×10^{-1}
	C2D03-R2-85/15-S11	15	13.8	100	2.9×10^{-3} to 5.9×10^{-1}
	C3D06-S11[e]	0	16.1	100	2.8×10^{-3} to 1.4×10^{-1}
	C3D06-R06-95/5-S11	5	15.6	100	4.5×10^{-3} to 1.6×10^{-1}
	C3D06-R06-90/10-S11	10	14.2	100	4.8×10^{-3} to 1.7×10^{-1}
	C3D06-R06-85/15-S11	15	13.8	100	5.4×10^{-3} to 3.8×10^{-1}

[a]By mixture weight.
[b]Initial dry unit weight at $\sigma'_m \approx 5$ kPa.
[c]Mean effective confining pressure where high-amplitude tests were performed.
[d]Range of shearing strain from low to high amplitude tests.
[e]Intact sands.
[f]Mixture composed of the sand C2D03 and the recycled rubber material R3 with 5 % rubber by weight.

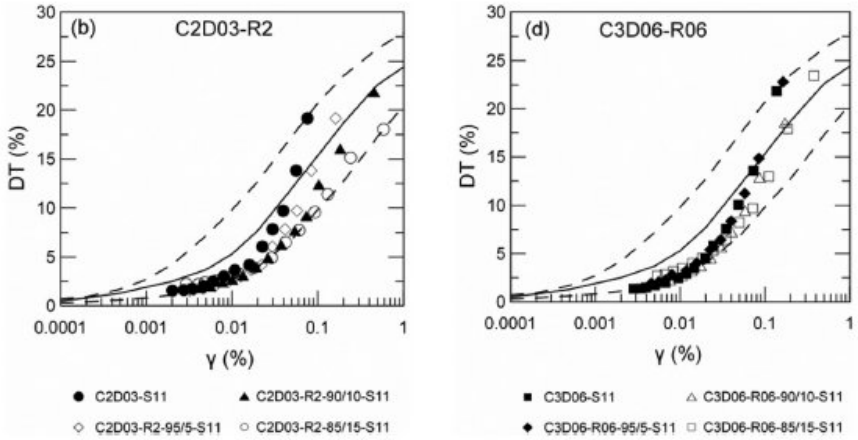

Figure 4.19: Effect of rubber content on DT-logγ curves of saturated specimens (Senetakis et al., 2012)

Figure 4.19 shows that as the rubber content increases, DT-logγ curves become more linear. (Senetakis et al., 2012)

To examine the mean confining pressure effect on the DT values, the results of two dry specimens of mixture group C3D06-R3 with rubber content of 10% and 15% by mixture weight are presented in Figures 4.20. Also curves for sands proposed by Seed et al. (1986) are plotted. Figure 4.20 shows that; at a specific shear stress amplitude, DT values increase as σ'_m decreases like the general trend. (Senetakis et al., 2012)

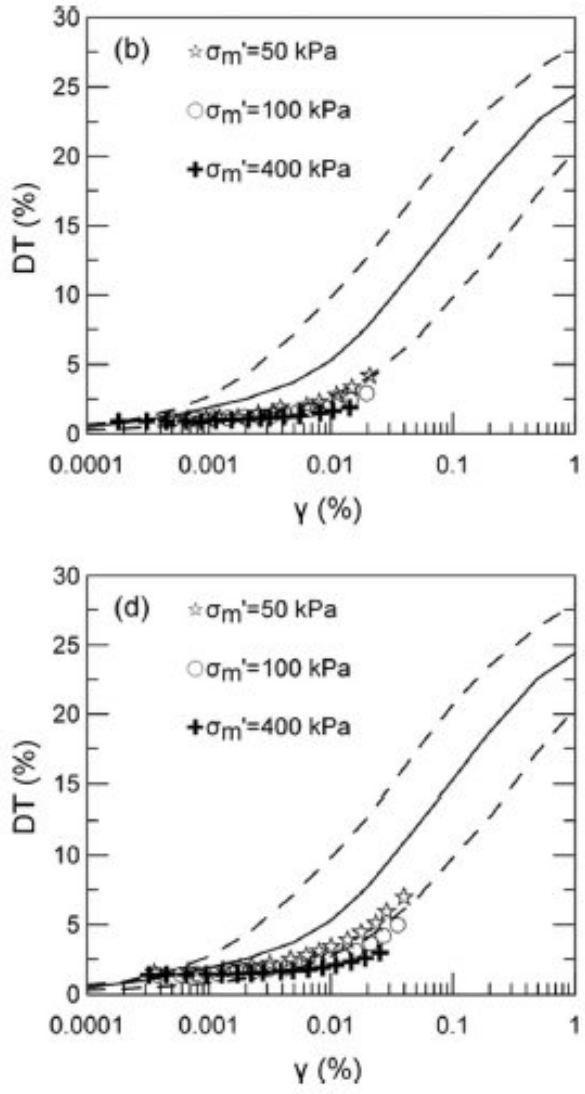

Figure 4.20: Representative DT-logγ curves of dry specimens: (b) specimen C3D06-R3-90/10 and (d) specimen C3D06-R3-85/15 (Senetakis et al., 2012)

To investigate the effect of the ratio of mean grain size of rubber solids versus soil solids ($D_{50,r}$/ $D_{50,s}$) on damping ratio, Ehsani et al. (2015) performed torsional

resonant column and dynamic triaxial experiments. Firoozkooh sandy soil (F161) which were taken from natural round silica sand mines of Firoozkooh township; has a mean grain size of D_{50}=0.22 mm, a coefficient of uniformity of C_u=2.14 and a specific gravity of 2.66. Coarse granular rubber (CR) and fine granular rubber (FR) have a specific gravity of 1.1. The grain-size distribution curves of soil and rubber materials are shown in Figure 4.21.

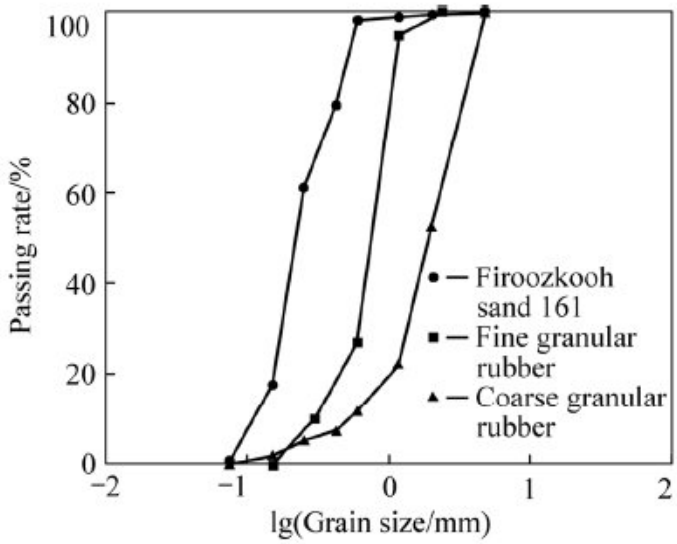

Figure 4.21: Grain-size distribution curves of soil and rubber materials (Ehsani et al., 2015)

Sand-coarse rubber mixture and sand-fine rubber mixture are named as F161-CR and F161-FR, respectively. Cyclic triaxial test samples has 70 mm in diameter and 140 mm and height while resonant column specimens has 70 mm in diameter and 100 mm in height. The maximum dry density and optimum moisture values for mixture groups are shown in Table 4.13.

Table 4.13: Maximum dry density and optimum moisture of mixtures (Ehsani et al., 2015)

No.	Mixture group	ω_{opt}/%			γ_{max}/(kN·m^{-3})		
		10%	15%	30%	10%	15%	30%
1	F161-CR	17.5	18	19.5	16.1	15.9	14.8
2	F161-FR	17.5		19.5	16.5		12.8

Dynamic experiments were performed on nine wet mixtures with rubber content 10% to 30% under 300 kPa confining pressure. Testing program is listed in Table 4.14.

Table 4.14: Cyclic triaxial and torsioal resonant column testing program (Ehsani et al., 2015)

No.	Mixture group	$D_{50,r}/D_{50,s}$	Test type	Rubber content by sand volume (volume fraction)		
				10%	15%	30%
1	F161-CR	11.07	Cyclic triaxial	●	●	
			Resonant column	●	●	●
2	F161-FR	2.13	Cyclic triaxial	●		●
			Resonant column	●		●

As a representative of pure sand, damping curves obtained by Kokusho (1980) were illustrated in all figures. For sand-coarse rubber and sand-fine rubber mixtures, the damping variations for mixtures with rubber content 10% to 30% at the same $D_{50,r}/D_{50,s}$ are shown in Figure 4.22 and 4.23, respectively.

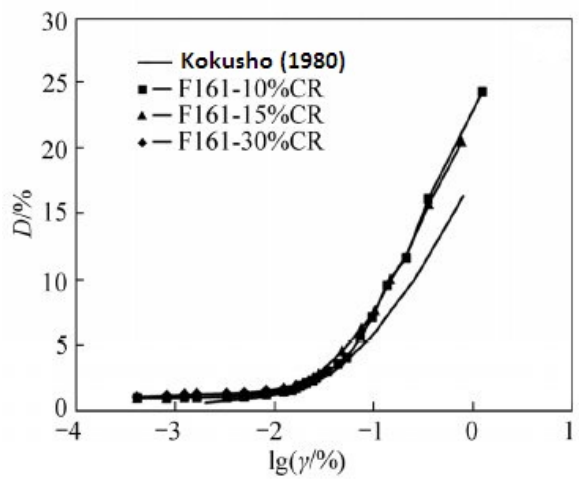

Figure 4.22: Effect of rubber percentage on D-lgγ of mixtures having $D_{50,r}/D_{50,s}$=11.07 (Ehsani et al., 2015)

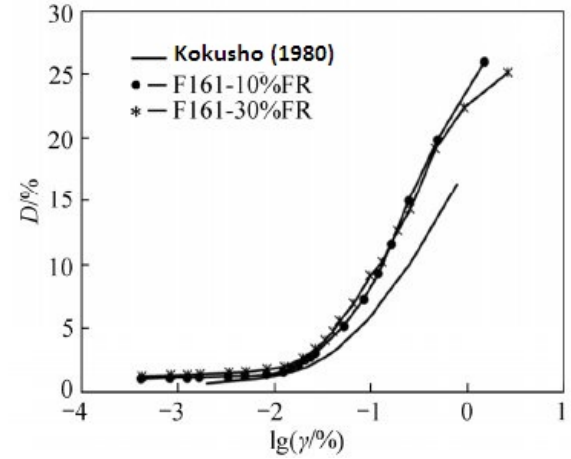

Figure 4.23: Effect of rubber percentage on D-lgγ of mixtures having $D_{50,r}/D_{50,s}$=2.13 (Ehsani et al., 2015)

Figure 4.22 and 4.23 show that, rubber content has no significant effect on damping at the same $D_{50,r}/ D_{50,s}$. However, damping values are significantly higher than those for pure sand. (Ehsani et al., 2015)

Damping curves of mixtures at the rubber contents of 10% and 30% are illustrated for various $D_{50,r}/ D_{50,s}$ in Figures 4.24 and 4.25, respectively.

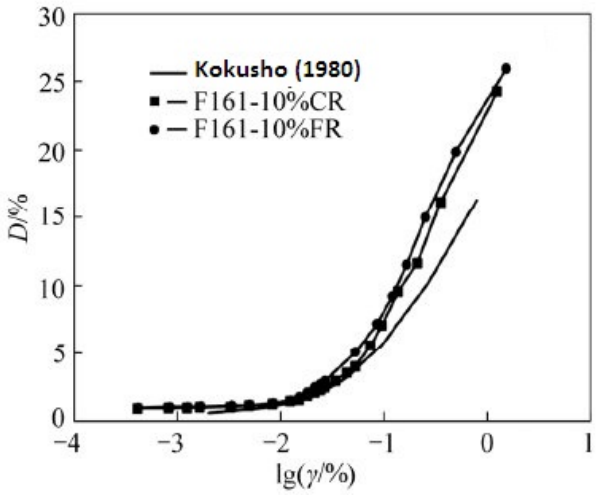

Figure 4.24: Effect of ratio of mean grain size of rubber solids versus soil solids ($D_{50,r}/ D_{50,s}$) on D-lgγ of mixtures having 10% rubber by sand volume (Ehsani et al., 2015)

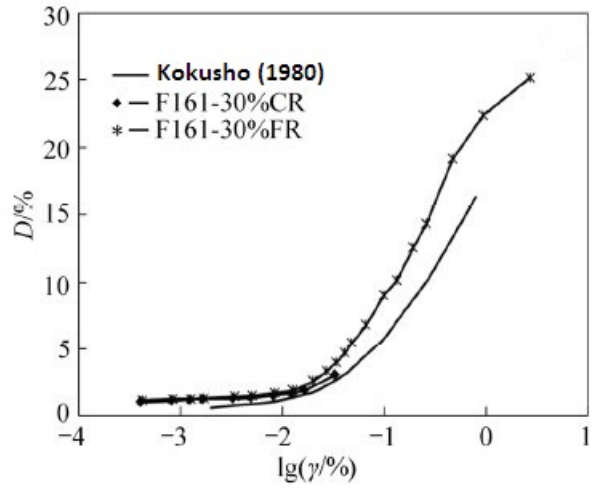

Figure 4.25: Effect of ratio of mean grain size of rubber solids versus soil solids ($D_{50,r}/ D_{50,s}$) on D-lgγ of mixtures having 30% rubber by sand volume (Ehsani et al., 2015)

Figures 4.24 and 4.25 show that; especially in high shear strain amplitudes, as the $D_{50,r}/ D_{50,s}$ increases the damping of the mixture relatively decreases at the same rubber content. Compared to pure sand, damping values are higher as expected. (Ehsani et al., 2015)

4.3 Investigations about Fiber/Soil Mixtures

There are only limited studies about effect of fiber on dynamic soil properties. Amir-Faryar and Aggour (2016) had a study about effect of fiber inclusion on dynamic properties of clay. Resonant column test was performed on mixtures of clay with two different types of fiber: monofilament and fibrillated fiber. Tested soil was synthetic soil Kaolinite which had LL=49, PL=29 and PI=20. Properties of polypropylene fibers are summarized in Table 4.15.

Table 4.15: Properties of polypropylene fibers (Amir-Faryar and Aggour, 2016)

Properties	Monofilament fibre	Fibrillated fibre
Specific gravity	0.91	0.91
Tensile strength	552–758 MPa (80–110 ksi)	552–758 MPa (80–110 ksi)
Denier	6	1500
Thickness	0.030 mm (0.0012 in)	0.48 mm (0.019 in)
Melting point	Above 160 °C (320 °F)	Above 160 °C (320 °F)
Flash point	Above 329 °C (624 °F)	Above 329 °C (624 °F)
Autoignition temperatures	Above 357 °C (675 °F)	Above 357 °C (675 °F)
Electrical and thermal conductivity	Low	Low
Acid and salt resistance	High	High
Alkali resistance	Alkali proof	Alkali proof

Fort his study fiber contents are 0%, 0.2%, 0.4% and 0.6%. Dynamic test results are shown in Figures 4.26, 4.27 and 4.28.

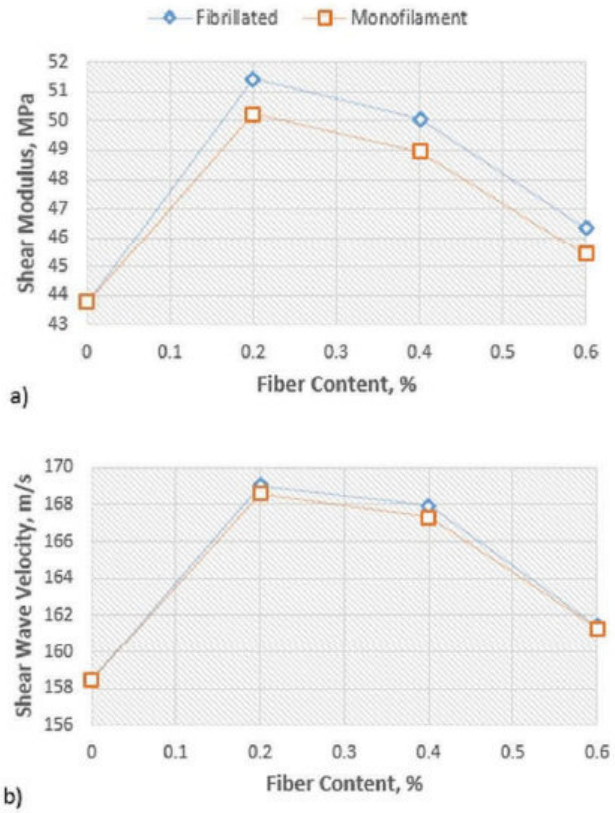

Figure 4.26: a) Maximum shear modulus vs fiber content b)shear wave velocity vs fiber content (Amir-Faryar and Aggour, 2016)

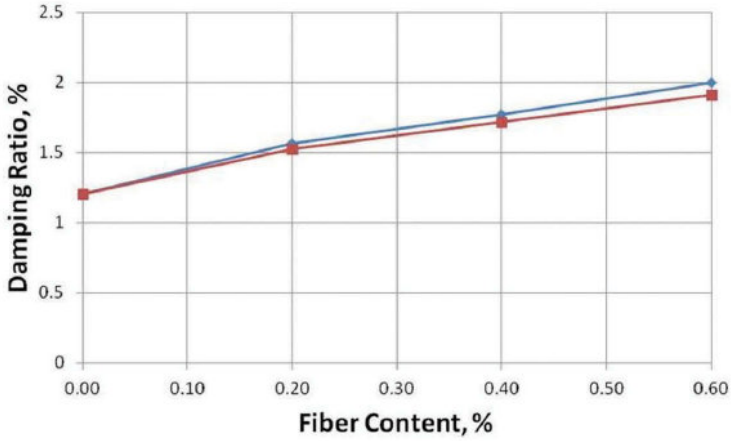

Figure 4.27: Minimum damping ratio vs fiber content (blue line is fibrillated and red line is monofilament fiber) (Amir-Faryar and Aggour, 2016)

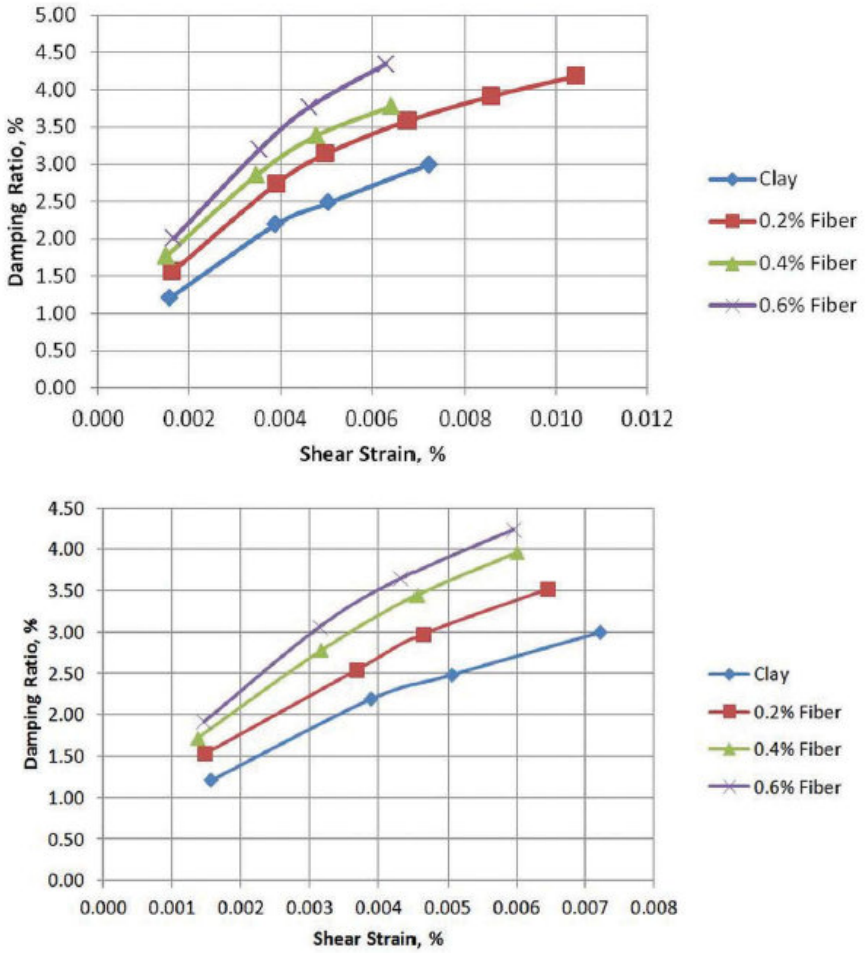

Figure 4.28: Damping vs shear strain for fibrillated fiber (up) and monofilament fiber (below) (Amir-Faryar and Aggour, 2016)

Figure 4.26 shows that fiber content has increasing effect on the maximum shear modulus and the shear wave velocity. And for both fiber types, largest values are belong to 0.2% fiber content mixtures. (Amir-Faryar and Aggour, 2016)

Figure 4.27 and 4.28 show that fiber content has increasing effect on the damping ratio of clay and also damping values increase with the shear strain for both fiber types. (Amir-Faryar and Aggour, 2016)

The effect of fiber content on damping for sands will be examined in the next chapter.

5. RUBBER AND FIBER EFFECT ON DAMPING

5.1 Rubber Effect

In the previous chapter, studies about soil/rubber mixtures are explained. To examine the rubber effect on damping more closely, curves are redrawn and interpreted. Firstly, Nakhaei et. al (2012) data in Figure 4.7 and 4.8 at shear strain γ=0.1% are choosen. Relative density of the mixture is changing from 91.14% to 92.25% which means the mixture is very dense. Fine content of soil is 8.5% and plasticity index is 4. Specific gravities of soil and granulated rubber are 2.65 and 1.1, respectively. Granulated rubber particles are nonspherical shapes the dimensions are tanging from 0.15 to 9.5 mm. Damping ratio vs. confining pressure and damping ratio vs. granulated rubber curves are drawn in Figure 5.1 and 5.2, respectively.

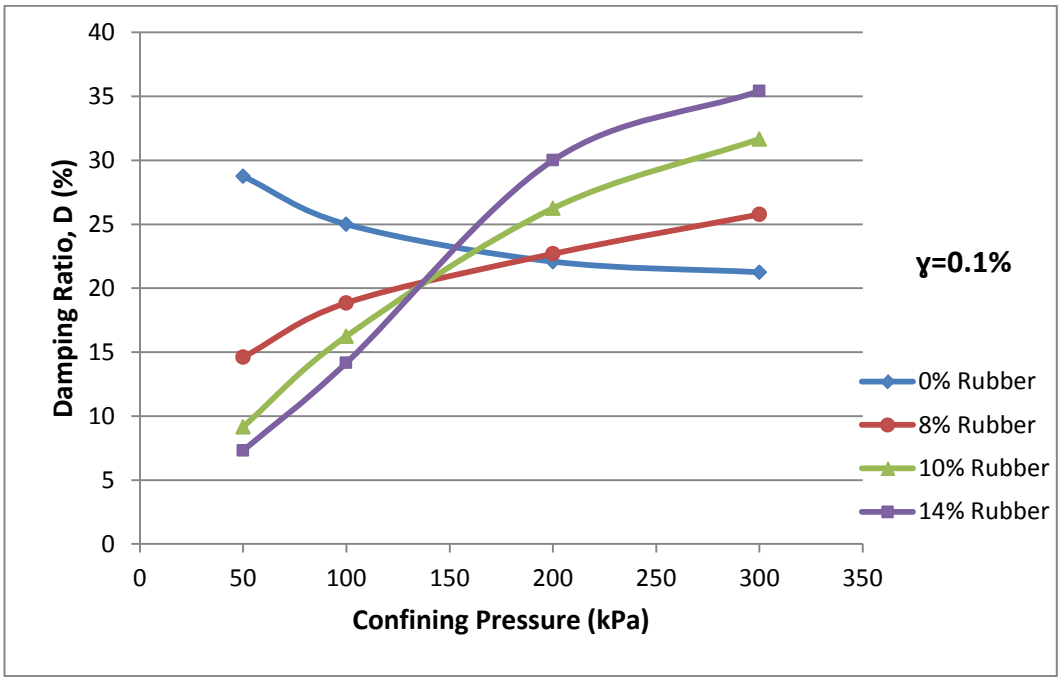

Figure 5.1: Nakhaei et. al (2012) data damping ratio vs. confining pressure

As seen in the Figure 5.1, there is a turning point approximetely at 150 kPa. When the confining pressure is smaller than 150 kPa, damping ratio decreases as the rubber content increases which is unlike the trend. However, when the confining pressure is higher than 150 kPa, damping ratio increases as the rubber content increases which is

expected. It means to see the effect of rubber on damping ratio positively, adequate amount of confining pressure is needed.

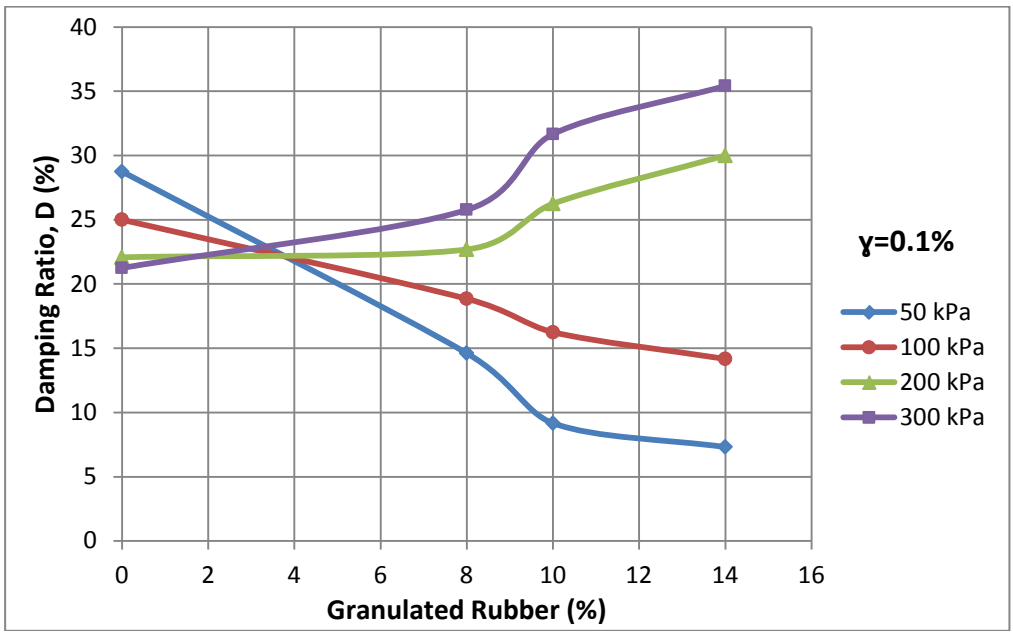

Figure 5.2: Nakhaei et. al (2012) data damping ratio vs. granulated rubber

Figure 5.2 shows that, the soil with no rubber follow the general trend that damping decreases as the confining pressure increases. However, when the rubber content increases, damping increases for confining pressure at 200 and 300 kPa but decreases for confining pressure at 50 and 100 kPa. There is also a turning point approximetely at rubber content 3%.

Senetakis et al. (2012) data in Figure 4.19 at shear strain value γ=0.1% are plotted. C2D03-R2 and C3D06-R06 specimens are saturated. C2D03 and C3D06 are parent soils which are fluvial sands (classified as SP) and have mean grain size 0.27 and 0.56, respectively. R2 and R06 are parent granulated rubbers which have mean grain size 1.50 and 2.80, respectively. Applied confining pressure is 100 kPa. In Table 4.7 and 4.8, properties of materials can be seen. Damping vs. granulated rubber curves are plotted in Figure 5.3.

Figure 5.3 shows that, C2D03-R2 has higher damping than C3D06-R06 at the 0% rubber content.However, with the increase of rubber content, decrease in the damping ratio of C2D03-R2 is higher than C3D06-R06. It means rubber content affects C3D03-R2 more than C3D06-R06. Likewise in Figure 5.2, there is a turning point appromimetely at rubber content 3%.

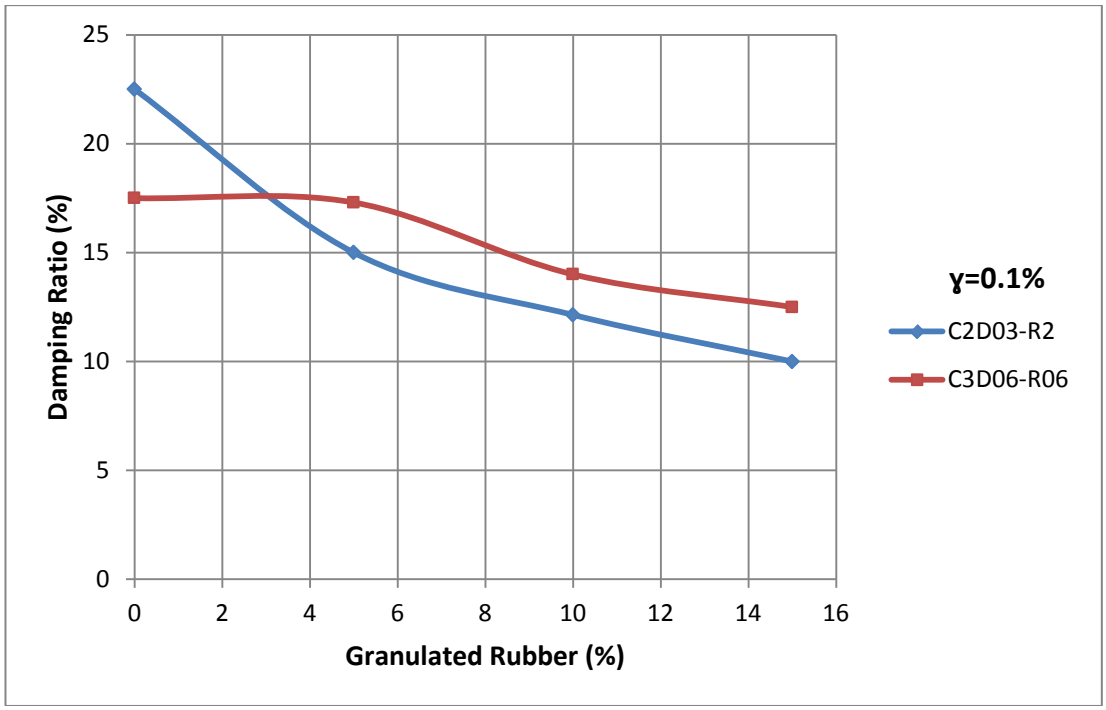

Figure 5.3: Senetakis et al. (2012) data damping ratio vs. granulated rubber

If confining at 100 kPa curve of Nakhaei et al. (2012) is compared with Senetakis et al. (2012), it can be seen that the behaviour is same for all samples; with the increase of rubber content damping decreases. That means confining pressure is not enough to see the effect of rubber content. Also damping values of Nakhaei et al. (2012) is a bit much higher because this sample is more dense.

5.2 Fiber Effect

Torabi (2011) had a study about cyclic and post cyclic static behaviour of fiber reinforced sand which showed that the inclusion of fiber increase the liquefaction resistance and the shear strengt of sand. However fiber effect on damping did not examined. In this chapter the effect of fiber content on damping ratio is interpretted with using the data of Torabi (2011).

In the experimental study, cyclic triaxial tests were performed on Akpınar sand mixed with fiber which is made of pure homopolymer polypropylene and called FORTA MIGHTY-MONO fiber. Akpınar sand and fiber properties are shown in Table 5.1 and 5.2, respectively. And also grain size distibution curve is shown in Figure 5.4. Akpınar sand is classified as SP according to USCS.

Table 5.1: Properties of sand (Torabi, 2011)

Property	Value
Specific Gravity	2.69
Maximum void ratio	0.874
Minimum void ratio	0.558
Permeability (m/s)	$4x10^{-4}$
Sand fraction (%)	99
Fine materials (%)	1
Effective grain size D_{10} (mm)	0.22
D_{60} (mm)	0.35
$D3_0$ (mm)	0.27
Coefficient of uniformity C_u	1.60
Coefficient of curvature C_c	1.00
c (kPa)	0
ø(deg)	40

Table 5.2: Fiber properties (Torabi, 2011)

Color	White
Structure	Single Fiber
Specific Weight	0.91
Length	19 mm
Water Absorption	0
Tensile Stress	570-660 MPa

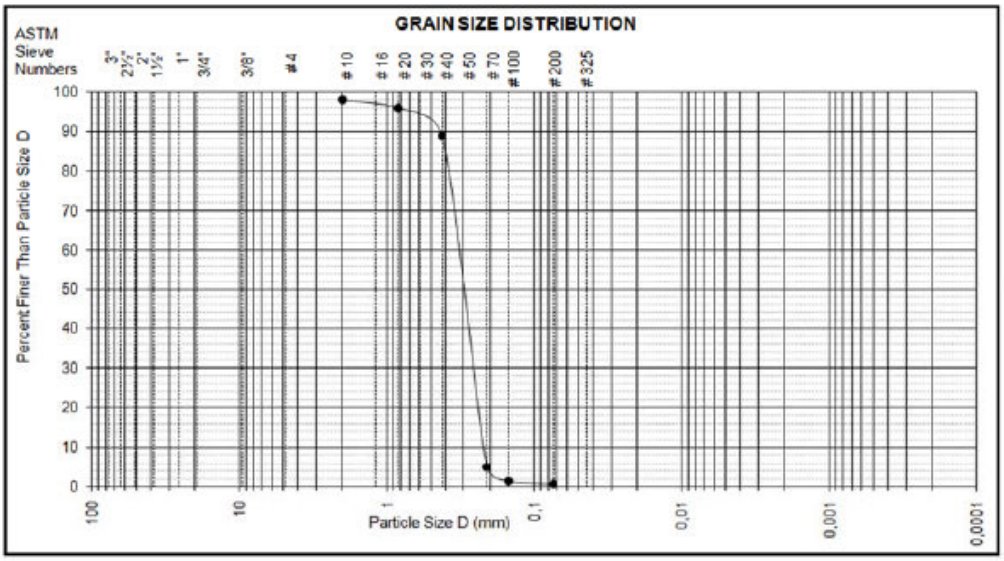

Figure 5.4: Grain size distribution curve of Akpınar sand (Torabi, 2011)

The fiber contents are 0.1%, 0.5% and 1% which are mixed with soil throughly by hand to obtain uniform mixture. The relative density of the mixtures are approximetely 60%. And the applied confining pressure is 100 kPa. Experimental properties of tests which are examined for damping ratio are summarized in Table 5.3.

Table 5.3: Experimental properties of cyclic load on mixtures (Torabi, 2011)

No	A_1 (cm^2)	V_1 (cm^2)	γ_n (kN/m^3)	σ_c (kPa)	CSR ($\pm\Delta\sigma/2\sigma_c$)	NC ±2.5	ΔU (kPa)	B (%)	D_r (%)	Fiber (%)
3.19	19.37	193.22	16.35	100	0.27	8	100	96	60	0
19.83	19.35	193.3	16	100	0.30	6	100	98	60	0.1
34.07	19.32	193.22	16.1	100	0.33	48	100	98	61	0.5
30.33	19.40	193.36	16.11	100	0.35	48	100	98	62	1

From the experimental data of Torabi (2011), damping ratios are calculated with the hysteresis loop method. And also shear modulus values are determined. Damping ratio and shear ratio results for four experiments are shown in Figures 5.5 and 5.6, respectively.

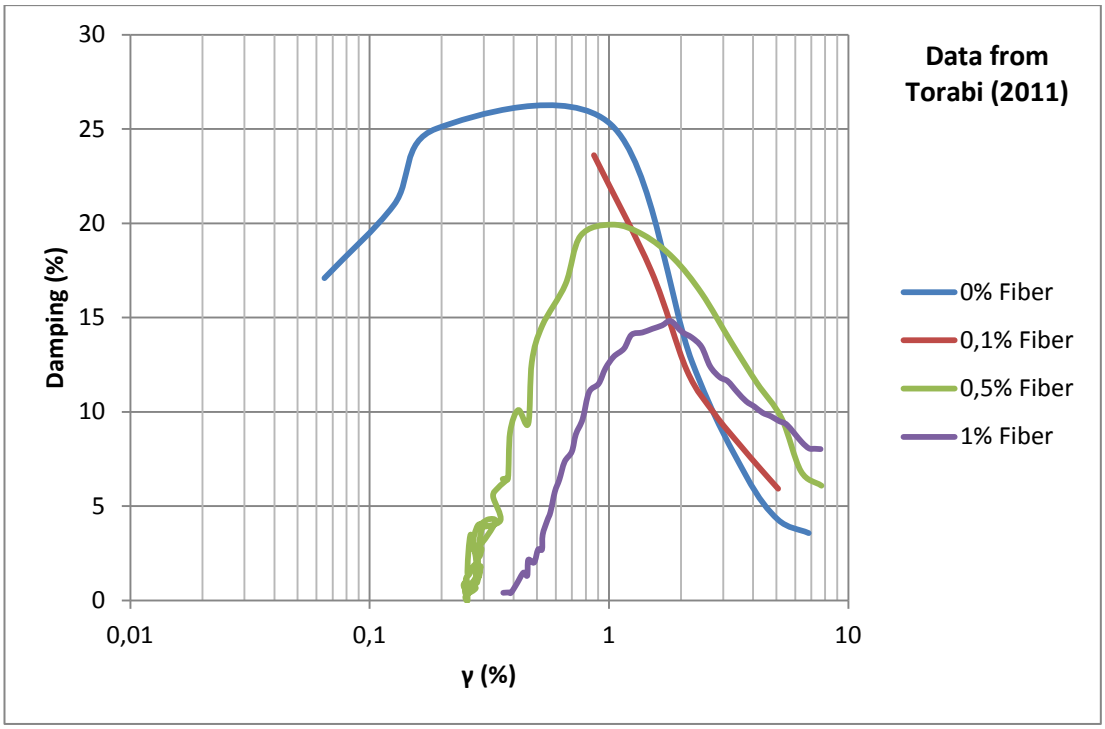

Figure 5.5: Damping vs. γ, Akpınar sand with fiber content of 0%, 0.1%, 0.5% and 1%

As seen in Figure 5.5, damping ratio firstly increases than decreases as the shear strain increases for 0%, 0.5% and 1%. However 0.1% fiber has no increasing effect on damping ratio. Figure 5.6 shows that, G decreases with increase of shear strain as expected. However, fiber content has no significant contribution on shear modulus for large strain levels.

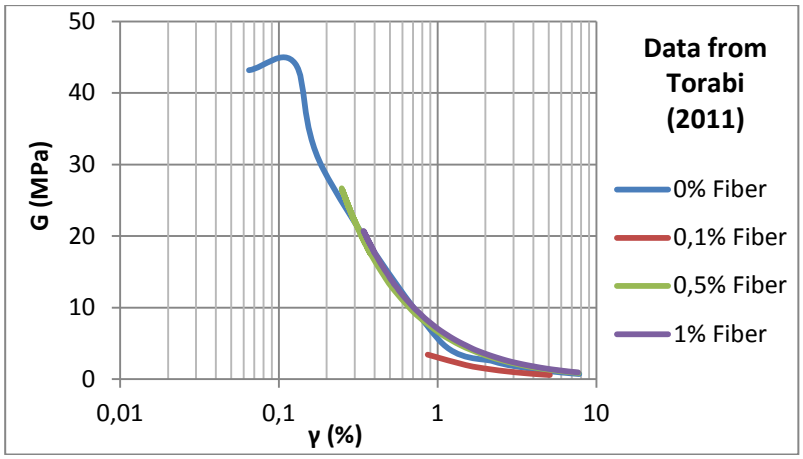

Figure 5.6: G vs. γ, Akpınar sand with fiber content of 0%, 0.1%, 0.5% and 1%

As explained in previous chapters, damping must be increase with shear strain for 0% fiber. To examine this decreasing behaviour in Figure 5.5 closely, hysteresis loops were drawn for cycles which damping ratio is increasing and decreasing separately. Figures 5.7 and 5.8 show the hysteresis loops for 0% fiber content and 0.5% fiber content, respectively.

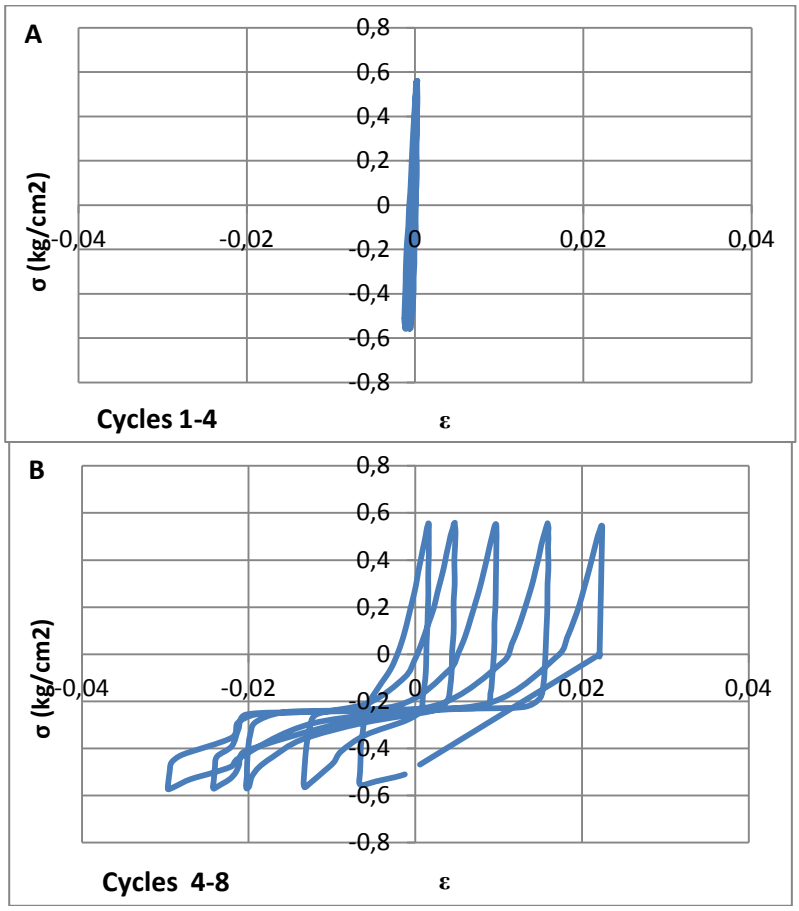

Figure 5.7: Hysteresis loops of Akpınar sand with 0% fiber content (A) cycles 1-4, (B) cycles 4-8 (data: Torabi, 2011)

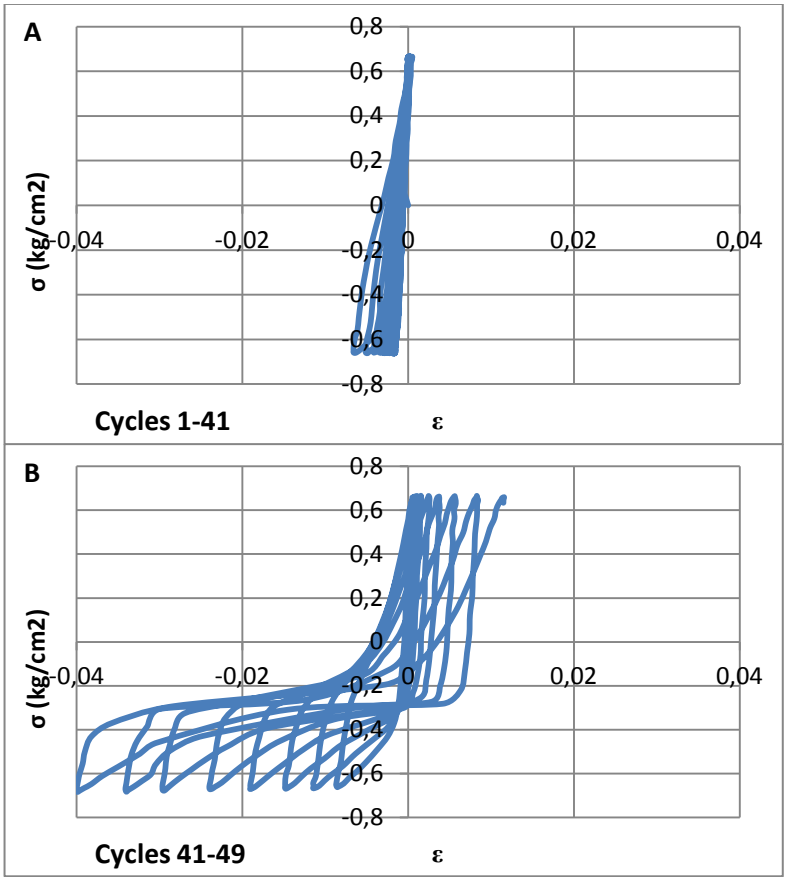

Figure 5.8: Hysteresis loops of Akpınar sand with 0.5% fiber content (A) cycles 1-41, (B) cycles 41-49 (data: Torabi, 2011)

Hysteresis loops can show that at some point there is rubber-membrane penetration effect which takes part in the damping behaviour due to the increasing of excess pore water pressure. Pore water pressure (PWP) curves are illustrated with the damping ratios in Figures 5.9 and 5.10 for 0% fiber and 0.5% fiber, respectively.

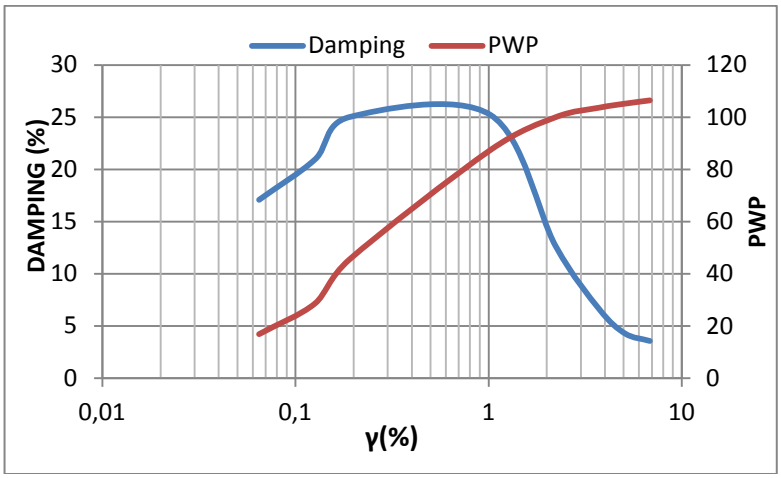

Figure 5.9: Damping vs. γ, PWP vs. γ, Akpınar sand with fiber content of 0% (data: Torabi, 2011)

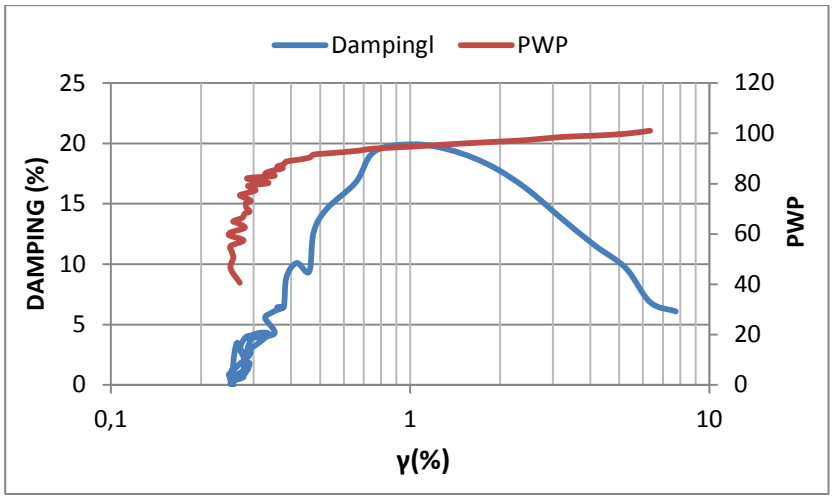

Figure 5.10: Damping vs. γ, PWP vs. γ, Akpınar sand with fiber content of 0.5% (data: Torabi, 2011)

To see clearly the effect of fiber content, Figure 5.11 is illustrated.

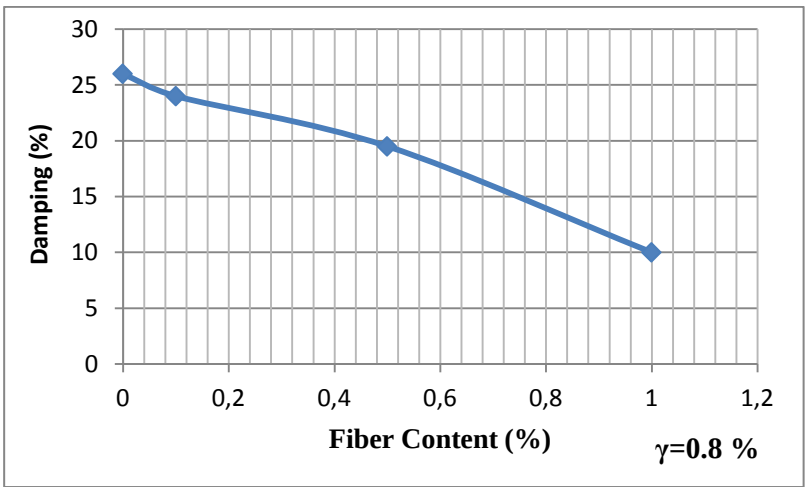

Figure 5.11: Damping vs. fiber content of Akpınar sand at γ=0.8% with confining pressure 100 kPa (data: Torabi, 2011)

It shows that, at 100 kPa confining pressure as the fiber content increases damping ratio decreases as following the trend of Nakhaei et al. (2012) and Senetakis et al. (2012) shown in Figures 5.1, 5.2 and 5.3.

In Figure 5.11, damping values of fiber content 0%, 0.1%, 0.5%, 1% at 100 kPa confining pressure and γ= 0.8% are compared with the damping values of Nakhaei et al. (2012) in Figure 5.1.

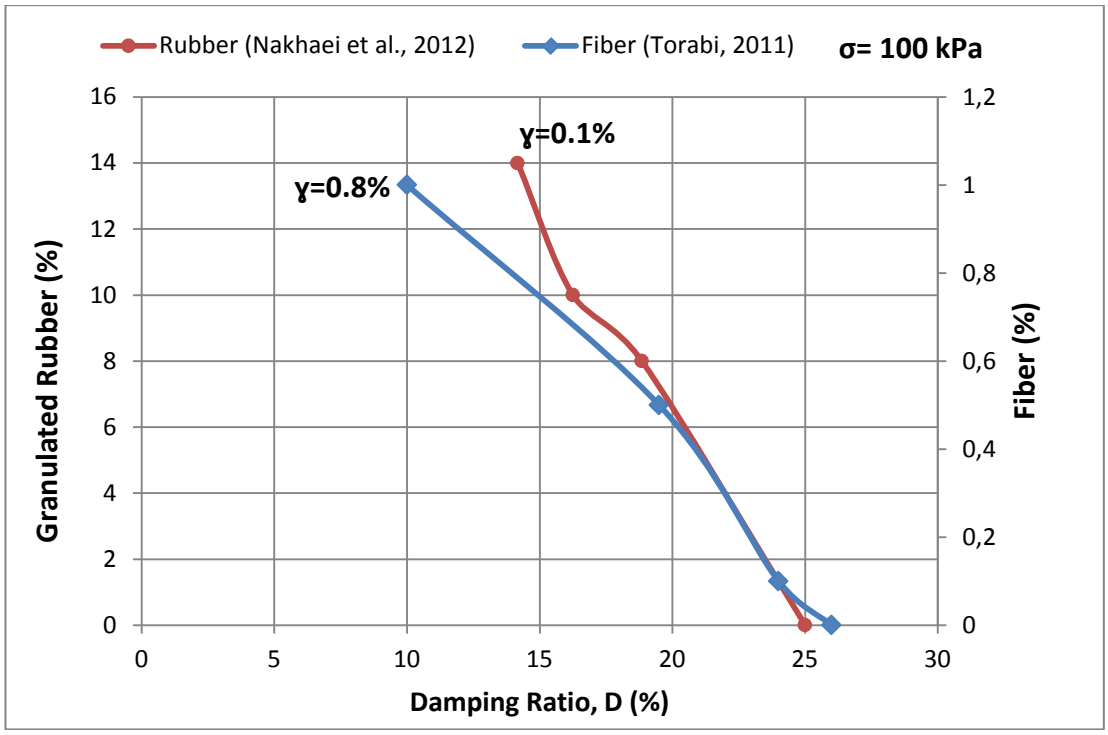

Figure 5.12: Comparison of damping ratio from Nakhaei et. al (2012) data and Torabi (2011) data at 100 kPa confining pressure

6.CONCLUSION

Earthquake is an important fact for humanity. The behaviour of soil under cyclic loading like earthquake is very important and must be analyzed to solve problems. It is possible to decrease the affect of earthquake or other cyclic loadings with improving the dynamic soil properties. In this thesis, factors affecting soil damping are examined through past studies. Soil damping is affected by density, number of cycles, plasticity index, overconsolidation ratio, consolidation stress, compaction stress, saturation, mean grain size and uniformity coefficient. Only relative density and saturation affect soil damping positively. As a possible increasing factor on soil damping, soil mixed with granulated rubber and fiber are analyzed.

Increase of traffic cause to excess waste tire. Rubber is a lightweight material and has high elasticity and good fatique properties. Rubber is already used for engineering applications like backfill material, highway embankments, soil reinforcement etc. Some studies are done on rubber-soil mixtures to investigate the effect on soil stiffness (elasticity and shear modulus) and damping. Results show that rubber soil mixtures have higher damping capacity than soil without rubber. (Zheng-Yi and Sutter, 2000; Nakhaei et al., 2012) However the applied stress has an important affect. As expected, damping ratio decreases as confining pressure increases however rubber-soil mixture the behaviour is opposite. So how bigger the applied stress the damping ratio is higher. According to Nakhaei et al. (2012) curves, adequate confining pressure is 150 kPa to increase the damping ratio for soil-rubber mixtures. If the curves from Nakhaei et al. (212) and Senetakis et al. (2012) at 100 kPa are examined, it can be seen that the damping ratio decreases.

Fibers are used as a reinforcement in contruction materials for improvement of soil properties since prehistoric times. For example in Mesopotamia, straw was adding to mud bricks to provide integrity, control the growth of cracks and improve soil properties. Freitag (1986) examined compacted cohesive soils with fiber inclusion. As a result, inclusion of fiber increases strength and toughness. Also Akbulut et al. (2007) mixed recycled short monofilament fibers in clayey soil which showed

increase in compressive and shear strength of clay. There are only limited studies about effect of fiber on dynamic soil properties. Amir-Faryar and Aggour (2016) had a study about effect of fiber inclusion on dynamic properties of clay. Results show that fiber content has increasing effect on the damping ratio, maximum shear modulus and the shear wave velocity. But it must be noted that the deformation levels are low.

Torabi (2011) had a study about cyclic and post cyclic static behaviour of fiber reinforced sand which showed that the inclusion of fiber increase the liquefaction resistance and the shear strength of sand. However fiber effect on damping did not examined. The effect of fiber content on damping ratio is interpretted with using the experimental data of Torabi (2011).

Results show that shear modulus decreases with increase of shear strain as expected. However, fiber content has no significant contribution on shear modulus for large strain levels. Damping ratio firstly increases than decreases as the shear strain increases for 0%, 0.5% and 1%. However 0.1% fiber has no increasing effect on damping ratio. But damping must be increase with shear strain for 0% fiber. To examine this decreasing behaviour hysteresis loops were drawn for cycles which damping ratio is increasing and decreasing separately. Hysteresis loops can show that at some point there is rubber-membrane penetration effect which takes part in the damping behaviour due to the increasing of excess pore water pressure.

Fiber vs damping ratio curve shows that, at 100 kPa confining pressure as the fiber content increases damping ratio decreases as following the trend of Nakhaei et al. (2012) and Senetakis et al. (2012) for high deformation levels. To comprehend the effect of fiber on damping, further investigations are needed.

REFERENCES

Ahmed, I., Lovell, C.W. (1993) "Rubber soils as lightweight geomaterials." *Lightweight Artificial and Waste Materials for Embankments over Soft Soils, Transportation Research Record,* No. 1422, National Academy Press, Washington, DC, pp.61–70.

Airey, D.W., Wood, D.M. (1987) "An evaluation of direct simple shear tests on clay." *Geotechnique,* Vol.37, No.1, pp. 25-35.

Akbulut, S., Arasan, S. and Kalkan, E. (2007) "Modification of clayey soils using scrap tire rubber and synthetic fibres." *Applied Clay Science,* 38, 23–32

Amir-Faryar, B., Aggour, M.S. (2016) "Effect of fibre inclusion on dynamic properties of clay." *Geomechanics and Geoengineering,* 11:2, 104-113,

Anderson, D.G, Phukunhapkan, A., Douglas, B.J., Martin, G.R. (1983) Cyclic behaviour of six marine clays." *Proc. of the 1983 ASCE Convention,* Session No. 52- Evaluation of Seafloor Soil Properties under Cyclic Loads, Houstan, Texas.

Beatty, J.R. (1981) "Physical properties of rubber compounds." Chapter 10 of *Mechanics of Pneumatic Tires,* S. K. Clark, Ed., U.S. Department of Transportation, National Highway Traffic Safety Admin., Washington, DC 20590, pp. 871–885.

Cho, G.C., and Santamarina, J.C. (2001) "Unsaturated particulate materials-particle level studies." *J. Geotech. Geoenviron. Eng.*, 127(1), 84–96.

Chung, M., Yokel, Y., Drnevich, V.P. (1984) "Evaluation of dynamic properties of sands by resonant column testing." *Geotechnical Testing Journal,* ASTM, Vol.7, No.2, pp.60-69.

Coulter, S.E., Phillips, R. (2003) "Simulating submarine slope instability initiation using centrifuge model testing." Paper ISSMM-062 1st International symposium on submarine mass movements and their consequences, EGS-AGUEUG Joint Assembly Meeting, Nice, Kluwer Academic Publishers, Netherlands.

Dobry, R., Vucetic, M. (1987) "State-of-the-art report: Dynamic properties and response of soft clay deposits." *Proc. Int. Symp. on Geotechnical Engineering of Soft Soils,* Vol. 2, 51-87.

Doroudian, M., Vucetic, M. (1995) "A direct simple shear device for measuring small-strain behavior." *Geotech. Testing J.,* ASTM, 18(1), 69-85.

Drnevich, V.P., Hall, J.R., Jr., Richart, F.E., Jr. (1966) "Large amplitude vibration effects on the shear modulus of sand." University of

Michigan Report to Waterways Experiment Station, Corps of Engineers, U.S. Army Contract DA-22-079-eng-340, Oct., 1966.

Drnevich, V.P., Richart, F.E., Jr. (1970) "Dynamic prestraining of dry sand." *Journal of SMFD*, Proc. of ASCE, Vol.96, SM2, pp. 453-469.

Drnevich, V.P. (1972) "Undrained cyclic shear of saturated sand." *Journal of Soil Mechanics and Foundations Division*, ASCE, 98, SM8, pp. 807- 825.

Drnevich, V.P. (1978) Drnevich resonant column apparatus operating manual.

Drnevich, V.P., Hardin, B.O, Shippy, D.J. (1978) "Modulus and damping of soils by the resonant-column method." *Dyn. Geotech. Testing*, Special Tech. Pub. No. 654, Am. Soc. for Testing and Mat., Philadelphia, Pa., 91-125.

Edil, T.B., Bosscher, P.J. (1994) "Engineering properties of tire chips and soil mixtures." *Geotechnical Testing Journal*, GTJODJ, Vol. 17, No. 4, December 1994, pp. 453–464.

Ehsani, M., Shariatmadari, N., Mirhosseini, S.M. (2015) "Shear modulus and damping ratio of sand-granulated rubber mixtures." *Journal of Central South University*, 22, 3159-3167.

Eleazer, W.E., Barlaz, M.B. (1992) "Technologies for utilization of waste tires in asphalt pavement." *Utilization of Waste Materials in Civil Engineering Construction: Proceedings*, Material Engineering Division, ASCE, New York, Sept. 1992, H. Inyang and K. Bergeson, Eds., pp. 193–201.

Fang, H.Y., Chaney, R.C, Pandit, N.S. (1981) " Dynamic shear modulus of soft silt." *International Conference on Recent Advances in Geotechnical Earthquake Engineering and Soil Dynamics*, Vol. II, pp. 575-580.

Goto, S., Nishio, S., Yoshimi, Y. (1994) "Dynamic properties of gravels sampled by ground freezing." *Ground failures under seismic conditions, Geotech. Spec. Publ. No.* 44, ASCE, Reston, Va., 141 -157.

Goto, S., Suzuki, Y., Nishio, S., Oh-Oka, H. (1992) "Mechanical properties of undisturbed Tone River gravel obtained by in-situ freezing method." *Soils and Found.*, Tokyo, Japan, 32(3), 15-25.

Hara, A., Kiyota, Y. (1976) "Dynamic behaviour of sand in small strain levels." *Proc. of 11th Annual Meeting of JSSMFE*, pp. 331-334 (in Japanese).

Hardin, B.O., Richart, F.E. (1963) "Elastic wave velocities in granular soils." *Journal of Soil Mechanics and Foundations*, ASCE, 89, SM1,33-65.

Hardin, B.O. (1965) "The nature of damping in sands." *J. Soil Mech. and Found. Div.*, ASCE, 91(1), 63-97.

Hardin, B.O., Black, W.L. (1968) "Vibration modulus of normally consolidated clay." *Journal of Soil Mechanics and Foundations*, ASCE, 94, SM2, 353-369.

Hardin, B.O., Drnevich, V.P. (1972) "Shear modulus and damping in soils: design equations and curves." *J. Soil Mech. and Found. Div.,* ASCE, 98(7), 667-692.

Hashiba, T. (1971) "Simple shear apparatus using an inclinometer." *Soils and Foundations,* JSSMFE, Vol.11, No.3, pp. 113-119.

Hatanaka, M., Suzuki, Y., Kawasaki, T., Endo, M. (1988) "Cyclic undrained shear properties of high quality undisturbed Tokyo gravel." *Soil and Found.,* Tokyo, Japan, 28(4), 57 -68.

Hatanaka, M., Uchida, A. (1995) "Effects of test methods on the cyclic deformation characteristics of high quality undisturbed gravel samples." *Static and dynamic properties of gravelly soils. Geotech. Spec. Pub. No.* 56, ASCE, Reston, Va. 136- 16I.

Houbrechts, J., Schevenels, M., Lombaert, G., Degrande, G., Rücker, N., Cuellas, V., Smekol, A. (2011) "The test procedures for the determination of the dynamic soil characteristics." *Railway Induced Vibration Abatament Solutions Collaborative Project*, RIVAS, WP 1.3, Deliverable 1.1, Version 6.

Humphrey, D. N., Sandford, T. C., Cribbs, M. M., and Manion, W. P. (1993) "Shear strength and compressibility of tire chips for use as retaining wall backfill." *Lightweight Artificial and Waste Materials for Embankments over Soft Soils, Transportation Research Record,* No. 1422, National Academy Press, Washington, DC, pp. 29–35.

Hynes, M. E. (1988) "Pore water pressure generation characteristics of gravels under undrained cyclic loadings," *PhD dissertation, Univ. of California,* Berkeley, Calif.

Iida, R., Matsumoto, N., Yasuda, N., Watanabe, K., Sakaino, N., Ohno, K. (1984) "Large-scale tests for measuring dynamic shear moduli and damping ratios of rockfill materials." *Sixteenth Joint Meeting. U.S.Japan Panel on Wind and Seismic Effects,* Washington, D.C.

Ishibashi, I., Zhang, X. (1993) "Unified dynamic shear moduli and damping ratios of sand and clay." *Soils and Foundations,* 33(1): 182-191.

Ishihara, K. (1996) *Soil Behaviour In Earthquake Geotechnics,* Oxford University Press, Great Clerandon Street.

Iwasaki, T., Tatsuoka, F., Takagi, Y. (1976) "Dynamic shear deformation properties of sand for wide strain range." *Report of Civ. Engrg. Inst., No. 1085,* Ministry of Construction, Tokyo, Japan.

Iwasaki, T., Tatsuoka, F. (1977) "Effects of grain size and grading on dynamic shear moduli of sand." *Soils and Foundations,* JSSMFE, Vol.17, No.3, pp. 19-35.

Iwasaki, T., Tatsuoka, F., Takagi, Y. (1978) "Shear modulus of sands under torsional shear loading." *Soils and Foundations,* JSSMFE, Vol.18, No.1, pp.39-56.

Iwasaki, T., Tatsuoka, F., Tokida, K., Yasuda, S. (1978) "A practical method for assessing soil liquefaction potential based on case studies in various sites in Japan." *Proceeding of the 2nd International Conference on Microzonation for Safer Construction- Research and Application*, Vol.2, pp. 885-896.

Jennings, D.C. (1964) "Periodic response of a general yielding structure." *J. Engrg. Mech. Div.*, ASCE, 90(2),131-166.

Khouri, N.Q (1984) "Dynamic properties of soils." Master Thesis, Department of Civil Engineering, Syracuse University.

Kitsunezaki, C. (1982) "Some basic problems of shear wave logging by means of the suspension sonde." *Journal of Mining College*, Akita University, Series A, 6(2), pp. 93-108.

Kim, T.C, Novak, M. (1981) "Dynamic properties of some cohesive soils of Ontario." Canadian Geotechnical Journal, 18, pp. 371-389.

Kokusho, T. (1980) "Cyclic triaxial test of dynamic soil properties for wide strain range." *Soils and Foundations*, Japanese Society of Soil Mechanics and Foundation Engineering, 20(2).

Kokusho, T. (1981) "Dynamic properties of deformation and damping properties of coarse soil for wide range." *Japanese Central Electric Power Research Institude*, Report No. 380002 (in Japanese).

Kokusho, T., Yoshida, Y., Esashi, Y. (1982) "Dynamic properties of soft clay for wide strain range." Soils Found 22(4):1–18.

Kokusho, T. (1987) "In situ dynamic soil properties and their evaluation." *Proceedings of the 8th Asian Regional Conference on Soil Mechanics and Foundation Engineering*, Kyoto, Vol.2, pp. 215-435.

Kokusho, T., Tanaka, Y. (1994). "Dynamic properties of gravel layers investigated by in-situ freezing sampling." *Groundfailures under seismic conditions. Geotech. Spec. Publ. No.* 44, ASCE, Reston, Va., 121-140.

Konno, T., Hatanaka, M., Ishihara, K., Ibe, Y., Iizuka, S. (1994) "Gravelly soil properties evaluation by large scale in-situ cyclic shear tests." *Groundfailures under seismic conditions. Geotech. Spec. Pub/.No.* 44, ASCE, Reston, Va., 177-200.

Kramer, S.L. (1996). *Geotechnical Earthquake Engineering*, Prentice Hall, New Jersey.

Kumar, J., Madhusudhan, B. N. (2011) "Dynamic properties of sand from dry to fully saturated states." Geotechnique, 62(1), 45–54.

Kuribayashi, E., Iwasaki, T., Tatsuoka, F. (1974) "Effects of stress conditions on dynamic properties of sands." *Bulletin Intl. of Seismology and Earthquake Engineering,* Vol. 12, Tokyo, Japan.

Kuribayashi, E., Iwasaki, T., Tatsuoka, F. (1975) " Effect of stress-strain condition on dynamic properties of sand." *Proc. of JSCE*, No.242, October, pp.105-114.

Lee, J.H., Salgado, R., Bernal, A., and Lovell, C.W. (1999) "Shredded tires and rubber-sand as lightweight backfill." *Journal of Geotechnical and Geoenvironmental Engineering,* American Society of Civil Engineers, Vol. 125, No. 2, pp. 132–141.

Lee, M.K.W., Finn, W.D.L. (1982) "Dynamic effective stress response analysis of soil deposits with energy transmitting boundary including assessment of liquefaction potential." *Rev. Dept. of Civ. Eng.*, Soil Mech. Series No. 38, Univ. of British Columbia, Vancouver, Canada.

Leon, J.L, Jaime, A., Rabago, A. (1974) "Dynamic properties of soils-preliminary study." Institude of Engineering, UNAM, (in Spanish).

Leon, J.L, Rufgo, A. (1975) "Dynamic tests on clays from valley of Mexico." *5th Pan American Conference on Soil Mechanics*, Vol.I, pp. 43-53.

Liang, R. Y. and Lee, S. (1996) "Short-term and long-term aging behavior of rubber modified asphalt paving mixture." *Recycled Rubber, Aggregate, and Filler in Asphalt Paving Mixtures, Transportation Research Record,* No. 1530, National Academy Press, Washington, DC, pp. 11–17.

Macky, T.A, Saada, A.S (1984) "Dynamics of anisotropic clays under large strains." *Journal of Geotechnical Engineering*, ASCE, Vol.110, No.4, April, pp.487-504.

Madhusudhan, B.N., Kumar, J. (2013) "Damping of sands for varying saturation" *J.Geotech. Geoenviron. Eng.*, ASCE, 139(9), 1625-1630.

Marcuson, W.F., Wahls, H.E. (1972) "Time effects on dynamic shear modulus of clays." *Journal of Soil Mechanics and Foundations,* ASCE, 98, SM12,1359-1373.

Maupin, G. W., Jr. (1996) "Hot mix asphalt rubber applications in Virginia." *Recycled Rubber, Aggregate, and Filler in Asphalt Paving Mixtures, Transportation Research Record,* No. 1530, National Academy Press, Washington, DC, pp. 18–24.

Menq, F.Y. (2003) "Dynamic properties of sandy and gravelly soils. PhD dissertation, University of Texas at Austin.

Michaels, P. (1998) "In situ determination of soil stiffness and damping" *J.Geotech. Geoenviron. Eng.*, ASCE, 124(8), 709-719

Nakhaei, A., Marandi, S.M., Kermani, S.Sani, Bagheripour, M.H (2012) "Dynamic properties of granular soils mixed with granulated rubber" *Soil Dynamics and Earthquake Engineering*, Elsevier Ltd., 43, 124-132.

Nigbor, R.L., Imai, Y. (1994) "The suspension P-S velocity logging method." *Geophysical Characterization of Sites*, A special volume by TC10 for XIII ICSMFE, New Delhi, pp.57-61.

Oh-oka, H., Itoh, K., Sugimura, Y., Hirosawa, M. (1979) "Stress-strain behaviour of dry sand and normally consolidated clay by inter-laboratory cooperative cyclic shear tests." Proc. of 11th Joint Meeting, U.S.-

Japan Panel on Wind and Seismic Effects, UJNR, Tsukuba, Japan, September.

Ray, Richard P., Woods, Richard D. (1988) "Modulus and damping due to uniform and variable cyclic loading" *J. Geotech. Engrg.*, ASCE, 114(8), 861-876.

Rayhani, M. H. T., El Naggar, M. H. (2007) "Dynamic properties of soft clay and loose sand from seismic centrifuge tests" *Geotech. Geol. Eng*., Springer

Rayhani, M.H.T., El Naggar, M.H. (2008) "Characterization of glyben for seismic application." Geotech Test J ASTM 31(1), paper ID: GTJ100552.

Richart, F.E., Hall, J.R., Woods, R.D. (1970) *Vibration of Soils and Foundations*, Prentice Hall

Rollins, K. M., Evans, M.D., Diehl, N.B., Daily, W.D. (1998) " Shear modulus and damping relationships for gravels" *J.Geotech. Geoenviron. Eng.*, ASCE, 124(5), 396-405.

Romo, M.P., Jaime, A. (1986) "Dynamic characteristics of some clays of the Mexico valley and seismic response of the ground." Institudo de Ingenieria, Technical Report, Institudo de Ingenieria (in Spanish).

Schnabel, B., Lysmer, J., Seed, H.B. (1972) "SHAKE: A computer program for earthquake response analysis of horizontally layered sites." *EERC 72-12*, University of California, Berkeley, California.

Schwarz, S.D., Musser, J.M., Jr. (1972) "Various techniques for making in situ shear wave velocity measurements - a description and evaluation." Proceedings, International Conference of Microzonation, Seattle, Washington, Vol.2, pp.594-608.

Seed. H. B., Idriss, I. M. (1970) "Soil moduli and damping factors for dynamic response analyses." *EERC Report 70-10*, University of California, Berkeley, Calif.

Seed, H. B., Wong, R. T., Idriss, I. M., Tokimatsu, K. (1984) "Moduli and damping factors for dynamic analyses of cohesionless soils." *Rep. No. EERC* 84-14, Earthquake Engineering Research Center, Univ. of California, Berkeley, Calif.

Seed, H. B., Wong, R. T., Idriss, I. M., Tokimatsu, K. (1986) "Moduli and damping factors for dynamic analyses of cohesionless soils." *J. Geotech. Engrg.*, ASCE, 112(11), 1016-1032.

Seid-Karbasi, M. (2003) "Input motion time histories for dynamic testing in the c-core centrifuge facilities." Report No. 2003/01, University of British Columbia.

Senetakis, K., Anastasiadis, A., Pitilakis, K. (2011) "Dynamic properties of dry sand/rubber (SRM) and gravel/rubber (GRM) mixtures in a wide range of shearing strain amplitudes." *Soil Dynamics and Earthquake Engineering*, Elsevier Ltd., 33, 38-58.

Senetakis, K., Anastasiadis, A., Pitilakis, K., Souli, A. (2012) "Dynamic behavior of sand/rubber mixtures, PartII: effect of rubber content on G/GO–γ–DT curves and volumetric threshold strain." *Journal of ASTM International*, Vol. 9, No. 2.

Shamoto, Y. (1984) " Applicability of nonlinear stress-strain model to undisturbed soils under cyclic loading." Shimizu Research Bulletin, No.3, Tokyo, Japan, March.

Shamoto, Y., Nishio, S., Baba, K. (1986) "Cyclic stress strain behavior and liquefaction strength of diluvial gravels utilizing freezing sampling." *Symp. on Deformation and Strength Characteristics and Testing Methods of Coarse Grained Granular Materials*, JSSMFE, Tokyo, Japan, 89-94.

Sherif, M. A., Ishibashi, I. (1976) "Dynamic shear modulusfor dry sands." *J. of Geotechnical Engineering Division*, ASCE, Vol.102, No. GT 11, pp.1171-1184.

Sherif, M. A., Ishibashi, I., Gaddah, A. H. (1977) "Damping ratio for dry sands." *J. Geotech. Engrg. Div.*, ASCE, 103(7), 743-756.

Shibata, T., Soelarno, D.S. (1975) "Stress-strain characteristics of sands under cyclic loading." *Proceeding of the Japan Society of Civil Engineering*, No.239, pp. 57-65 (in Japanese).

Shibuya, S., Kong, X. J., and Tatsuoka, E. (1990) "Deformation characteristics of gravels subjected to monotonic and cyclic loadings." *Proc.8th Japan Earthquake Engrg. Symp.*, 1, 771-776.

Silver, M. L., Seed, H. B. (1969) "The behavior of sands under seismic loading conditions." *Report No. EERC 69-16*, Earthquake Engineering Research Center, Univ. of California, Berkeley, Calif.

Silver, M. L., Seed, H. B. (1971) "Deformation chararacteristics of sands under cyclic loading." *J. of SMFD*, Proc, of ASCE, Vol.102, No. GT 11, pp. 1171-1184.

Shamoto, Y., Nishio, S., Baba, K. (1986) "Cyclic stress strain behavior and liquefaction strength of diluvial gravels utilizing freezing sampling." *Symp. on Deformation and Strength Characteristics and Testing Methods of Coarse Grained Granular Materials*, JSSMFE, Tokyo, Japan, 89-94.

Shibuya, S., Kong, X. J., Tatsuoka, E (1990) "Deformation characteristics of gravels subjected to monotonic and cyclic loadings." *Proc.8th Japan Earthquake Engrg. Symp.*, 1, 771-776.

Stoll, R. (1985) "Computer-aided studies of complex soil moduli." *Proc., Measurement and use of shear wave velocity for evaluating dynamic soil properties*, ASCE, Reston, Va., 18-33.

Streeter, V.L., Wylie, E.B., Richart, F.E., Jr. (1974) "Soil motion computation by characteristics method." *J. Geotech. Engrg. Div.*, ASCE, 100(3), 247-263.

Sung, Y.W. (1997) "The dynamic properties of Keelung River Clay of Peitou region in Taipei Basin." *Thesis*, Department of Civil Engineering, National Central University, Taiwan. (*in Chinese*)

Tatsuoka, F., Iwasaki, T., Takagi, Y. (1978) "Histeretic damping of sand under cyclic loading and its relation to shear modulus." *Soils and Foundations*, JSSMFE, Vol.18, No.2, pp. 25-40.

Tatsuoka, F., Iwasaki, T., Sudo, H. (1979) "Stress conditions and stress histories affecting shear modulus and damping of sand under cyclic loading." *Soils and Foundations*, JSSMFE, Vol.19, No.2, pp.29-43.

Torabi, M. (2011) "Cyclic and post cyclic static behaviour of fibre reinforced sand."

Uchida, K., Sawada, T., Hasegawa, T. (1980) "Dynamic properties of sand subjected to initial shear stress." *Proc. of International Symposium on Soils under Cyclic and Transient Loading*, Swansen, United Kingdom, pp.121-132.

Upton, R. J. and Machan, G. (1993) "Use of shredded tires for lightweight fill." *Lightweight Artificial and Waste Materials for Embankments over Soft Soils, Transportation Research Record,* No. 1422, National Academy Press, Washington, DC, pp. 36–45.

Vucetic, M., Lanzo, G., Doroudian, M. (1998) "Damping at small strains in cyclic simple shear test" *J.Geotech. Geoenviron. Eng.*, ASCE, 124(7), 585-594.

Vucetic, M, Dobry, R. (1991) "Effect of soil plasticity on cyclic response." *J. Geotech. Engrg.*, ASCE, 117(1), 89-107.

Wang, J.S. (2004) "Soil dynamic properties of the resonant column test." *Thesis*, Department of Civil Engineering, National Central University, Taiwan. (*in Chinese*)

Witchmann, T., Triantafyllidis, T. (2013) "Effect of uniformity coefficient on G/G_{max} and damping ratio of uniform to well-graded quartz sands" *J.Geotech. Geoenviron. Eng.*, ASCE, 139, 59-72.

Wu, C.P., Hwang, J.H., Chien, T.K. (2008) "Dynamic properties of saturated compacted soils" *Geotechnical Earthquake Engineering and Soil Dynamics IV Congress*, ASCE.

Yasuda, N., Matsumoto, N. (1993) "Dynamic deformation characteristics of sand and rockfill materials." *Can. Geotech. J.*, Ottawa, Canada, 30, 747-757.

Yasuda, N., Matsumoto, N. (1994) "Comparisons of deformation characteristics of rockfill materials using monotonic and cyclic loading laboratory tests and in-situ tests." *Can. Geotech. J.*, Ottawa, Canada, 31(2),162-174.

Yu, P., Richart, F.E (1984) "Stress ratio effects on shear modulus of dry sands." *Journal of Geotechnical Engineering*, ASCE, 110, gt3, 331-345.

Zeghal, M., Elgamal, A.W., Tang, H.T., Stepp, J.C. (1995) "Lotung downhole array. II: evaluation of soil nonlinear properties." *J. Geotech. Eng.*, 121(4):363–378.

Zen, K., Umehara, Y., Hamada, K. (1978) "Laboratory tests and in situ seismic survey on vibratory shear modulus of clayey soils with various plasticities." Proceedings of the 5th Japanese Eartquake Engineering Symposium, pp. 721-728.

Zhang, X. J. (1994) "Effect of coupled motions on the dynamic properties of sands" *Ph.D Dissertation, U. of Maryland at Collage Park*

Zhang, X.J., Aggour, M.S (1996) "Damping determination of sands under different loadings" *Eleventh World Conference on Earthquake Engineering*, Elsevier Science Ltd., Paper No. 364.

Zhang, X.J., Aggour, M.S (2004) "Effects of coupled vibrations on the dynamic properties of sands." *13th World Conference on Earthquake Engineering*, Vancouver, B.C., Canada, Paper No.1475.

Zheng-Yi, F., Sutter, K. G. (2000) "Dynamic properties of granulated rubber/sand mixtures " *Geotechnical Testing Journal*, GTJODJ, Vol. 23, No. 3, September 2000, pp. 338–344.

CURRICULUM VITAE

Name Surname **: Yeşim Ünal**

Place and Date of Birth **: Balıkesir - 15.04.1989**

E-Mail **: ysm_89@yahoo.com**

EDUCATION **:**

- **B.Sc.** **:** 2013, Yeditepe University, Faculty of Engineering, Civil Engineering